

EXPLORING BACTERIOPHAGE Q $\beta$  VIRUS LIKE PARTICLE AS A PLATFORM FOR  
ANTICANCER VACCINE DEVELOPMENT

By

Shivangi Chugh

A DISSERTATION

Submitted to  
Michigan State University  
in partial fulfillment of the requirements  
for the degree of

Chemistry – Doctor of Philosophy

2023

## ABSTRACT

Vaccination is a powerful strategy to combat different diseases and provide long term immunity with no overt toxicities. Our lab has been exploring the ability of bacteriophage Q $\beta$ , a virus like particle (VLP) in eliciting immune response against several antigens. Q $\beta$  is an attractive candidate for vaccine applications due to its exceptionally stable and highly organized icosahedral structure. It provides a platform to overcome the low immunogenicity of many peptide antigens and tumor-associated carbohydrate antigens (TACA). This thesis will focus on the design and development of Q $\beta$ -based anticancer vaccine against human breast cancer and Bovine Leukemia Virus causing enzootic bovine leukosis.

Human Mucin-1 (MUC1) is a high molecular weight transmembrane glycoprotein that is found on the apical borders for luminal or glandular epithelial cellular surfaces of many tissues. Of the ~1.4 million tumor patients diagnosed each year in the US, about 900,000 patients were found to overexpress MUC1 and were associated with poor prognosis compared to those with low levels of MUC1. It can be aberrantly overexpressed (>100-fold) on the cell surface of a wide range of human carcinoma including prostate, lung, ovarian pancreatic, colon and more than 90% of breast cancer. MUC1 protein is cleaved into two subunits MUC1-N (N-terminus) and MUC1-C (C-terminus), which are associated by non-covalently interactions. MUC1 has thus become a highly attractive target for the development of new anti-cancer agents. In chapter 1, the current MUC1-C based immunotherapies including monoclonal antibodies, peptide vaccines, antibody-drug conjugates and cytotoxic T cells were reviewed for a deeper understanding of MUC1-C glycoprotein as an oncogenic target. In the following chapters (chapter 2 and chapter 3) both domains of MUC1 protein; MUC1-N and MUC1-C were investigated as antigenic epitopes for Q $\beta$ -based vaccines against human breast cancer. In chapter 2, a spontaneous mouse breast cancer model (MUC1/MMTV) was developed by crossing mouse mammary tumor virus (MMTV)-polyoma middle T (PyMT) mice with human MUC1 transgenic (MUC1.Tg) mice. While the xenograft tumor

model is relatively straightforward to establish, it is unable to represent well the genetic and histological complexity of human tumors. To better mimic the immunosuppressive environment and heterogeneity of human breast cancer, spontaneous tumor models are attractive. The translational potential of the Q $\beta$ -<sup>t</sup>MUC1 vaccine with a short glycopeptide (<sup>t</sup>MUC1)SAPDT\*RPAP (\* denotes *O*-linked glycan) from the MUC1-N domain was evaluated. The Q $\beta$ -<sup>t</sup>MUC1 conjugate produced a robust immune response including binding and killing a wide range of MUC1-expressing tumor cells. It also significantly prolonged the overall survival of MUC1/MMTV mice vaccinated with Q $\beta$ -<sup>t</sup>MUC1 conjugate laying the groundwork for its clinical translation to human patients. In chapter 3, preliminary results for Q $\beta$ -MUC1-C vaccine were demonstrated, which explored two MUC1-C epitopes. The MUC1-C vaccine displayed encouraging results to be developed as an anti-metastatic therapeutic candidate.

Bovine leukemia virus (BLV) is a C-type retrovirus of cattle that causes huge economic losses with the infection rate escalated in the majority of countries worldwide. The National Animal Health Monitoring System estimated that BLV is present in 89% of US dairy operations. BLV causes enzootic bovine leukosis including frequent persistent lymphocytosis and lymphoma. In chapter 4, an anti-BLV vaccine was developed by constructing a peptide-Q $\beta$  conjugate using the envelope glycoprotein gp51 peptide-epitope. The gp51-peptide epitope is known to be putative receptor-binding site and directly implicated in virus infectivity. Q $\beta$ -gp51 peptide vaccine construct elicited robust immune response with long lasting antibodies persisting for over 539 days, making it the first BLV peptide-based vaccine candidate to generate such a long-term immunity, an important criterion for an effective vaccine.

*Dedicated to my beloved parents  
Sunil Chugh and Sunita Chugh  
who have supported me endlessly in this journey  
and to my late grandparents, to whom I am forever grateful.*

## ACKNOWLEDGEMENTS

First and foremost, I would like to express my deepest appreciation to my advisor Prof. Xuefei Huang for his unwavering support, patience and understanding throughout my time here at Michigan State University. He has been the best mentor I could have asked for, I have learnt immensely from him and not just in the field of science but also in several aspects of life in general. I have always appreciated his open-door policy to have scientific discussions despite of his busy schedule. He has always inspired me to be an honest and independent scientist. I want to thank him for giving me this amazing opportunity, it was a privilege to be mentored by a great scientist, a fantastic and fun-loving human being.

I would also like to thank all my committee members Prof. James Geiger, Prof Xiangshu Jin and Prof. Vilma Yuzbasiyan-Gurkan. Their advice, suggestions and feedback over the years have helped me to gain different perspective towards my research and scientific problems. I would like to thank Prof. Vilma Yuzbasiyan-Gurkan and Dr. Cheryl Swenson for being great collaborators on one of my projects. It has been an enriching experience to have worked with such an amazing team. I have always appreciated the motivation and confidence they have instilled in me. Additionally, I want to thank Prof. Kirstin Parkin for teaching me the basics of immunology, I have always admired her style of teaching; Dr. Anthony Schillmiller for troubleshooting all the mass spectrometry errors I have ever encountered; Dr. Matthew Bernard for teaching me the underlying principles of flow cytometry.

To my labmates in the Huang group, thank you for providing a supportive and encouraging environment to work in. A special shoutout to Dr. Herbert Kavunja, Dr. Sherif Ramadan, Dr. Setare Nick and Dr. Xuanjun Wu for their invaluable and unlimited assistance in my research projects. I appreciated their help for developing my scientific skills and research knowledge. I also want to thank Dr. Shuyao Lang, Dr. Zahra Rashidijahanabad, Dr. Zibin Tan, Dr. Kunli Liu, Dr. Hunter McFall-Boegeman, Dr. Vincent Shaw and Dr. Tianlu Li for their

suggestions and help for analyzing my research queries. And all the other members in the Huang lab: Dr. Weizhun Yang, Dr. Jicheng Zhang, Dr. Changxin Huo, Dr. Peng Wang, Dr. Kedar Baryal, Dr. Mengxia Sun, Dr. Xingling Pan, Dr. Somnath Bhagat, Dr. Dushen Chen, Chia-wei Yang, Ida Shafieichaharberoud, Cameron Talbot, Po-han Lin, Athar Nakisa, Morgan Mayieka, Vindula Alwis and Shiva Amin and my mentee and an amazing person Jessica for the conversations and support over the years.

Finally and most importantly, I am indebted to my family and friends. In particular, I would not have been where I am now without the unconditional love and support from my parents. Thanking them is the least I can ever do, I am forever grateful for their sacrifices and their endless motivation that they have provided me throughout my life. I owe everything to them. To my sister, my first mentor, and my best friend, thank you for being your awesome great self and inspiring me every single day. A special mention to my brother-in law, Kanav who has taught me life lessons when I first moved to the United States and the cutest and most loving nephew, Ranveer, whose undeniable love towards me cannot be ever matched by anyone else. I would also like to thank my friends Dr. Ashweta Sahni, Dr. Supreet Kaur, Priyali Prakash, Akhil Sai Konda, Pramit Sawant, Akash Gondalia, Aditya Nair, Ashwathy Nair, Ashwin Koppayi, Dr. Jurick Lahiri and Dr. Grace Hubbell for filling my life with fun, love and laughter.

To my boyfriend and the love of my life, Dushyant who has loved and supported me unconditionally since the day I met him. He is my best friend, my biggest cheerleader and the only person who can make me angry and happy at the same time. We have come a long way and this journey would not have been this much fun and exciting without him at every step of my life. Lastly, to my fur babies Zoey and Yogurt who have been the best roommates I could have asked for. They have kept me sane, happy and motivated during the most difficult times of my life.

## TABLE OF CONTENTS

LIST OF ABBREVIATIONS.....	viii
CHAPTER 1: MUC1-C: The Hidden Target for Cancer Immunotherapy?.....	1
REFERENCES.....	26
CHAPTER 2: Effective Tumor Protection by Q $\beta$ -tMUC1 Vaccine in a Spontaneous Tumor Model Resembling Human Triple Negative Breast Cancer.....	32
REFERENCES.....	54
APPENDIX.....	56
CHAPTER 3: Investigating Epitopes of MUC1-C Protein as an Antigenic Target for Anti-Cancer Vaccine Developmen.....	58
REFERENCES.....	76
CHAPTER 4: Design and Synthesis of Bovine Leukemia Virus Associated Peptide Based Q $\beta$ Conjugate Eliciting Long-lasting Neutralizing Antibodies in Mice.....	79
REFERENCES.....	100
APPENDIX.....	104

## LIST OF ABBREVIATIONS

ADCC	Antibody dependent cell-mediated cytotoxicity
BLV	Bovine Leukemia Virus
BSA	Bovine serum albumin
CAR	Chimeric antigen receptor
CD	Cytoplasmic domain
CDC	Complement-dependent cytotoxicity
CIA	Cell invasion assay
CT	Cytoplasmic tail
CTL	Cytotoxic T cell
DC	Dendritic cell
DMEM	Dulbecco's modified Eagle's medium
DMSO	Dimethyl sulfoxide
ECD	Extracellular domain
EGFR	Epidermal growth factor receptor
ELISA	Enzyme-linked immuno-sorbent assay
ERK	Extracellular signal-regulated kinase
FACS	Fluorescence activated cell sorting
FBS	Fetal bovine serum
FDA	Food and Drug Administration
FITC	Fluorescein isothiocyanate
HRP	Horseradish peroxidase
IgG	Immunoglobulin G
IgM	Immunoglobulin M
KLH	Keyhole limpet hemocyanin

LCMS	Liquid chromatography–mass spectrometry
mAb	Monoclonal antibody
MALDI-TOF	Matrix assisted laser desorption ionization-time of flight
MFI	Mean fluorescence intensities
MHC I	Major histocompatibility complex class I
MHC II	Major histocompatibility complex class II
MPLA	Monophosphoryl lipid A
mQ $\beta$	Mutant Q $\beta$
MS	Mass spectrometry
MUC1	Mucin 1
MUC1-C	Mucin-1 C-terminal subunit
MUC1-N	Mucin-1 N-terminal subunit
MW	Molecular weight
MWCO	Molecular weight cut-off
NSCLC	Non-small cell lung cancer
OD	Optical density
PBS	Phosphate-buffered saline
PBST	Phosphate-buffered saline tween
Q $\beta$	Bacteriophage Q-beta (Qubavirus durum)
SDS-PAGE	Sodium dodecyl-sulfate polyacrylamide gel electrophoresis
SEA	Sea-urchin sperm protein, enterokinase and agrin
SEC	Size exclusion chromatography
Ser	Serine
TACA	Tumor-associated carbohydrate antigen
TACE	Tumor necrosis factor-alpha converting enzyme
TCR	T-cell receptor
TEM	Transmission electron microscopy
Th	Helper T cell
Thr	Threonine
TLR	Toll-like receptors
TM	Transmembrane

Tn	Thomsen-nouveau antigen
VLP	Virus like particle
VNTR	Variable number tandem repeat

## **Chapter 1 MUC1-C: The Hidden Target for Cancer Immunotherapy?**

### **1.1 Introduction**

Cancer is a disease with uncontrollable growth of cells in the body leading to abnormalities in body's function resulting in high mortality worldwide. Amongst the various treatments for cancer, immunotherapy is an attractive strategy that stimulates the immune system of the body to fight against cancer. There are various types of cancer immunotherapies including monoclonal antibodies (mAbs), chimeric antigen receptor (CAR) T-cells, oncolytic viruses, checkpoint inhibitors, cytokines, immunomodulators, and cancer vaccines.

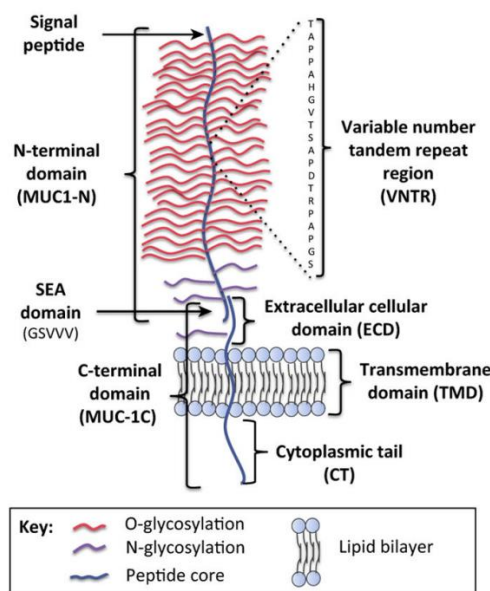
A critical step to achieve an effective anti-cancer immunotherapy is the selection of an antigenic target. Mucins are high molecular weight glycoproteins that are present on the apical borders of reproductive tracts, salivary glands, gastrointestinal tracts, respiratory tract, and urinary tracts.<sup>1</sup> Human mucins are encoded by 22 genes, designated MUC1 to MUC22, which can be classified as secreted, transmembrane and soluble proteins based on their structure and physiological nature.<sup>2</sup> The transmembrane mucins (MUC1, MUC4, MUC12, MUC13, MUC16 and MUC17) are heavily glycosylated with an extracellular domain containing variable number of tandem repeat (VNTR) units, a transmembrane domain and a cytoplasmic tail. These glycoproteins are responsible for many crucial cellular functions like providing a mucosal barrier against pathogenic invasion, cell adhesions, cell signaling, regulation of stress-induced death pathways.

MUC1 (CD227) was the first transmembrane mucin identified and structurally characterized.<sup>3,4,5,6</sup> It can be aberrantly overexpressed (> 100-fold) on the cell surface of a wide range of human carcinoma including prostate, lung, ovarian pancreatic, colon and more than 90% of breast cancer.<sup>7, 8</sup> MUC1 expression in normal epithelial cells is polarized with the protein mainly present at the apical surface of the cells. However, in cancer cells,

MUC1 expression loses the cellular polarity, thus becoming accessible to the immune system.<sup>2, 9, 10</sup> These findings supported MUC1 being ranked as one of the top cancer antigens by the National Cancer Institute Project for the Acceleration of Translational Research.<sup>11</sup>

MUC1 is composed of two subunits, i.e., *N*- and *C*-terminal subunits. The MUC1-*N* subunit forms a heterodimer with the MUC1-*C* subunit, which is localized on the cell surface. The MUC1-*N* terminal subunit (MUC1-*N*) is a polypeptide consisting of 20-125 tandem repeats each with 20 amino acids in length. The tandem repeat contains multiple Ser and Thr residues (PDTRPAPGSTAPPAHGVTSA), which can be glycosylated leading to up to five *O*-glycans per repeat (**Fig. 1**).<sup>12</sup>

**(A) Full length MUC1:**



**(B) MUC1-C N-glycosylation:**

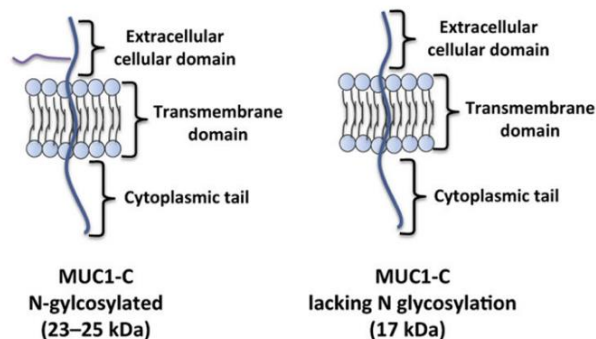


**Figure 1. Schematic representation of full length MUC1 protein and sites of N-glycosylation.** (A) The full length MUC1 is subdivided as *N*-terminal subunit (MUC1-*N*) consisting of variable number of tandem repeats and *C*-terminal subunit (MUC1-*C*). The cleavage of MUC1 takes place around the sea-urchin sperm protein, enterokinase and agrin (SEA) domain, forming a stable heterodimeric complex. (B) The extracellular domain (ECD) of MUC1-*C* contains one site (asparagine residue) for *N*-glycosylation. The molecular weight of MUC1-*C* subunit can range between 17 kDa – 25 kDa depending on the extent of *N*-glycosylation. This figure is reproduced with permission from the publisher.<sup>13</sup>

MUC1 is translated as a single polypeptide chain, which can undergo proteolysis.

One major site of cleavage is at the SEA domain in the endoplasmic reticulum (ER) forming

two subunits, i.e., *N*- and *C*-terminal subunits (**Fig. 1A**). The two subunits form a heterodimer during post-translational glycosylation. The SEA domain is a highly conserved 120 amino acid domain and the cleavage site is 59 amino acids proximal to the transmembrane domain between Gly<sup>316</sup>-Ser<sup>317</sup>.<sup>14-16</sup> Other studies emphasized the crucial role of enzymes such as tumor necrosis factor-alpha converting enzyme (TACE-ADAM 17) and membrane type matrix metalloproteinase MMP14 (MT1-MMP) in the MUC1 cleavage.<sup>17,18</sup> The heterodimer formed is stable when subjected to high temperature, reducing agents like  $\beta$ -mercaptoethanol or acidic condition but dissociates in sodium dodecyl sulfate.<sup>19, 20</sup> The rate at which this cleavage takes place is between 5-30 min at 37 C and it is pH-dependent with maximum cleavage observed at physiological pH conditions.<sup>21</sup>

Many strategies including cancer vaccines, mAbs, antibody-drug conjugates (ADCs), targeted radiotherapy, aptamers and peptide-based therapies have targeted MUC1-N tandem repeats as antigens.<sup>22-26</sup> In one of these studies, mice were immunized with a MUC1 cDNA vaccine containing MUC1-N (22 tandem repeats) plasmid, which significantly reduced the number of lung metastases.<sup>27</sup> Another study reported the use of anti-MUC1 antibodies (GP1.4) to treat MUC1-positive tumors in the pancreas. The mechanism involved internalization of the GP1.4 antibody after binding to MUC1 on cellular surface to the intracellular region through the macropinocytotic pathway.<sup>28</sup> This leads to reduced epidermal growth factor receptor (EGFR) signaling, which inhibited extracellular signal-regulated kinase (ERK) phosphorylation suppressing proliferation and migration of cancer cells.<sup>29</sup> A group of scientists used dendritic-cell based vaccine loaded with MUC1-derived peptide to target non-small cell lung cancer (NSCLC). The patients who received this vaccine had prolonged survival due to anti-tumor immune response.<sup>30</sup> A peptide-based vaccine (ImMucin) encoding for 21 amino acids in signal domain of MUC1-N region targeted MUC1-expressing tumors. Balb/c mice with DA3 metastatic mammary

tumors overexpressing MUC1 immunized with ImMucin exhibited robust anti-tumor immune response that increased their overall survival.<sup>31</sup> The peptide sequence within ImMucin is also known to be epitopes to both human major histocompatibility complexes (MHC) class 1 and 2 alleles leading to MUC1-specific T cell activation. ImMucin has successfully completed Phase I/II clinical trial in multiple myeloma and received orphan drug status by FDA and EMA.<sup>32</sup>

After cleavage, the MUC1-N subunit can be shed from the surface of cancerous cells as detected at increased levels in the plasma obtained from the breast cancer patients.<sup>33, 34</sup> Many clinical trials involving mAbs (AS1402; huHMFG-1) and BrevaRex (AR-20.5) that targeted the VNTR region in MUC1-N domain were unsuccessful. AS1402 induced potent antibody-dependent cellular cytotoxicity (ADCC) response against MUC1- positive tumor cells. BrevaRex, a murine anti-MUC1 monoclonal antibody, formed immune complexes (antigen/antibody complexes) binding with receptors on dendritic cells. Despite the promising preclinical results, the clinical development of mAbs AS1402 (huHMFG-1) and BrevaRex (AR-20.5) failed, which was presumably due to MUC1-N shed in the blood circulation sequestering the antibodies and preventing them from reaching the surface of tumor cells.<sup>35-38</sup>

An alternative target for MUC1 based immunotherapies is MUC1-C that remains anchored on the cell surface. MUC1-C is mainly composed of a 58-amino acid extracellular domain (ECD), a 28 amino-acid transmembrane (TM) domain followed by a 72-amino acid cytoplasmic tail (CT). The ECD also contains of one *N*-glycosylation site.<sup>39</sup> MUC1-C is involved in various cellular functions, as its ECD can function as a binding site for galectin-3 that interacts with tyrosine kinase EFGR at the cell membrane. This leads to the activation of phosphoinositide 3-kinase (PI3K)-AKT and mitogen-activated protein kinase (MEK)-ERK pathways, which are vital for cancer cell survival and proliferation.<sup>40, 41</sup> MUC1-C can

be localized to the nucleus and activate the Wnt/b-catenin, signal transducer and activator of transcription (STAT) and NF (nuclear factor)-kB RelA pathways that promote survival of cancerous cells and induce their transformation.<sup>42</sup> *In vitro* and *in vivo* xenograft models have supported that the inhibition of this C-terminal subunit directly blocks its oncogenic function and thereby inducing apoptosis in breast cancer cells.<sup>43</sup> Various other studies have demonstrated that transfection of MUC1-negative cells with MUC1-C alone resulted in oncogenic activities such as increased growth rate, anchorage-independent cell growth, and resistance to apoptosis of cancerous cells with chemotherapy agents), which were previously attributed to the full length MUC1.<sup>44, 45, 46</sup>

There have been many excellent reviews on targeting MUC1 for anti-cancer therapy, which primarily focus on the MUC1-N region.<sup>22-26, 39, 47-50</sup> In this review, the various modes of therapeutic tools involving mAbs, peptide-epitopes, cytotoxic T-cells (CTLs), and ADCs that target MUC1-C for potential anti-cancer therapies will be summarized.

### **Immunotherapeutic tools targeting MUC1-C**

#### **A) Cytotoxic T-cell epitopes spanning the MUC1-C domain**

The cellular adaptive immune system comprises of two types of T cells, i.e., helper T cells (T<sub>h</sub>) and CTLs. CTLs expressing CD8 on their surface can recognize and kill tumor cells in the body through T cell-mediated cytotoxicity. This can be achieved either by direct cell-cell contact or the release of various cytokines such as interferon-gamma (IFN- $\gamma$ ) and tumor necrosis factor-alpha (TNF- $\alpha$ ). Tsang et. al. successfully identified nine potential CD8<sup>+</sup> CTL epitopes from MUC1 and highlighted their importance in enhancing a potent immune response. Of the nine CD8<sup>+</sup> epitopes, seven are in the MUC1-C region and two epitopes are in the VNTR region of MUC1-N.<sup>51</sup> Based on the epitopes identified, scientists discovered enhancer agonist peptides that can more potently activate T-cells to lyse human tumor cells. These agonist peptides cover the human leukocyte antigen (HLA)-A2, HLA-

A3 and HLA-A23 MHC class I alleles, which are major histocompatibility complexes (MHC) controlled by chromosome 6. The MHCs present the peptide epitopes to T-cell receptors to activate T cells and provide immune defence.<sup>52</sup> In comparison to the native peptide epitopes, incubation with these agonist peptides generated T-cell lines more efficiently from the peripheral blood mononuclear cells (PBMCs) of cancer patients, enhanced the production of IFN- $\gamma$  by peptide-activated human T cells and lysed human tumor cell targets in an MHC-restricted manner. Point mutations in the native peptide epitope sequences were performed to synthesize fourteen agonist peptides in the MUC1-C region and three in the VNTR region. These agonist peptide epitopes with single amino acid substitution at the HLA class I-binding site were then scanned for matches to consensus motifs for HLA-A2-, HLA-A3-, and HLA-A24-binding peptides by using a computer algorithm.<sup>53</sup> The algorithm ranks potential MHC-binding peptides according to the predicted one-half-time dissociation of peptide/MHC complexes, but it was unsuccessful in predicting the MHC binding and HLA-A2 binding ability to activate human T cells to produce interferon.

Five agonist peptides (C1A, C2A, C3A, C8A, C9A) from MUC1-C domain were evaluated for their immunogenicity. **Table 1** depicts the sequences of the native and the mutant agonist epitopes with their predicted and actual binding ability to form stable complexes with HLA-A2 molecules in T2 cell binding and stability assay.<sup>51</sup> Three HLA-A2-binding peptides for the MUC1-C domain, designated C1 (AA 1172-1181), C2 (AA 1177-1186), and C3 (AA 1240-1248), were identified, as well as their corresponding potential agonists with higher predicted binding affinity (designated C1A, C2A, and C3A, respectively). Two HLA-A2-binding peptides were also identified from the VNTR region, designated V1 (AA 150-158) and V2 (AA 141-149) as well as two corresponding potential agonists with higher predicted binding affinity (designated V1A and V2A, respectively).

Three agonist epitopes C2A (position 1177), V1A (position 150) and V2A (position 141) exhibited higher binding affinity than their native peptide epitopes. The binding of C2A peptide was 10 to 16-fold higher than the control flu peptide; another known strong HLA-A2 binding peptide.

Peptide	Location	Position	Sequence	Class I allele	Predicted binding*	Actual binding <sup>#</sup>
C1	C domain	1172–1181	ALAIVYLIAL	A2	49	249
C1A			<b>Y</b> LAIVYLIAL		226	245
C2	C domain	1177–1186	YLIALAVCQC	A2	52	211
C2A			<b>Y</b> LIALAVC <b>QV</b>		736	299
C3	C domain	1240–1248	SLSYTNPAV	A2	70	326
C3A			<b>Y</b> LSYTNPAV		320	342
V1	VNTR region	150–158	STAPPAHGV	A2	1	166
V1A			<b>Y</b> LAPPAHGV		320	486
V2	VNTR region	141–149	APDTRPAPG	A2	0	210
V2A			<b>Y</b> LDTRPAPV		128	647
C4	C domain	432–441	ALAIVYLIAL	A3	5	NA
C4A			ALFIVYLI <b>A</b> K		900	NA
C5	C domain	483–491	STDRSPYEK	A3	3	NA
C5A			SLFRSPYE <b>K</b>		300	NA
C6	C domain	462–471	TYHPMSEYPT	A24	6	NA
C6A			<b>K</b> YHPMSEY <b>A</b> L		480	NA
C7	C domain	502–510	SYTNPAVAA	A24	5	NA
C7A			<b>K</b> YTNPA <b>V</b> A		400	NA

Amino acids that were changed to generate an agonist epitope are in bold

\* Predicted binding on the basis of reported motif [32]; score estimate of half time of disassociation of a molecule containing this sequence.

<sup>#</sup>Peptides were used at a concentration of 12.5 µg/ml in a binding assay with T2-A2 cells. Results are expressed as mean fluorescence intensity (MFI). NA: A functional binding assay was not available for HLA-A3 and HLA-A24 peptides

**Table 1. Predicted binding and T2-cell binding assay for MUC1 HLA-A2-, HLA-A3-, and HLA-A24-binding peptides and their potential agonists.** This figure is reproduced with permission from the publisher.<sup>51</sup>

The immunogenicity of these agonist and native peptides were evaluated for their abilities to generate CTLs *in vitro*. The T cell lines generated from the agonist peptides (T-C1A, T-C2A, and T-C3A) produced higher levels of IFN- $\gamma$  as evaluated by enzyme linked immunosorbent assay (ELISA) than those stimulated with the respective native peptides. In the cytotoxicity analysis, the agonist T-cell lines C1A, C3A lysed the MCF-7 (human breast carcinoma cell line, 86 % HLA-A2<sup>+</sup>, 48 % MUC1<sup>+</sup>) tumor cells more efficiently compared to their corresponding native T-cell lines whereas the cytotoxicity assay results for C2 and C2A had only minor differences. As the negative control, there was no lysis of the SK-Mel

(melanoma cell line ,100 % HLA-A2<sup>+</sup>, MUC1<sup>neg</sup>) demonstrating the specificity for MUC1. The results corroborated that the T cells generated specifically from agonist epitopes of the MUC1-C and VNTR region are able to lyse human tumor cells endogenously expressing native MUC1 in an antigen-specific and HLA-A2 restricted manner.

## **B) Novel polyclonal and monoclonal antibody targeting the minimal fragment of MUC1-C**

MUC1 is aberrantly overexpressed on the surface of cancer cells and when it is introduced into MUC1-negative cells leads to increased cell growth and resistance to cancer cell apoptosis by chemotherapeutic drugs. As discussed previously, MUC1 can be cleaved. Two subunits may be generated, i.e., a high molecular weight species (150-300 kDa) with the VNTR region and a low molecular weight species (20-35 kDa; MUC1\*) with the cytoplasmic tail.<sup>54</sup> The low molecular weight MUC1 species (20-35 kDa; MUC1\*) contains part the MUC1-C subunit discussed previously. The MUC1\* was found to be composed of the cytoplasmic tail, the transmembrane domain and 45 amino acids (N-1110-1154-C) from the ECD, the minimal fragment of MUC1-C ECD protein on the surface of cancer cells and tissues that was able to mimic the oncogenic functions of full-length MUC1.<sup>54</sup>

The main focus of the study led by Bamdad et. al. is to investigate the expression patterns of MUC1\* and examine its specific role in mediating growth of cancerous cells in comparison to the full-length MUC1 protein. MUC1\* remains membrane bound after the high molecular weight MUC1-N is cleaved and released from the surface of the cells. A set of antibodies targeting different regions of MUC1 was used to characterize and distinguish MUC1\* from full-length MUC1. The commercially available VU4H5 antibody binds to the VNTR region and Ab-5 antibody targets the cytoplasmic tail of MUC1. However, there were no commercially available antibodies that recognized the extracellular domain of

MUC1\*. To fill this gap, novel polyclonal and monoclonal anti-MUC1\* antibodies have been developed to distinguish the full length MUC1 and MUC1\* proteins.<sup>54</sup> The anti-MUC1\* antibodies were elicited against the forty-five amino acid peptide (N-1110-1154-C) that is N-terminal to the transmembrane domain (**Fig. 2A, B**). Anti-MUC1\* was characterized by western blot, immunoprecipitation, immunohistochemistry (IHC) and fluorescence activated cell sorting (FACS). MUC1\* was stained by anti-MUC1\* antibodies in MUC1-positive cells like T47D, ZR-75-1, ZR-75-30, BT474, DU145, and Capan 2. It showed no reaction to the MUC1-negative cells including HCT116, 3Y1 and HEK293.

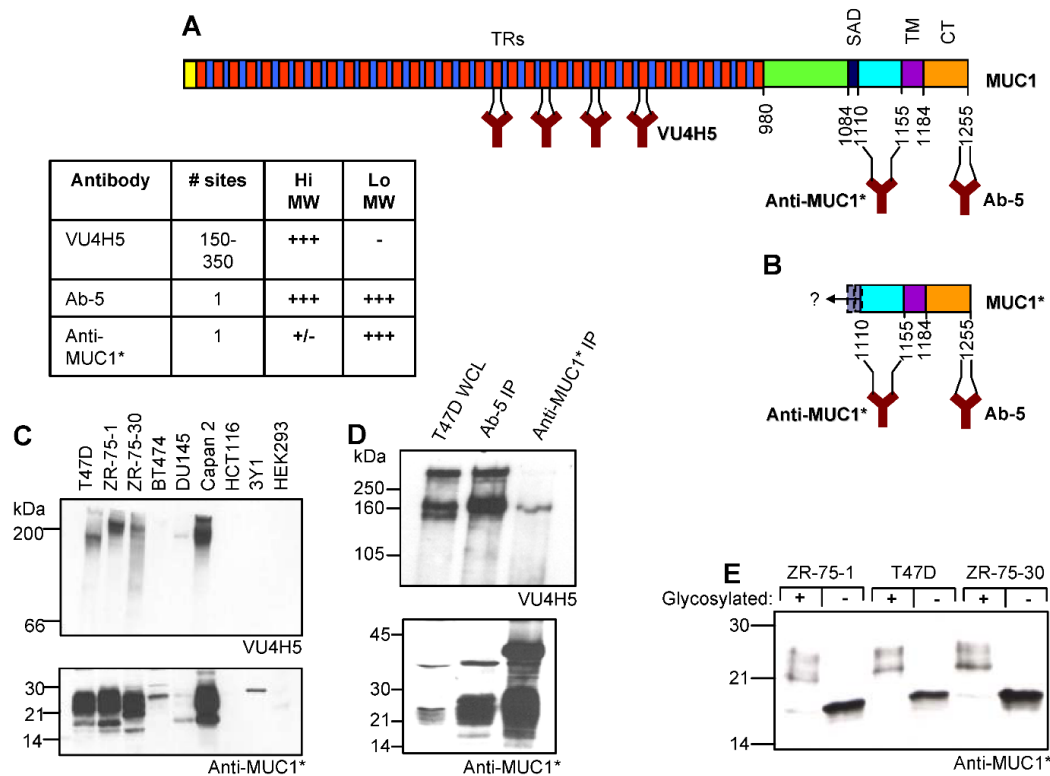


**Figure 2. Schematic representation of full-length MUC1 and the membrane-bound minimal fragment MUC1\* along with antibody recognition sites** A. Full-length MUC1 protein depicting the recognition sites for antibody VUH5, AB-5 and Anti-MUC1\* B. Minimal fragment, MUC1\*, with the cytoplasmic tail, transmembrane domain, and at least 45 amino acids from the extracellular domain (ECD) C. Western blot analysis of whole cell lysates of MUC1-positive cultured cancer cells (Lanes 1-6; T47D, ZR-75-1, ZR-75-30, BT474, DU245 and Capan 2) versus MUC1-negative cells (Lanes 7-9; HCT116, 3Y1 and HEK293) D. Immunoprecipitation of T47D cells with control antibody Ab-5 versus Anti-MUC1\*. Gels were probed with either control antibody VU4H5 (upper) or Anti-MUC1\* (lower). E. Western blot analysis of T47D, ZR-75-1, ZR-75-30 pre- and post-deglycosylation and blotted with Anti-MUC1\* depicting 16-18 kDa as the actual molecular weight of cleaved MUC1 (MUC1\*). F. The table summarizing the reactivities of antibodies to either full-length MUC1 (high molecular weight; Hi MW) or cleaved MUC1 (MUC1\*; low molecular weight; Lo MW). This figure is reproduced with permission from the publisher.<sup>54</sup>

To further confirm that the stained MUC1\* species is indeed MUC1 protein, the lysates from MUC1-positive cancer cells (T47D, ZR-75-1, ZR-75-30, BT474, DU245 and Capan 2) were immunoprecipitated by the anti-MUC1\* antibodies and analysed by western blot. VU4H5 and Ab-5 were used as controls, which weakly immunoprecipitated cell-

associated MUC1 species as compared to anti-MUC1\* antibodies suggesting that the predominant form on cancer cells is the cleaved MUC1 fragment (**Fig. 2C, D**). This membrane-bound cleavage product MUC1\* showed 20-35 kDa in molecular weight for the glycosylated protein and an approximately 16 kDa for the un-glycosylated form (**Fig. 2E**). On analysis of immediately-adjacent sections of cancerous breast, lung and colon tissues by fluorescence imaging, it was revealed that MUC1\* was distributed over the entire cell surface of cultured cancer cells. In contrast, the full-length MUC1 protein stained by VU4H5 was either not present or present in minor amounts restricted to the cytoplasm. Furthermore, anti-MUC1\* antibodies produced more intense staining than the VU4H5 even though there is a much higher probability for this tandemrepeat antibody (VU4H5) as it can bind to hundreds of epitopes per receptor compared to a single epitope available per receptor for anti-MUC1\*. One critical finding was that some cancer tissue samples stained positive for MUC1\* but negative for full-length MUC1.<sup>54</sup> For example, some colon cancer specimen was stained positive by anti-MUC1\* with the most intense staining depicted in the most diseased area of the specimen. In contrast, VU4H5 only faintly stained the areas in proximity to the margins of malignancy with no staining in the diseased region. This observation highlighted that most cancerous specimens may give false negative MUC1 staining when stained with antibodies targeting the VNTR region of MUC1. These evidences demonstrated that MUC1\* is the predominant species on cultured cancerous cells and tissue specimens and can be used as an important epitope for cancer diagnostics.

The cell growth characteristics of cells expressing the cleaved MUC1\* protein was studied in comparison to those with the full length MUC1 protein. The number of cells increase primarily due to two factors, i.e., 1) through the increase in cell growth; and 2) through increasing cell survival factors such as resistance to chemotherapy induced cell death. To evaluate this, the single clones of MUC1\*<sub>1110</sub> (construct whose extracellular

domain was terminated after forty-five amino acids N-1110-1255-C) and MUC1 were transfected in MUC1-negative cells (3Y1 or HCT116).<sup>54</sup> A clonogenic assay revealed that the MUC1\*<sub>1110</sub> clones produced more, bigger and denser colonies than those with the full length MUC1. Further analysis using chemotherapeutic agents such as cytarabine (AraC), cisplatin or etoposide depicted that the cells transfected with either full length MUC1 or the cleaved MUC1\*<sub>1110</sub> became resistant to death induced by these agents. Additionally, a cell cycle experiment was performed to analyze the increase in cell growth by measuring the ratio of the number of cells in G2/M phase (indicator of cell division) to the number of cells in the G1 phase of HCT116 transfected cells with either full length MUC1 or the cleaved MUC1\*<sub>1110</sub>.<sup>54</sup> The results reported that the transfection of MUC1\*<sub>1110</sub> increased the ratio of G2:G1 much more than that of cells transfected with the full length MUC1. This could also be indicative of the fact that the full length MUC1 protein undergoes a significant amount of proteolysis to the MUC1\* form.

It is generally known that class I growth factor receptors can trigger cell growth by dimerizing the ECD of the receptor. To test this, MUC1\* expressing cells were treated with a bivalent antibody against MUC1\*<sub>1110</sub>-ECD, which stimulated tumor cell proliferation and transient phosphorylation of ERK1/2, a key step in the MAP kinase activation signaling cascade. These results suggested that MUC1\* might act as a growth receptor or co-receptor. The potential ligand for MUC1\* was identified as non-metastatic protein 23 (NM23), a nucleoside diphosphate kinase-A (NDPK-A) enzyme through ligand fishing experiment, specifically of H1 and H2 isoforms using N-terminal microsequencing in cancer cell lysates.<sup>55</sup> NM23 is cytoplasmic but often secreted by cancer cells, which is linked to both metastasis suppression and metastasis promotion.<sup>56, 57</sup> NM23 bounded to the extracellular domain of MUC1\* with nanomolar affinity and stimulated the growth of NM23 transfected MUC1-positive cancer cells.

### C) Cell penetrating peptide epitopes targeting MUC1-C

MUC1-C has been known to be involved in many critical oncogenic activities and one of those functions is its involvement in uncontrolled growth of cancerous cells and resistance to chemotherapy induced apoptosis.<sup>43, 58, 59</sup> To inhibit this, agents have been developed to directly target the glycoprotein. One such inhibitor is a cell penetrating peptide GO-201 that blocks the oligomerization of MUC1-C glycoprotein, which prevents it to be transported to the nucleus and mitochondria.<sup>42, 60</sup>

The N-terminal region of MUC1-CD consists a CQC motif that has been shown to be of utmost importance in MUC1 oligomerization and maintenance of the redox balance in human breast cancer cells.<sup>61-64</sup> This cysteine-dependent oligomerization when targeted abrogates MUC1 induced transformation and its nuclear localization, which causes growth arrest and apoptosis of carcinoma cells. A peptide inhibitor derived from the N-terminal region of the cytoplasmic domain of MUC1 has been synthesized, which consists the CQC motif (CQCRRKNYGQLDIFP), designated as GO-201. To enhance the entry into cells, the peptide inhibitor, GO-201 was further functionalized with a poly D-arginine transduction domain. A control peptide CP1 was synthesized with the CQC sequence mutated to AQA (Fig. 3).

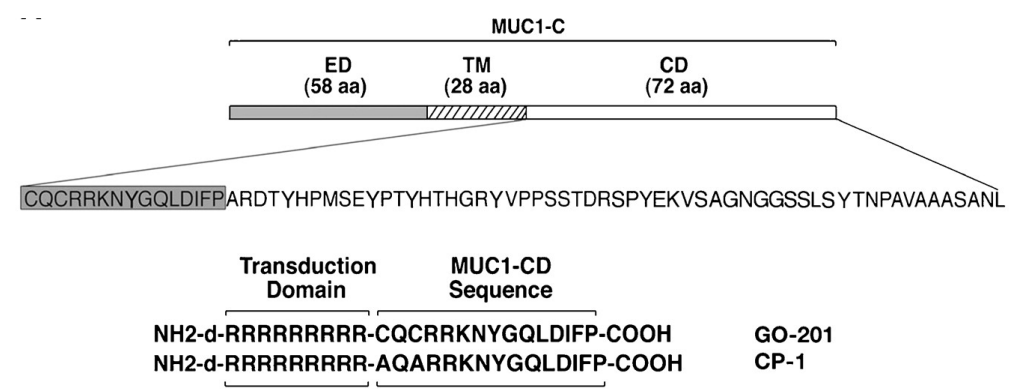


**Figure 3. Schematic representation of the cytoplasmic domain (CD) with 72 amino acid sequence of MUC1-C subunit. GO-201 peptide sequence (shaded) with 15 amino acids at the N-terminus along with the control peptide CP1 sequence. Both peptides were**

synthesized with poly-d-arginine transduction domain. This figure is reproduced with permission from the publisher.<sup>60</sup>

For analysis of the binding affinity of the synthesized peptides to the MUC1-CD, the BIAcore sensor chip was immobilized with His-tagged MUC1-CD. The dissociation constant  $K_d$  for GO-201 to His-MUC1-CD was calculated to be 30 nM, which was similar to the  $K_d$  for MUC1-C oligomerization.<sup>61</sup> Incubation of MUC1-CD with GO-201 significantly decreased the formation of MUC1 oligomers with the simultaneous increase in monomers as detected by polyacrylamide gel electrophoresis. In contrast, incubation with CP1 had no such effects highlighting the significance of CQC motif. The protein binding results were consistent with similar experiments performed with HEK293 cells for assessing MUC1 oligomerization. A time-dependent increase in cellular uptake was evaluated by the mean fluorescence intensity of FITC-labeled GO-201 and CP1 peptides in both ZR-75-1 and MCF-7 cells. Previous work has revealed that the increase in levels of reactive oxygen species (ROS) above the reducing capacity of the cells could lead to DNA damage due to the formation of double-strand breaks.<sup>65</sup> This was consistent with the exposure of ZR-75-1 and MCF-7 cells to GO-201 leading to high ROS levels and activation of DNA damage response whereas treatment with CP1 did not lead to apparent responses. In addition, treatment with GO-201 initiated S-phase growth arrest in human breast cancer cells (ZR-75-1 and MCF-7) as evident by a distinct sub-G1 DNA peak and prominent uptake of propidium iodide, which is consistent with induction of late apoptosis/necrosis and loss of membrane integrity respectively. As a control, GO-201 had negligible to no effect in non-malignant MCF-10A breast cancer cells.

To investigate the anti-tumor activity *in vivo*, GO-201 was administered to mice implanted with ZR-75-1 cells at 10mg/kg/d for 21 days in comparison to 50mg/kg/d dosage of CP1 or just PBS alone. Tumor regression and prolonged delays in regrowth were

observed for GO-201, which was partially explained by the induction of tumor necrosis. The control peptide and vehicle had no anti-tumor activities. Administration of GO-201 was also well-tolerated with no observable acute toxicities at the mentioned dosage in Balb-c nu/nu female mice. To further emphasize that the CQC motif is the Achilles heel of the MUC1 oncoprotein, a shorter peptide (CQCRRKN) designated as GO-202 was used as a control peptide. The tumorigenicity results for GO-202 were similar to those of GO-201 with 15 MUC1 amino acids. The mice treated with GO-201 and GO-202 did not have any observable tumors till day 152. The experiment was repeated and it gave similar results for the xenograft models with MCF-7 and estrogen-independent breast cancer cells, MDA-MB-231.

#### **D) Monoclonal antibodies targeting MUC1-C**

Antibodies targeting the extracellular domain of MUC1-C (58 A.A, N-1097-1154-C) and MUC1-C\* (45 A.A, N-1110-1154-C) were developed through the phage display process.<sup>66</sup> In this process, the phage phenotype is directly linked to its encapsulated genotype, which ultimately leads to the presentation of libraries of molecules on the surface of the phage.<sup>66, 67</sup> Antigens mimicking the MUC1-ECD and MUC1-C\* were generated as human Fc-fused forms to present them in their natural conformation during the antibody screening process (**Fig. 4**). A total of 600 phage clones was examined for binding specificities against MUC1-C and MUC1-C\* with 24 human antibodies isolated through

phage display antibody panning.

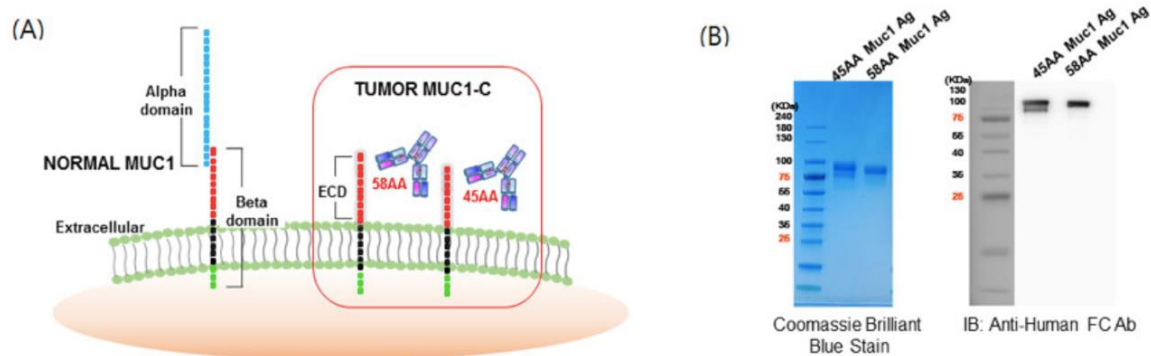


**Figure 4. Schematic representation of MUC1 and potential binding sites for antibodies targeting 58 amino acids and 45 amino acids (AA) in the MUC1-C domain.** (A) The ECD of MUC1-C depicting the binding domains to generate MUC1-C (58 AA and 45 AA) antibodies. (B) Purification of the expressed antigens (45 AA MUC1 Ag and 58 AA MUC1 Ag) using protein A column and characterizing it through Coomassie blue stain and western blot against anti-human Fc antibody. This figure is reproduced with permission from the publisher.<sup>66</sup>

Five clones were selected based on their strong binding to the MUC1 expressing cells and the mammalian expression system was used to produce the antibodies in full-sized IgG1 format. Amongst the five clones, two (SKM1-06, 07) displayed minimal expression whereas the other three (SKM1-02, 13, 20) had relatively robust expression (**Fig. 5A**). Various immunological assays such as ELISA, dual FACS analysis, bio-layer interferometry (BLI) assay and confocal image analysis were used to validate the specificities and functionalities of the selected three clones (SKM1-02, 13, 20) and MIN-C2 (anti-MUC1 $\beta$  domain;  $\beta$  domain is referred to the MUC1-C domain consisting of ECD, TM and CT domains) antibody was used as a reference.

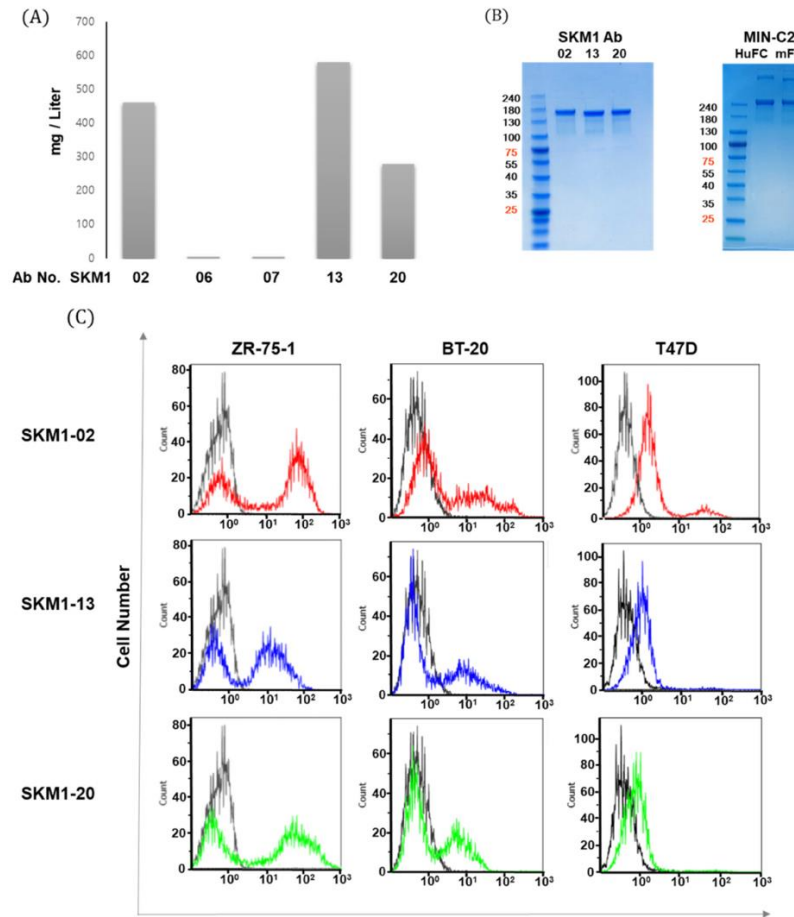


**Figure 5. Expressing MUC1-C specific antibodies and its binding evaluation of MUC1-positive breast cancer cells.** (A) The expression level (mg/ L) of the five antibodies expressed through Expi-CHO cells and purified by protein A column. (B) Purified SKM1 antibodies (left panel) characterized by SDS-PAGE and compared with MIN-C2 antibody developed by Minerva Biotechnologies (right panel). (C) FACS analysis of SKM1-02(red line), 13(blue line), 20(blue line) antibodies with MUC1-positive breast cancer cells (ZR-75-1, BT-20 and T47D). This figure is reproduced with permission from the publisher.<sup>66</sup>

The top three clones SKM1-02, 13, 20 were subjected to FACS analysis of MUC1-expressing cell lines; ZR-75-1, T47D and BT-20 (TNBC; triple negative breast cancer). TNBC is one of the most aggressive forms of breast cancer (**Fig. 5C**). It is termed as ‘triple-negative’ because it lacks the common receptors (estrogen or progesterone) found in other breast cancer cells and express little or no HER2 protein. It accounts for 10-15% of all breast cancers with very high rate of growth and metastasis.<sup>68</sup> ELISA and the direct interaction experiment between the antibody and the MUC1-C antigen using BLI were also performed. The results depicted that SKM1-02 antibody possessed the highest binding capability

compared to the other two antibodies. Furthermore, SKM1-02 Ab had similar binding to MUC1-C and MUC1-C\* antigen whereas the SKM1-20 clone exclusively bound to the MUC1-C 58 aa ECD epitope. Similar results were obtained with immunofluorescence staining, which revealed overlapping staining for SKM1-02 Ab and the control antibody MIN-C2 suggesting that both antibodies share similar binding sites within the MUC1-ECD on the breast cancer cell surface.

Translocation of MUC1-C to the nucleus is like a domino, where one step influences the next. It begins with beta-catenin repression of E-cadherin expression, which further destabilizes the adherens junctions. This causes cytoskeletal rearrangement, which ultimately results in the loss of inhibition of cell-cell contact.<sup>69</sup> To evaluate these antibodies (SKM1-02, 13, 20) as potential anti-metastatic candidates for their inhibitory roles in the invasion of MUC1-expressing breast cancer cells (ZR-75-1, T47D, BT-20), cancer cell invasion and cancer growth inhibition assays were performed. The results demonstrated that all three antibodies with high levels of migration inhibition. To develop these antibodies as a viable therapeutic drug, their thermal stability and affinity were explored. SKM1-02 mAb displayed superior qualities with dissociation constant of 6.5 nM against MUC1-C and was even able to bind to the antigen at 72 °C. These results showed that these antibodies can be developed as highly effective therapeutic candidates against human breast cancer, especially TNBC.

In one study, Kwon et. al. demonstrated the binding of the anti-MUC1 mAb to the recombinant and native MUC1-C protein present on the membrane surface of MUC1-positive breast cancer cells.<sup>70</sup> Anti-MUC1 recognized the ECD region of MUC1-C glycoprotein. The human cDNA encoding the polypeptide sequence (rhMUC1-EC192) of 192 amino acids from the extracellular region of MUC1-C (N-961-1152-C) for mAb (anti-

MUC1) was obtained from MCF-7 cells. Female balb/c mice were immunized with this purified recombinant human MUC1 protein to successfully obtain the anti-MUC1 mAb from the immunized mice. Anti-MUC1 (MUC1-1H7 clone, IgG1) binds efficiently to rhMUC1-EC192 protein with the Kd of 15nM as analyzed by surface plasmon resonance (SPR). The western blot analysis with the lysates of MUC1-positive (MCF-7, ZR-75-1, T47D) and MUC1-negative (MDA-MB-231) breast cancer cells revealed that anti-MUC1 antibody was unable to recognize MUC1 protein in any of the samples. However, the mAb successfully immunoprecipitated native-state MUC1 protein in MCF-7, ZR-75-1 and T47D cell lysates. The results depicted that anti-MUC1 antibody was able to recognize and bind only to the MUC1-C in its native form.

The efficiency of the anti-MUC1 mAb was assessed, and its specificity and binding affinity were determined.<sup>70</sup> It revealed that the anti-MUC1 mAb bound with significant immunofluorescence staining both on the surface and intracellular locations of intact cells with MUC1 overexpression (MCF-7, T47D and ZR-75-1). This signifies that anti-MUC1 was able to recognize the MUC1-C ECD whereas the control antibody (anti-MUC1-CT2) failed to show any intracellular staining without permeabilization. To evaluate internalization of the antibody, confocal imaging was carried out with an amine-reactive fluorescent label (DyLight 488). The results suggested that the anti-MUC1 mAb was predominantly internalized in T47D cells and significantly delayed the proliferation of these cancer cells. This suggests a potential correlation between the internalization of anti-MUC1 antibody and its anti-proliferative effect on MUC1-positive breast cancer cells.

*In-vivo* biodistribution of anti-MUC1 was evaluated in a mouse xenograft model to demonstrate its effectiveness in targeting of the tumor cells versus the healthy cells. It used total flux of fluorescence of DyLight-labeled antibody.<sup>70</sup> It clearly demonstrated that the

mAb localized in the breast tumor region only, sparing any other vital organs. The results were also confirmed with confocal imaging showing prominent staining in T47D and ZR-75-1 derived tumors but relatively weaker staining in MCF-7 derived tumors. Anti-MUC1 mAb recognized and bound to the extracellular region of MUC1 in breast cancer cells with tumor-specific localization. However, further work is still required to enhance its potency as it was effective in anti-proliferative assays against only in T47D breast cancer cells compared to three other MUC1<sup>+</sup> cancer cell lines (ZR-75-1, MCF-7 and MDA-MB-231) tested.

In another work, Kufe et. al. developed and investigated a mAb (3D1) against the  $\alpha 3$  helix region of the ECD of MUC1-C subunit.<sup>71</sup> Hybridomas were generated from mice immunized with MUC1-C/ECD protein and clone 3D1 was selected based on its high reactivity with  $K_D$  of 17nM against MUC1-N p62/MUC1-C ECD p58 heterodimer. A stable heterodimer formation establishes when the 62-aa fragment of MUC1-N consisting the amino acid sequence of LGL (p62-LGL) binds with the amino acid sequence of LTL in the 58-aa MUC1-C ECD region. Point mutations in p62-LGL to AGA and MUC1-C ECD LTL to ATA abrogated the heterodimer formation, depicting the significance of LXL motifs. When the MUC1-N p62/ MUC1-C heterodimer was disrupted, the binding of mAb 3D1 was not affected. This indicated that 3D1 is not reactive to MUC1-N/MUC1-C junction. Another interesting observation was that mAb 3D1 displayed no detectable affinity to the MUC1-N p62 region confirming that the mAb recognizes and binds only to an epitope in the MUC1-C ECD region (**Fig. 6**).

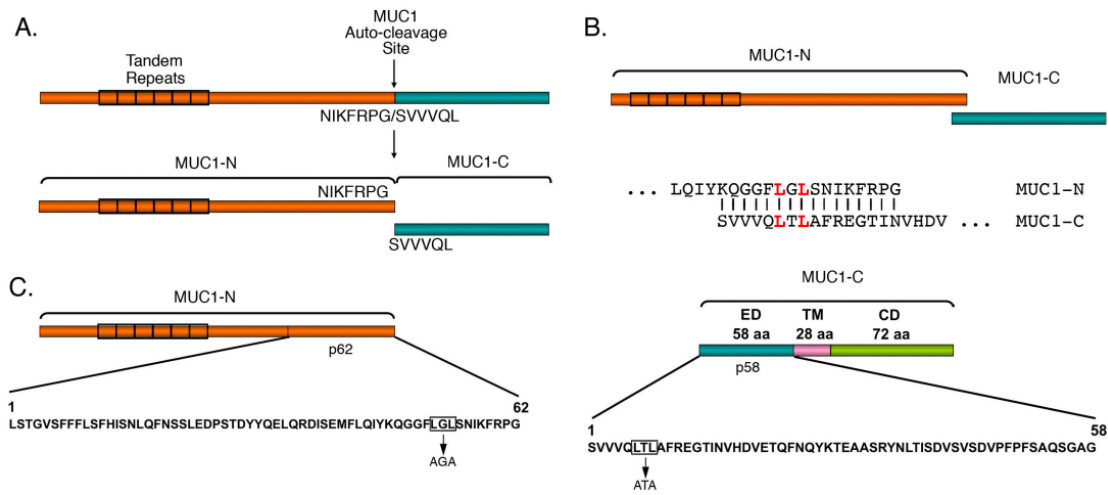


**Figure 6. Heterodimer (p62/p58) formation and leucine residue mutation leading to attenuation of heterodimer formation.** (A) Auto-cleavage site (G<sup>^</sup>SVVV) forming MUC1-N and MUC1-C subunit. (B) Alignment of MUC1-N and MUC1-C subunit at the junction (C) Sequence of p62 MUC1-N protein (left panel; LGL → AGA ) and p58 MUC1-C protein (right panel; LTL → ATA) highlighting the site of leucine residue mutation leading to attenuation of cleavage. This figure is reproduced with permission from the publisher.<sup>71</sup>

The  $\alpha$ 3 helix region (VHDVETQFNQ) residing in MUC1-C ECD is largely conserved in humans, cynomolgus monkeys and mice, which when mutated at D19 residue to glutamic acid led to decrease in binding of mAb 3D1.<sup>71</sup> The numbering system is based on the amino acid sequence in the p58 region (N-1-58-C). This binding was further abrogated when site-directed mutagenesis occurred in other conserved residues (V20 and T22), clearly demonstrating that mAb 3D1 binds to the  $\alpha$ 3 helix (**Fig. 7**).<sup>16</sup>



knockdown expression of MUC1 in MDA-MB-468 triple negative breast cancer cells. Additionally, the surface binding of mAb 3D1 to various types of cancer cells was depicted by its specific binding to H441 non-small cell lung cancer (NSCLC) lines, primary NSCLC cells from resected tumors, ZR-75-1 luminal breast cancer cells and formalin-fixed, paraffin-embedded (FFPE) sections of tumors expressing MUC1-C but not the normal epithelial cells.

### **E) Antibody-drug conjugates targeting MUC1-C**

Antibody drug conjugates or ADCs are a class of targeted immunotherapy in which a therapeutic mAb delivers chemotherapeutic drugs to the tumor cells sparing the healthy cells. These immunoconjugates are not only highly selective but also stable and potent.<sup>72</sup> The 3D1 mAb further proved to be advantageous when it successfully delivered monomethyl auristatin E (MMAE) when conjugated using a cleavable maleimido caproyl-valine-citrulline linker. 3D1-MMAE ADC was internalized at 37 °C in HCT116/MUC1 cells with half-maximal lethal concentration (LC<sub>50</sub>) of 3.8 nM whereas it was ineffective in killing HCT116/null cells.<sup>71</sup> To assess the toxicity of this ADC, human MUC1-transgenic (MUC1-Tg) mice were administered with 15 mg/kg i.v of mAb 3D1-MMAE conjugate, based on the pharmacokinetic studies of mAb 3D1 performed in C57BL/6 mice. Compared to wild type mice, human MUC1-Tg mice are a suitable model to test the toxicity of mAb 3D1-MMAE ADC as it expresses MUC1 in similar patterns and levels as those found in humans. The findings depicted no evident weight loss in the mice or any histopathologic damage to diverse types of normal tissues expressing MUC1 like lung, colon and kidney. Effective inhibition was observed when mAb 3D1-MMAE ADCs were administered in nude mice with HCC827 NSCLC xenografts along with no overt toxicities. To assess the clinical development potential, mAb 3D1-MMAE ADC was humanized by

complementarity determining region (CDR) grafting and it also exhibited significant antitumor activity in MUC1-Tg mice against mouse MC-38/MUC1 colon cancer with no associated adverse effects on MUC1-C expressing healthy tissues.

## **Conclusions and Future Outlook**

In summary, the MUC1-C domain has displayed its crucial role in many critical cellular functions making it an oncogenic protein. The identification of seven potent CTL epitopes derived from the MUC1-C domain opens another platform to employ these CTL antigens in various immunotherapies like recombinant-based vector vaccines. With further investigations, scientists were able to identify the 45 amino acid fragment (MUC1\*) in the MUC1-C as the predominant form of MUC1 protein on the surface of cancer cells and tissues that was able to mimic the oncogenic functions of full-length MUC1. In addition, MUC1\* proved to be diagnostically more effective in staining the most diseased portions of certain MUC1 expressing cancers, which were not effectively stained by full-length MUC1. The research findings highlighted the importance of understanding of the interactions between the MUC1\* protein with its ligand in the development of the peptide-based inhibitors like GO-201, which directly targets MUC1\* oligomerization and ultimately induced apoptosis of human breast cancer cells. The generation of novel antibody; SKM1-02 using phage display; anti-MUC1 and antibody drug conjugate; 3D1-MMAE, have provide promising leads targeting the extracellular domain of MUC1-C protein with high selectivity and potency.

These research findings toward understanding oncogenic role of MUC1-C protein were critical in using it as an immunotherapeutic target. On the other hand, much more studies are still required to deeply understand its mechanistic role. Strategic developments in a preclinical

setting that aim at defining the functions of this membrane-bound glycoprotein is of utmost importance.

## REFERENCES

- (1) Devine, P. L.; McKenzie, I. F. Mucins: structure, function, and associations with malignancy. *Bioessays* **1992**, *14* (9), 619-625. DOI: 10.1002/bies.950140909.
- (2) Rachagani, S.; Torres, M. P.; Moniaux, N.; Batra, S. K. Current status of mucins in the diagnosis and therapy of cancer. *Biofactors* **2009**, *35* (6), 509-527. DOI: 10.1002/biof.64.
- (3) Gendler, S. J.; Burchell, J. M.; Duhig, T.; Lamport, D.; White, R.; Parker, M.; Taylor-Papadimitriou, J. Cloning of partial cDNA encoding differentiation and tumor-associated mucin glycoproteins expressed by human mammary epithelium. *Proc Natl Acad Sci U S A* **1987**, *84* (17), 6060-6064. DOI: 10.1073/pnas.84.17.6060.
- (4) Lan, M. S.; Batra, S. K.; Qi, W. N.; Metzgar, R. S.; Hollingsworth, M. A. Cloning and sequencing of a human pancreatic tumor mucin cDNA. *J Biol Chem* **1990**, *265* (25), 15294-15299.
- (5) Ligtenberg, M. J.; Vos, H. L.; Gennissen, A. M.; Hilkens, J. Episialin, a carcinoma-associated mucin, is generated by a polymorphic gene encoding splice variants with alternative amino termini. *J Biol Chem* **1990**, *265* (10), 5573-5578.
- (6) Siddiqui, J.; Abe, M.; Hayes, D.; Shani, E.; Yunis, E.; Kufe, D. Isolation and sequencing of a cDNA coding for the human DF3 breast carcinoma-associated antigen. *Proc Natl Acad Sci U S A* **1988**, *85* (7), 2320-2323. DOI: 10.1073/pnas.85.7.2320.
- (7) Kufe, D.; Inghirami, G.; Abe, M.; Hayes, D.; Justi-Wheeler, H.; Schlom, J. Differential reactivity of a novel monoclonal antibody (DF3) with human malignant versus benign breast tumors. *Hybridoma* **1984**, *3* (3), 223-232. DOI: 10.1089/hyb.1984.3.223.
- (8) Brockhausen, I.; Yang, J. M.; Burchell, J.; Whitehouse, C.; Taylor-Papadimitriou, J. Mechanisms underlying aberrant glycosylation of MUC1 mucin in breast cancer cells. *Eur J Biochem* **1995**, *233* (2), 607-617. DOI: 10.1111/j.1432-1033.1995.607\_2.x.
- (9) Drubin, D. G.; Nelson, W. J. Origins of cell polarity. *Cell* **1996**, *84* (3), 335-344. DOI: 10.1016/s0092-8674(00)81278-7.
- (10) McCaffrey, L. M.; Macara, I. G. Epithelial organization, cell polarity and tumorigenesis. *Trends Cell Biol* **2011**, *21* (12), 727-735. DOI: 10.1016/j.tcb.2011.06.005.
- (11) Cheever, M. A.; Allison, J. P.; Ferris, A. S.; Finn, O. J.; Hastings, B. M.; Hecht, T. T.; Mellman, I.; Prindiville, S. A.; Viner, J. L.; Weiner, L. M.; et al. The prioritization of cancer antigens: a national cancer institute pilot project for the acceleration of translational research. *Clin Cancer Res* **2009**, *15* (17), 5323-5337. DOI: 10.1158/1078-0432.CCR-09-0737.
- (12) Brockhausen, I.; Melamed, J. Mucins as anti-cancer targets: perspectives of the glycobiologist. *Glycoconj J* **2021**, *38* (4), 459-474. DOI: 10.1007/s10719-021-09986-8.
- (13) Nath, S.; Mukherjee, P. MUC1: a multifaceted oncoprotein with a key role in cancer progression. *Trends Mol Med* **2014**, *20* (6), 332-342. DOI: 10.1016/j.molmed.2014.02.007.

- (14) Parry, S.; Silverman, H. S.; McDermott, K.; Willis, A.; Hollingsworth, M. A.; Harris, A. Identification of MUC1 proteolytic cleavage sites in vivo. *Biochem Biophys Res Commun* **2001**, *283* (3), 715-720. DOI: 10.1006/bbrc.2001.4775.
- (15) Levitin, F.; Stern, O.; Weiss, M.; Gil-Henn, C.; Ziv, R.; Prokocimer, Z.; Smorodinsky, N. I.; Rubinstein, D. B.; Wreschner, D. H. The MUC1 SEA module is a self-cleaving domain. *J Biol Chem* **2005**, *280* (39), 33374-33386. DOI: 10.1074/jbc.M506047200.
- (16) Macao, B.; Johansson, D. G.; Hansson, G. C.; Härd, T. Autoproteolysis coupled to protein folding in the SEA domain of the membrane-bound MUC1 mucin. *Nat Struct Mol Biol* **2006**, *13* (1), 71-76. DOI: 10.1038/nsmb1035.
- (17) Tsakadze, N. L.; Sithu, S. D.; Sen, U.; English, W. R.; Murphy, G.; D'Souza, S. E. Tumor necrosis factor-alpha-converting enzyme (TACE/ADAM-17) mediates the ectodomain cleavage of intercellular adhesion molecule-1 (ICAM-1). *J Biol Chem* **2006**, *281* (6), 3157-3164. DOI: 10.1074/jbc.M510797200.
- (18) Thathiah, A.; Carson, D. D. MT1-MMP mediates MUC1 shedding independent of TACE/ADAM17. *Biochem J* **2004**, *382* (Pt 1), 363-373. DOI: 10.1042/BJ20040513.
- (19) Ligtenberg, M. J.; Kruijshaar, L.; Buijs, F.; van Meijer, M.; Litvinov, S. V.; Hilkens, J. Cell-associated episialin is a complex containing two proteins derived from a common precursor. *J Biol Chem* **1992**, *267* (9), 6171-6177.
- (20) Julian, J.; Carson, D. D. Formation of MUC1 metabolic complex is conserved in tumor-derived and normal epithelial cells. *Biochem Biophys Res Commun* **2002**, *293* (4), 1183-1190. DOI: 10.1016/S0006-291X(02)00352-2.
- (21) Johansson, D. G.; Wallin, G.; Sandberg, A.; Macao, B.; Aqvist, J.; Härd, T. Protein autoproteolysis: conformational strain linked to the rate of peptide cleavage by the pH dependence of the N → O acyl shift reaction. *J Am Chem Soc* **2009**, *131* (27), 9475-9477. DOI: 10.1021/ja9010817.
- (22) Zhang, S.; Graeber, L. A.; Helling, F.; Ragupathi, G.; Adluri, S.; Lloyd, K. O.; Livingston, P. O. Augmenting the immunogenicity of synthetic MUC1 peptide vaccines in mice. *Cancer Res* **1996**, *56* (14), 3315-3319.
- (23) Xing, P.; Michael, M.; Apostolopoulos, V.; Prenzoska, J.; Marshall, C.; Bishop, J.; McKenzie, I. Phase-I study of synthetic muc1 peptides in breast-cancer. *Int J Oncol* **1995**, *6* (6), 1283-1289. DOI: 10.3892/ijco.6.6.1283.
- (24) Schettini, J.; Kidiyoor, A.; Besmer, D. M.; Tinder, T. L.; Roy, L. D.; Lustgarten, J.; Gendler, S. J.; Mukherjee, P. Intratumoral delivery of CpG-conjugated anti-MUC1 antibody enhances NK cell anti-tumor activity. *Cancer Immunol Immunother* **2012**, *61* (11), 2055-2065. DOI: 10.1007/s00262-012-1264-y.
- (25) Oei, A. L.; Moreno, M.; Verheijen, R. H.; Sweep, F. C.; Thomas, C. M.; Massuger, L. F.; von Mensdorff-Pouilly, S. Induction of IgG antibodies to MUC1 and survival in patients with epithelial ovarian cancer. *Int J Cancer* **2008**, *123* (8), 1848-1853. DOI: 10.1002/ijc.23725.

- (26) Apostolopoulos, V.; Pietersz, G. A.; Tsibanis, A.; Tsikkinis, A.; Drakaki, H.; Loveland, B. E.; Piddlesden, S. J.; Plebanski, M.; Pouniotis, D. S.; Alexis, M. N.; et al. Pilot phase III immunotherapy study in early-stage breast cancer patients using oxidized mannan-MUC1 [ISRCTN71711835]. *Breast Cancer Res* **2006**, *8* (3), R27. DOI: 10.1186/bcr1505.
- (27) Kamata, M.; Denda-Nagai, K.; Kubota, N.; Aida, S.; Takeda, K.; Irimura, T. Vaccination of mice with MUC1 cDNA suppresses the development of lung metastases. *Clin Exp Metastasis* **2002**, *19* (8), 689-696. DOI: 10.1023/a:1021332932531.
- (28) Hisatsune, A.; Kawasaki, M.; Nakayama, H.; Mikami, Y.; Miyata, T.; Isohama, Y.; Katsuki, H.; Kim, K. C. Internalization of MUC1 by anti-MUC1 antibody from cell membrane through the macropinocytotic pathway. *Biochem Biophys Res Commun* **2009**, *388* (4), 677-682. DOI: 10.1016/j.bbrc.2009.08.059.
- (29) Hisatsune, A.; Nakayama, H.; Kawasaki, M.; Horie, I.; Miyata, T.; Isohama, Y.; Kim, K. C.; Katsuki, H. Anti-MUC1 antibody inhibits EGF receptor signaling in cancer cells. *Biochem Biophys Res Commun* **2011**, *405* (3), 377-381. DOI: 10.1016/j.bbrc.2011.01.029.
- (30) Teramoto, K.; Ozaki, Y.; Hanaoka, J.; Sawai, S.; Tezuka, N.; Fujino, S.; Daigo, Y.; Kontani, K. Predictive biomarkers and effectiveness of MUC1-targeted dendritic-cell-based vaccine in patients with refractory non-small cell lung cancer. *Ther Adv Med Oncol* **2017**, *9* (3), 147-157. DOI: 10.1177/1758834016678375.
- (31) Kovjazin, R.; Volovitz, I.; Kundel, Y.; Rosenbaum, E.; Medalia, G.; Horn, G.; Smorodinsky, N. I.; Brenner, B.; Carmon, L. ImMucin: a novel therapeutic vaccine with promiscuous MHC binding for the treatment of MUC1-expressing tumors. *Vaccine* **2011**, *29* (29-30), 4676-4686. DOI: 10.1016/j.vaccine.2011.04.103.
- (32) Carmon, L.; Avivi, I.; Kovjazin, R.; Zuckerman, T.; Dray, L.; Gatt, M. E.; Or, R.; Shapira, M. Y. Phase I/II study exploring ImMucin, a pan-major histocompatibility complex, anti-MUC1 signal peptide vaccine, in multiple myeloma patients. *Br J Haematol* **2015**, *169* (1), 44-56. DOI: 10.1111/bjh.13245.
- (33) Hayes, D. F.; Sekine, H.; Ohno, T.; Abe, M.; Keefe, K.; Kufe, D. W. Use of a murine monoclonal antibody for detection of circulating plasma DF3 antigen levels in breast cancer patients. *J Clin Invest* **1985**, *75* (5), 1671-1678. DOI: 10.1172/JCI111875.
- (34) Abe, M.; Kufe, D. Structural analysis of the DF3 human breast carcinoma-associated protein. *Cancer Res* **1989**, *49* (11), 2834-2839.
- (35) de Bono, J. S.; Rha, S. Y.; Stephenson, J.; Schultes, B. C.; Monroe, P.; Eckhardt, G. S.; Hammond, L. A.; Whiteside, T. L.; Nicodemus, C. F.; Cermak, J. M.; et al. Phase I trial of a murine antibody to MUC1 in patients with metastatic cancer: evidence for the activation of humoral and cellular antitumor immunity. *Ann Oncol* **2004**, *15* (12), 1825-1833. DOI: 10.1093/annonc/mdh472.
- (36) Moreno, M.; Bontkes, H. J.; Scheper, R. J.; Kenemans, P.; Verheijen, R. H.; von Mensdorff-Pouilly, S. High level of MUC1 in serum of ovarian and breast cancer patients inhibits huHMFG-1 dependent cell-mediated cytotoxicity (ADCC). *Cancer Lett* **2007**, *257* (1), 47-55. DOI: 10.1016/j.canlet.2007.06.016.

- (37) Pegram, M. D.; Borges, V. F.; Ibrahim, N.; Fuloria, J.; Shapiro, C.; Perez, S.; Wang, K.; Schaedli Stark, F.; Courtenay Luck, N. Phase I dose escalation pharmacokinetic assessment of intravenous humanized anti-MUC1 antibody AS1402 in patients with advanced breast cancer. *Breast Cancer Res* **2009**, *11* (5), R73. DOI: 10.1186/bcr2409.
- (38) Ibrahim, N. K.; Yariz, K. O.; Bondarenko, I.; Manikhas, A.; Semiglazov, V.; Alyasova, A.; Komisarenko, V.; Shparyk, Y.; Murray, J. L.; Jones, D.; et al. Randomized phase II trial of letrozole plus anti-MUC1 antibody AS1402 in hormone receptor-positive locally advanced or metastatic breast cancer. *Clin Cancer Res* **2011**, *17* (21), 6822-6830. DOI: 10.1158/1078-0432.CCR-11-1151.
- (39) Taylor-Papadimitriou, J.; Burchell, J. M.; Graham, R.; Beatson, R. Latest developments in MUC1 immunotherapy. *Biochem Soc Trans* **2018**, *46* (3), 659-668. DOI: 10.1042/BST20170400.
- (40) Ramasamy, S.; Duraisamy, S.; Barbashov, S.; Kawano, T.; Kharbanda, S.; Kufe, D. The MUC1 and galectin-3 oncoproteins function in a microRNA-dependent regulatory loop. *Mol Cell* **2007**, *27* (6), 992-1004. DOI: 10.1016/j.molcel.2007.07.031.
- (41) Raina, D.; Kosugi, M.; Ahmad, R.; Panchamoorthy, G.; Rajabi, H.; Alam, M.; Shimamura, T.; Shapiro, G. I.; Supko, J.; Kharbanda, S.; et al. Dependence on the MUC1-C oncoprotein in non-small cell lung cancer cells. *Mol Cancer Ther* **2011**, *10* (5), 806-816. DOI: 10.1158/1535-7163.MCT-10-1050.
- (42) Ahmad, R.; Raina, D.; Joshi, M. D.; Kawano, T.; Ren, J.; Kharbanda, S.; Kufe, D. MUC1-C oncoprotein functions as a direct activator of the nuclear factor-kappaB p65 transcription factor. *Cancer Res* **2009**, *69* (17), 7013-7021. DOI: 10.1158/0008-5472.CAN-09-0523.
- (43) Kufe, D. W. MUC1-C oncoprotein as a target in breast cancer: activation of signaling pathways and therapeutic approaches. *Oncogene* **2013**, *32* (9), 1073-1081. DOI: 10.1038/onc.2012.158.
- (44) Ren, J.; Agata, N.; Chen, D.; Li, Y.; Yu, W. H.; Huang, L.; Raina, D.; Chen, W.; Kharbanda, S.; Kufe, D. Human MUC1 carcinoma-associated protein confers resistance to genotoxic anticancer agents. *Cancer Cell* **2004**, *5* (2), 163-175. DOI: 10.1016/s1535-6108(04)00020-0.
- (45) Tsutsumida, H.; Swanson, B. J.; Singh, P. K.; Caffrey, T. C.; Kitajima, S.; Goto, M.; Yonezawa, S.; Hollingsworth, M. A. RNA interference suppression of MUC1 reduces the growth rate and metastatic phenotype of human pancreatic cancer cells. *Clin Cancer Res* **2006**, *12* (10), 2976-2987. DOI: 10.1158/1078-0432.CCR-05-1197.
- (46) Li, Y.; Liu, D.; Chen, D.; Kharbanda, S.; Kufe, D. Human DF3/MUC1 carcinoma-associated protein functions as an oncogene. *Oncogene* **2003**, *22* (38), 6107-6110. DOI: 10.1038/sj.onc.1206732.
- (47) Gendler, S. J. MUC1, the renaissance molecule. *J Mammary Gland Biol Neoplasia* **2001**, *6* (3), 339-353. DOI: 10.1023/a:1011379725811.

- (48) Syrkina, M. S.; Vassetzky, Y. S.; Rubtsov, M. A. MUC1 Story: Great Expectations, Disappointments and the Renaissance. *Curr Med Chem* **2019**, *26* (3), 554-563. DOI: 10.2174/0929867324666170817151954.
- (49) Vlad, A. M.; Kettel, J. C.; Alajez, N. M.; Carlos, C. A.; Finn, O. J. MUC1 immunobiology: from discovery to clinical applications. *Adv Immunol* **2004**, *82*, 249-293. DOI: 10.1016/S0065-2776(04)82006-6.
- (50) Singh, R.; Bandyopadhyay, D. MUC1: a target molecule for cancer therapy. *Cancer Biol Ther* **2007**, *6* (4), 481-486. DOI: 10.4161/cbt.6.4.4201.
- (51) Jochems, C.; Tucker, J. A.; Vergati, M.; Boyerinas, B.; Gulley, J. L.; Schlom, J.; Tsang, K. Y. Identification and characterization of agonist epitopes of the MUC1-C oncoprotein. *Cancer Immunol Immunother* **2014**, *63* (2), 161-174. DOI: 10.1007/s00262-013-1494-7.
- (52) He, Q.; Jiang, X.; Zhou, X.; Weng, J. Targeting cancers through TCR-peptide/MHC interactions. *J Hematol Oncol* **2019**, *12* (1), 139. DOI: 10.1186/s13045-019-0812-8.
- (53) Parker, K. C.; Bednarek, M. A.; Coligan, J. E. Scheme for ranking potential HLA-A2 binding peptides based on independent binding of individual peptide side-chains. *J Immunol* **1994**, *152* (1), 163-175.
- (54) Mahanta, S.; Fessler, S. P.; Park, J.; Bamdad, C. A minimal fragment of MUC1 mediates growth of cancer cells. *PLoS One* **2008**, *3* (4), e2054. DOI: 10.1371/journal.pone.0002054.
- (55) Kim, B.; Lee, K. J. Activation of Nm23-H1 to suppress breast cancer metastasis via redox regulation. *Exp Mol Med* **2021**, *53* (3), 346-357. DOI: 10.1038/s12276-021-00575-1.
- (56) Steeg, P. S.; Bevilacqua, G.; Kopper, L.; Thorgeirsson, U. P.; Talmadge, J. E.; Liotta, L. A.; Sobel, M. E. Evidence for a novel gene associated with low tumor metastatic potential. *J Natl Cancer Inst* **1988**, *80* (3), 200-204. DOI: 10.1093/jnci/80.3.200.
- (57) Leary, J. A.; Kerr, J.; Chenevix-Trench, G.; Doris, C. P.; Hurst, T.; Houghton, C. R.; Friedlander, M. L. Increased expression of the NME1 gene is associated with metastasis in epithelial ovarian cancer. *Int J Cancer* **1995**, *64* (3), 189-195. DOI: 10.1002/ijc.2910640308.
- (58) Shigeta, K.; Hasegawa, M.; Kikuchi, E.; Yasumizu, Y.; Kosaka, T.; Mizuno, R.; Mikami, S.; Miyajima, A.; Kufe, D.; Oya, M. Role of the MUC1-C oncoprotein in the acquisition of cisplatin resistance by urothelial carcinoma. *Cancer Sci* **2020**, *111* (10), 3639-3652. DOI: 10.1111/cas.14574.
- (59) Kufe, D. Dependence on MUC1-C in Progression of Neuroendocrine Prostate Cancer. *Int J Mol Sci* **2023**, *24* (4). DOI: 10.3390/ijms24043719.
- (60) Raina, D.; Ahmad, R.; Joshi, M. D.; Yin, L.; Wu, Z.; Kawano, T.; Vasir, B.; Avigan, D.; Kharbanda, S.; Kufe, D. Direct targeting of the mucin 1 oncoprotein blocks survival and tumorigenicity of human breast carcinoma cells. *Cancer Res* **2009**, *69* (12), 5133-5141. DOI: 10.1158/0008-5472.CAN-09-0854.

- (61) Leng, Y.; Cao, C.; Ren, J.; Huang, L.; Chen, D.; Ito, M.; Kufe, D. Nuclear import of the MUC1-C oncoprotein is mediated by nucleoporin Nup62. *J Biol Chem* **2007**, *282* (27), 19321-19330. DOI: 10.1074/jbc.M703222200.
- (62) Yin, L.; Li, Y.; Ren, J.; Kuwahara, H.; Kufe, D. Human MUC1 carcinoma antigen regulates intracellular oxidant levels and the apoptotic response to oxidative stress. *J Biol Chem* **2003**, *278* (37), 35458-35464. DOI: 10.1074/jbc.M301987200.
- (63) Yin, L.; Huang, L.; Kufe, D. MUC1 oncoprotein activates the FOXO3a transcription factor in a survival response to oxidative stress. *J Biol Chem* **2004**, *279* (44), 45721-45727. DOI: 10.1074/jbc.M408027200.
- (64) Yin, L.; Kharbanda, S.; Kufe, D. Mucin 1 oncoprotein blocks hypoxia-inducible factor 1alpha activation in a survival response to hypoxia. *J Biol Chem* **2007**, *282* (1), 257-266. DOI: 10.1074/jbc.M610156200.
- (65) Lavin, M. F.; Delia, D.; Chessa, L. ATM and the DNA damage response. Workshop on ataxia-telangiectasia and related syndromes. *EMBO Rep* **2006**, *7* (2), 154-160. DOI: 10.1038/sj.embor.7400629.
- (66) Kim, M. J.; Choi, J. R.; Tae, N.; Wi, T. M.; Kim, K. M.; Kim, D. H.; Lee, E. S. Novel Antibodies Targeting MUC1-C Showed Anti-Metastasis and Growth-Inhibitory Effects on Human Breast Cancer Cells. *Int J Mol Sci* **2020**, *21* (9). DOI: 10.3390/ijms21093258.
- (67) Bazan, J.; Calkosiński, I.; Gamian, A. Phage display--a powerful technique for immunotherapy: 1. Introduction and potential of therapeutic applications. *Hum Vaccin Immunother* **2012**, *8* (12), 1817-1828. DOI: 10.4161/hv.21703.
- (68) Dass, S. A.; Tan, K. L.; Selva Rajan, R.; Mokhtar, N. F.; Mohd Adzmi, E. R.; Wan Abdul Rahman, W. F.; Tengku Din, T. A. D. A.; Balakrishnan, V. Triple Negative Breast Cancer: A Review of Present and Future Diagnostic Modalities. *Medicina (Kaunas)* **2021**, *57* (1). DOI: 10.3390/medicina57010062.
- (69) Rajabi, H.; Ahmad, R.; Jin, C.; Kosugi, M.; Alam, M.; Joshi, M. D.; Kufe, D. MUC1-C oncoprotein induces TCF7L2 transcription factor activation and promotes cyclin D1 expression in human breast cancer cells. *J Biol Chem* **2012**, *287* (13), 10703-10713. DOI: 10.1074/jbc.M111.323311.
- (70) Wu, G.; Kim, D.; Kim, J. N.; Park, S.; Maharjan, S.; Koh, H.; Moon, K.; Lee, Y.; Kwon, H. J. A Mucin1 C-terminal Subunit-directed Monoclonal Antibody Targets Overexpressed Mucin1 in Breast Cancer. *Theranostics* **2018**, *8* (1), 78-91. DOI: 10.7150/thno.21278.
- (71) Panchamoorthy, G.; Jin, C.; Raina, D.; Bharti, A.; Yamamoto, M.; Adeebge, D.; Zhao, Q.; Bronson, R.; Jiang, S.; Li, L.; et al. Targeting the human MUC1-C oncoprotein with an antibody-drug conjugate. *JCI Insight* **2018**, *3* (12). DOI: 10.1172/jci.insight.99880.
- (72) Beck, A.; Goetsch, L.; Dumontet, C.; Corvaia, N. Strategies and challenges for the next generation of antibody-drug conjugates. *Nat Rev Drug Discov* **2017**, *16* (5), 315-337. DOI: 10.1038/nrd.2016.268.

## Chapter 2 Effective Tumor Protection by Q $\beta$ -<sup>t</sup>MUC1 Vaccine in a Spontaneous Tumor Model Resembling Human Triple Negative Breast Cancer

### 2.1 Introduction

Cancer immunotherapy has become an important strategy to treat cancer complementing the traditional methods of surgery, radiation and chemotherapy.<sup>1,2</sup> Anti-cancer vaccine is an exciting direction for immunotherapy, which can potentially provide long lasting protection against cancer.<sup>3-5</sup> Mucin-1 (MUC1), a high molecular weight membrane-bound glycoprotein, is an attractive target for anti-cancer vaccine development. MUC1 is found on the apical borders of luminal or glandular epithelial cellular surface of many tissues.<sup>6,7</sup> In normal cells, it provides a physical barrier to pathogens and also acts as a lubricant. In contrast, on a wide range of cancer cells, the level of MUC1 expression can be more than 100-fold higher than that on normal cells. Furthermore, MUC1 on tumor cells often contain shortened *O*-linked glycans, which expose the protein backbone for immune recognition.<sup>8</sup> These unique glycoprotein structures distinguish tumor associated MUC1 (<sup>t</sup>MUC1) from those on normal cells.<sup>9</sup> With such contrasting structural and biochemical properties in normal *vs* cancer cells, <sup>t</sup>MUC1 has been rated as a top tumor associated antigen by the National Cancer Institute.<sup>10</sup>

The selection of MUC1 glycoprotein/glycopeptide antigen structures utilized for vaccine design is a critical step. A prominent structural feature of MUC1 is the 20-125 variable number tandem repeats (VNTR) with 20 amino acids in length (PDTRPAPGSTAPPAHGVTSA), each of which contains five potential sites of *O*-linked glycosylation on Ser and Thr residues.<sup>11</sup> There have been many innovative MUC1 based vaccine studies, using a variety of antigenic MUC1 structures.<sup>12-14</sup> It has been shown that focusing the immunogen design on a short glycopeptide SAPDT\*RPAP (\* denotes *O*-linked glycan) led to significantly enhanced vaccine efficacy. Prophylactic vaccination with the

conjugate of the <sup>1</sup>MUC1 glycopeptide with an immunogenic bacteriophage Q $\beta$  carrier reduced the tumor burden in a tumor metastasis and a xenograft model in mice.<sup>15</sup>

While the xenograft tumor model is relatively straightforward to establish, it is unable to represent well the genetic and histological complexity of human tumors.<sup>16</sup> To better mimic the immunosuppressive environment and heterogeneity of human breast cancer, spontaneous tumor models are attractive. Herein, a spontaneous mouse breast cancer model (MUC1/MMTV) was developed by crossing mouse mammary tumor virus (MMTV)-polyoma middle T (PyMT) mice with human MUC1 transgenic (MUC1.Tg) mice.<sup>17</sup> To evaluate the translational potential of the Q $\beta$  based MUC1 vaccine, MUC1/MMTV mice have been vaccinated with the Q $\beta$ -<sup>1</sup>MUC1 conjugate, which significantly improved mouse survival from breast cancer.

## **2.1 Results and Discussion**

### **2.1.1 Immunization with Q $\beta$ -<sup>1</sup>MUC1 vaccine at different timepoints resulted in similar antibody titers in MUC1/MMTV and MMTV mice**

To facilitate translation, a spontaneous breast cancer model was established based on the mouse mammary tumor virus promoter (MMTV)-polyoma virus middle T (PyMT) mice. These mice express the PyMT antigen under the direction of the MMTV promoter/enhancer, which promotes malignant transformation and leads to the development of multiple palpable mammary tumors in *all* female mice.<sup>17, 18</sup> This is a highly aggressive tumor model, as tumor can appear as early as 4 weeks post-natal in these mice and between the ages of 8-18 weeks, the solid tumors become completely invasive.<sup>19</sup>

Mouse mucins have very different sequences compared to human MUC1. As a result, unlike in humans, MUC1 is foreign in mice and immunogenic. To mimic the immunotolerance to MUC1, the MMTV mice were crossed with human MUC1 transgenic mice. The female offspring of the resulting mice double transgenic in MUC1 and PyMT (referred to as

MUC1/MMTV) all spontaneously develop palpable breast cancer at 5-7 primary sites resembling human triple negative breast cancer (TNBC) in 8-10 weeks, which progress very rapidly and share morphological similarities with human mammary carcinoma. Compared to xenograft models of mouse breast cancer, the MUC1/MMTV mouse can mimic more closely the human breast cancer clinical conditions with a native tumor microenvironment and immune tolerance to MUC1. Furthermore, these mice are immuno-competent, thus providing an appealing platform for evaluation of anti-MUC1 vaccines.

To determine the vaccine efficacy against the more clinically relevant spontaneous breast cancer, the Q $\beta$ -<sup>t</sup>MUC1 glycopeptide SAPDT\*RPAP (\* denotes *N*-acetyl galactosamine GalNAc) conjugate was prepared. Cohorts of 1-month old MUC1/MMTV and MMTV mice were immunized subcutaneously with one prime and four weekly boosters of Q $\beta$ -<sup>t</sup>MUC1 at 4 nmol <sup>t</sup>MUC1 per dose. Monophosphoryl lipid A (MPLA) was used as the adjuvant (**Fig. 8a**). The control groups of mice (MUC1/MMTV and MMTV) received Q $\beta$  + MPLA (Q $\beta$ ) or phosphate buffered saline (PBS) + MPLA (PBS) following an identical schedule.

a.

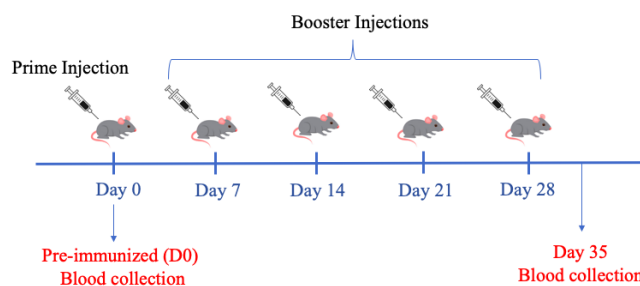
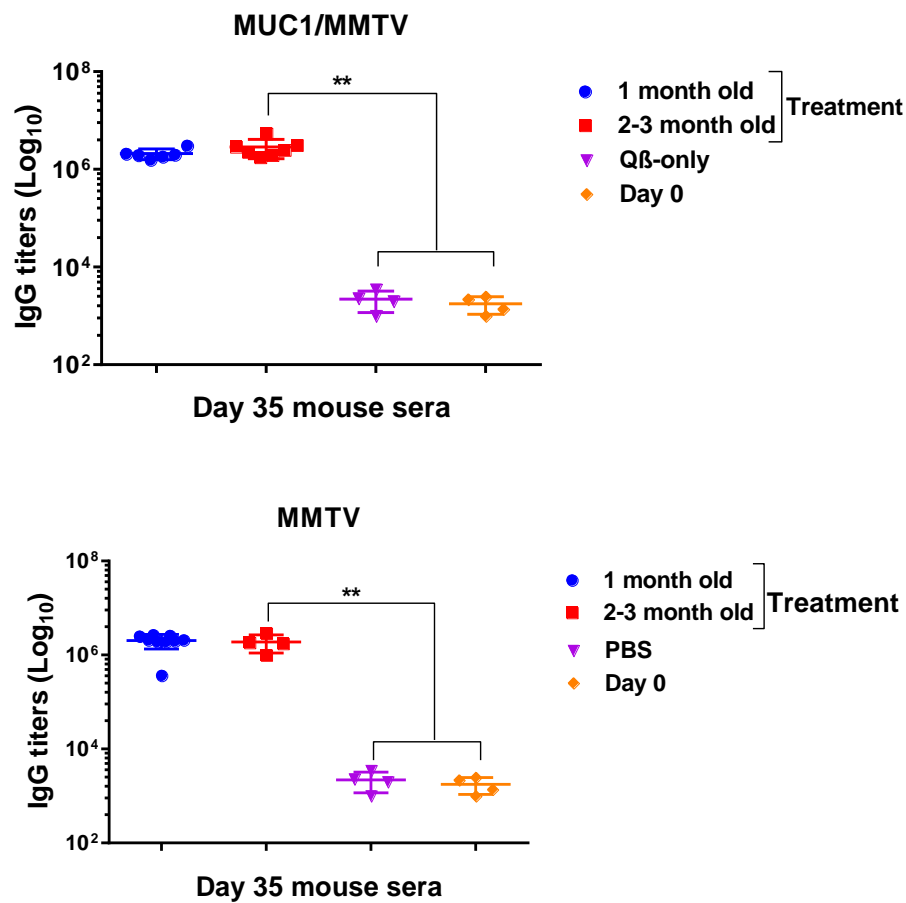


**Figure 8. Immunization protocol and assessment of anti-<sup>t</sup>MUC1 antibody in MUC1/MMTV and MMTV mice for two different age when mice were immunized (1-month and 2-3-month old).** a) Schematic representation of the immunization protocol for mice vaccinated with Q $\beta$ -<sup>t</sup>MUC1. Mice were vaccinated on days 0, 7, 14, 21 and 28 with 4 nmol <sup>t</sup>MUC1 per dose using MPLA adjuvant. Mice in the control groups were vaccinated with the protein carrier Q $\beta$ -only or PBS using the same protocol. Blood was collected on days 0, 6, 20, and 35 to generate sera for analyses. b) Anti-<sup>t</sup>MUC1 IgG titers of MUC1/MMTV and MMTV mice in treatment groups (1-month and 2-3-month old) on day 35 post-immunization. Statistical significance was determined by two-tailed unpaired Student's *t*-test using GraphPad Prism, \*\**p* < 0.01, \*\*\**p* < 0.001. Each symbol represents one mouse (*n* = 3–6 mice for each group).

Figure 8 (cont'd)

b.

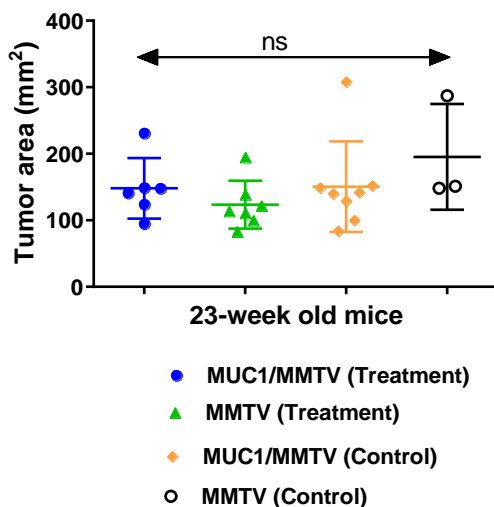


On day 35 after the initial injection, blood was collected from mice to harvest serum followed by enzyme linked immunosorbent assay (ELISA) analysis of the IgG antibody titers using BSA conjugate of the <sup>t</sup>MUC1 glycopeptide as the coating antigen to avoid the interference of anti-Qβ antibodies. As shown in **Fig. 8b**, Qβ-<sup>t</sup>MUC1 vaccine elicited a robust anti-<sup>t</sup>MUC1 IgG response in both MUC1/MMTV and MMTV mice. For MUC1/MMTV mice, the average IgG titers were 2.2 × 10<sup>6</sup> (1-month) and 2.9 × 10<sup>6</sup> (2-3-month) ELISA units respectively. For MMTV mice, the average IgG titers were similar at 2.0 × 10<sup>6</sup> (1-month) and 1.9 × 10<sup>6</sup> (2-3-month) ELISA units. The antibody responses in both MUC1/MMTV and MMTV mice were about three orders of magnitude greater for the treatment group of mice when compared with the post-immune sera from the groups of mice receiving the mock control of Qβ-only or PBS.

### 2.1.2 Immunization of MUC1/MMTV and MMTV mice at 1-month of age did not provide significant protection against tumor development

Following 4 weekly immunizations, mice were monitored for tumor growth twice a week. Mice in the treatment and the control group with MUC1/MMTV genotype started developing palpable mammary gland tumors at about the same time, approx. 16 weeks of age and similar outcome was observed for MMTV immunized mice. The tumor burden was calculated by averaging the tumor area (length x width) in mm<sup>2</sup> of the three-biggest tumors developed when the mice were 23-week of age (**Fig. 9a**), which was when a mouse in either the treatment or the control study reached the size required for euthanization (biggest tumor area >200 mm<sup>2</sup>). The overall survival of MUC1/MMTV mice in both treatment and control groups was monitored and no significant differences in their survival were observed (**Fig. 9b**).

a.



b.

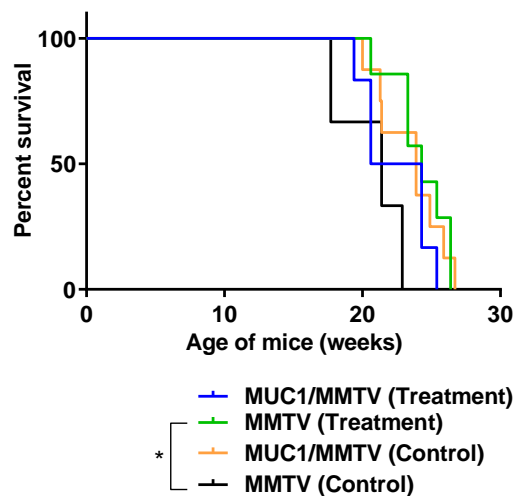


**Figure 9.** a) Tumor burden analysis of MUC1/MMTV and MMTV mice in the treatment group receiving Q $\beta$ -<sup>t</sup>MUC1 at 4 nmol of <sup>t</sup>MUC1 per dose with MPLA as an adjuvant at one month of age. Mice in the control groups were vaccinated with the protein carrier Q $\beta$ -only or PBS. Mice were immunized when they were 1-month of age and analyzed for their tumor burden twice a week. At the age of 23-weeks, tumor burden of each mouse was determined by averaging the area (length x width) of the three biggest tumors and reported in mm<sup>2</sup>. b) The days of survival since birth in both treatment and control groups of MUC1/MMTV and MMTV mice. Health conditions of the tumor bearing mice were observed and mice were euthanized when the biggest

## Figure 9 (cont'd)

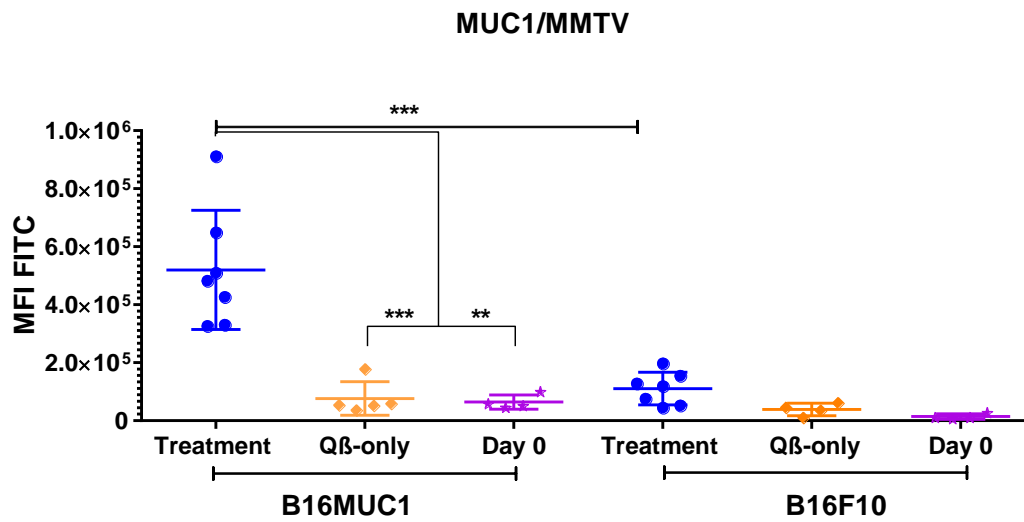
tumor area  $> 200 \text{ mm}^2$  and/or their body conditions significantly deteriorated due to tumor development. Statistical significance was determined by Log-rank Mantel-Cox test using GraphPad Prism, ns  $p > 0.05$ . Each symbol represents one mouse (n = 3–8 mice for each group).

### 2.1.3 Antibodies induced by Q $\beta$ -<sup>t</sup>MUC1 vaccine in MUC1/MMTV and MMTV mice when immunized at 2-3 months of age elicited strong binding to MUC1- expressing tumor cells

We hypothesize that the lack of tumor protection may be due to the immaturity of the immune system of mice when immunization started at one month. Thus, groups of female MUC1/MMTV and MMTV mice were immunized starting at the age of 2-3 months following the same immunization protocol. Following 4 weekly injections of Q $\beta$ -<sup>t</sup>MUC1 at 4 nmol dose of <sup>t</sup>MUC1, sera were collected on day 35 after the initial immunization. ELISA analysis showed that the average anti- <sup>t</sup>MUC1 IgG titers were  $2.9 \times 10^6$  and  $1.9 \times 10^6$  ELISA units for MUC1/MMTV mice and MMTV mice respectively. The anti-<sup>t</sup>MUC1 IgG titers in control mice receiving Q $\beta$  or PBS only were below 2,000 ELISA units.

The abilities of the induced anti-<sup>t</sup>MUC1 antibodies to bind with the native MUC1 protein present on tumor cells were analyzed through flow cytometry. To test the breadth of cancer cell recognition, the post-immune sera from both MUC1/MMTV mice and MMTV mice receiving Q $\beta$ -<sup>t</sup>MUC1 (treatment) were incubated with a variety of MUC1 expressing tumor cells including B16MUC1 melanoma, PANC-O2 pancreatic cancer cells, and ZR-75-1 breast cancer cells. To establish the MUC1 dependence of cell binding, the MUC1 negative B16F10 cells were used as a control. Sera from MUC1/MMTV mice immunized with Q $\beta$ -<sup>t</sup>MUC1 exhibited significantly stronger binding to all MUC1+ tumor cells as compared to sera from MUC1/MMTV mice immunized with Q $\beta$ -only or pre-immune sera (**Fig. 10a**). Importantly, the post-immune sera binding to the B16F10 cells not expressing MUC1 were much weaker, demonstrating the serum selectivity toward <sup>t</sup>MUC1 (**Fig. 10a**).

a.



b.

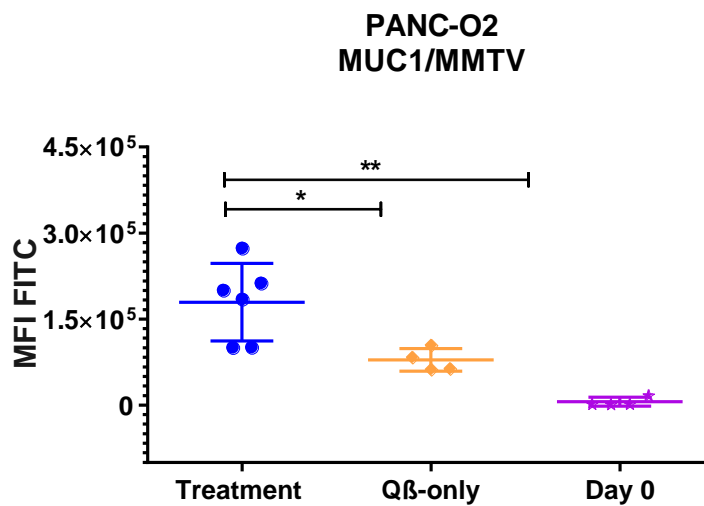
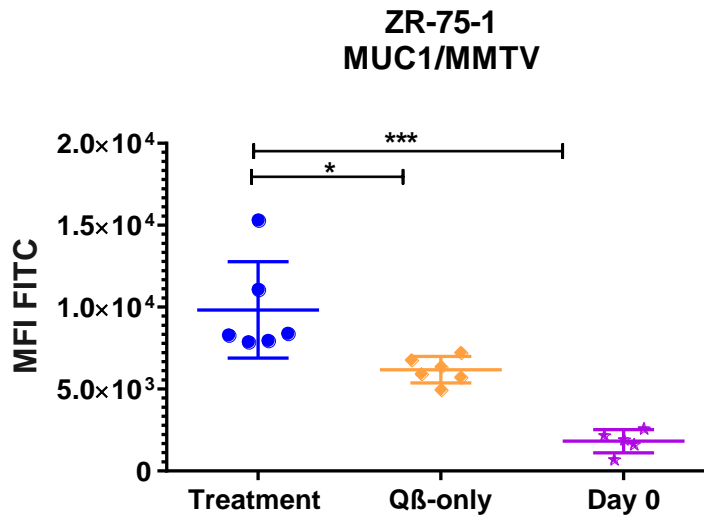


**Figure 10. Results for flow cytometry analysis of cell binding by post-immune sera (day 35) elicited in MUC1/MMTV mice receiving Qβ-<sup>t</sup>MUC1 with 4 nmol <sup>t</sup>MUC1 per dose.** Mice in the control groups were vaccinated with (the protein carrier; Qβ-only or placebo; PBS). Mice were immunized when they were 2-month of age and their mean fluorescence intensities following incubation with tumor cells and detection by fluorescently labelled secondary antibodies are reported. a) B16MUC1 and B16F10 cells. b) PANC-O2 cells. c) ZR-75-1 cells. Statistical significance was determined by two-tailed unpaired Student's t-test using GraphPad Prism, \* $p < 0.05$ , \*\* $p < 0.01$ , \*\*\* $p < 0.001$ . Each symbol represents one mouse ( $n = 5-6$  mice for each group).

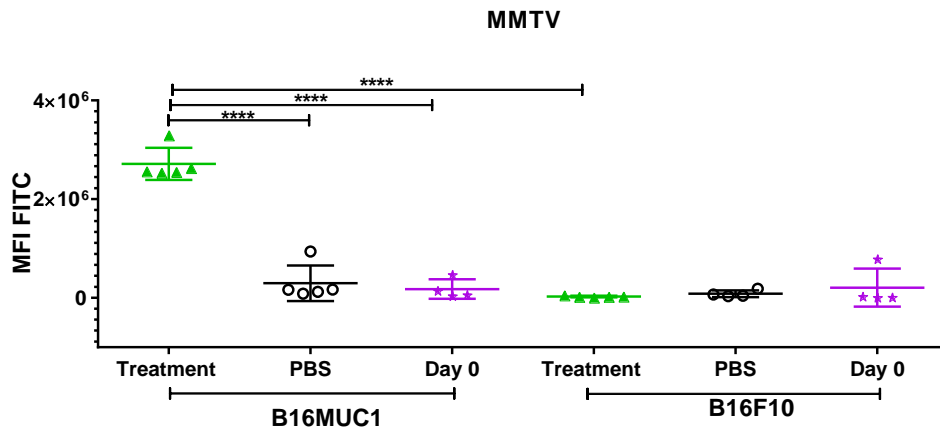
**Figure 10 (cont'd)**

c.

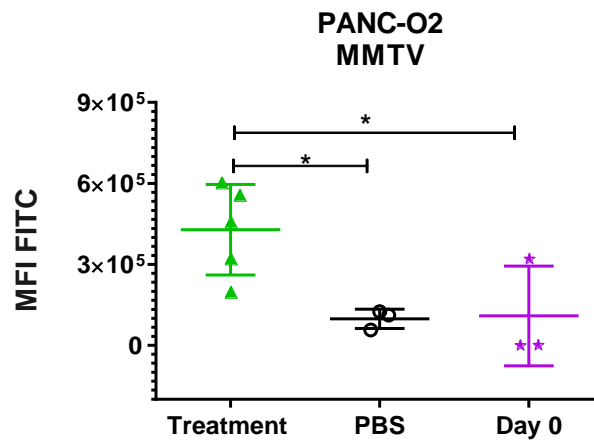


It is interesting to note that the binding of post-immune sera from MMTV mice receiving the Q $\beta$ - $\mu$ MUC1 vaccination was significantly higher to MUC1+ tumor cells (5-fold for B16MUC1 cells, 2-fold for PANC-O2 cells and 3-fold for ZR-75-1 cells) than that by sera from the treatment group with MUC1/MMTV background despite similar IgG titers from both groups (**Fig. 11**). The strong tumor cell binding in MMTV treatment group is likely because the  $\mu$ MUC1 is foreign in MMTV mice whereas it is a self-antigen in MUC1/MMTV mice, leading to limited repertoire of anti- $\mu$ MUC1 antibodies resulting in weaker binding of antibodies produced in MUC1/MMTV mice to MUC1+ tumor cells.

a.



b.



c.

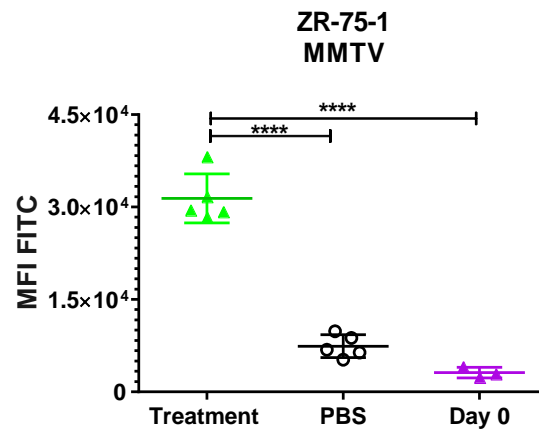


**Figure 11. Results for flow cytometry analysis of cell binding by post-immune sera (day 35) elicited in MMTV mice immunized with Q $\beta$ -MUC1 with 4 nmol <sup>125</sup>I-MUC1 per dose.** Mice in the control groups were vaccinated with (the protein carrier; mQ $\beta$ -only or placebo; PBS). Mice were immunized when they were 2-month of age and their mean fluorescence intensities are reported. a) B16MUC1 and B16F10 cells. b) PANC-O2 cells. c) ZR-75-1 cells. Statistical significance was determined by two-tailed unpaired Student's t-test using GraphPad Prism, \* $p < 0.05$ , \*\*\*\* $p < 0.0001$ . Each symbol represents one mouse ( $n = 5-6$  mice for each group).

### 2.1.4 Immunizing MUC1/MMTV and MMTV mice with Q $\beta$ -<sup>t</sup>MUC1 at a higher dosage of <sup>t</sup>MUC1 antigen (8 nmol) produced similar anti-<sup>t</sup>MUC1 immune responses as the 4 nmol <sup>t</sup>MUC1 dosage

As the dose of a vaccine may impact the immune responses, we next investigated the effect of dose by immunizing MUC1/MMTV and MMTV mice with Q $\beta$ -<sup>t</sup>MUC1 at the double dose of <sup>t</sup>MUC1 (8 nmol) following the identical immunization protocol. These mice produced significantly higher IgG titers as compared to the control groups receiving mock immunization with PBS or Q $\beta$ -only (**Fig. 12**). On the other hand, no statistically significant differences in anti-<sup>t</sup>MUC1 IgG titers were observed between the mice receiving 4 nmol vs 8 nmol of the antigen.

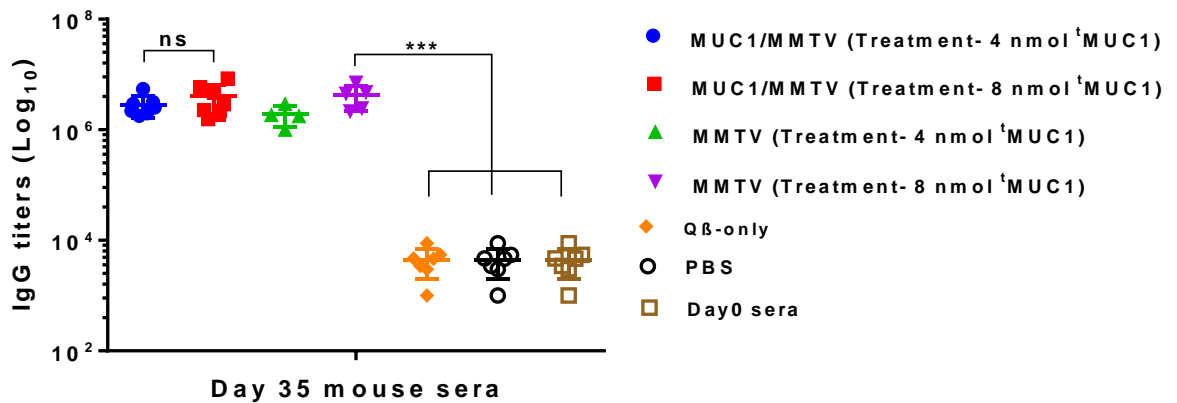
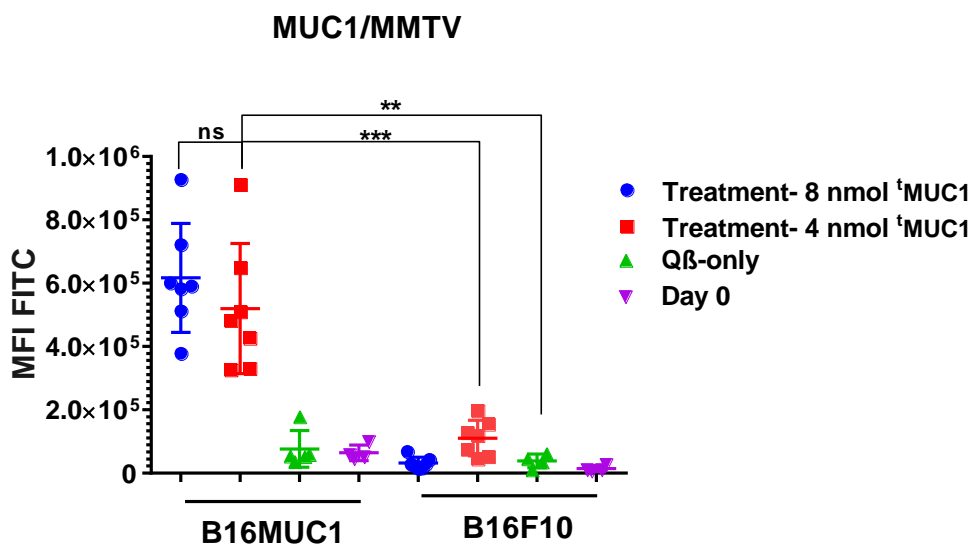


**Figure 12.** a) Comparison of post-immune sera (day 35) of MUC1/MMTV and MMTV mice in the treatment group receiving Q $\beta$ -<sup>t</sup>MUC1 with 4 nmol and 8 nmol <sup>t</sup>MUC1 per dose. Mice in the control groups were vaccinated with the protein carrier Q $\beta$ -only or PBS. Mice were immunized when they were 2-month of age and their IgG antibody titers are reported. Statistical significance was determined by two-tailed unpaired Student's t-test using GraphPad Prism, \*\*\* $p < 0.001$ . Each symbol represents one mouse ( $n = 3-8$  mice for each group).

Similar to the ELISA results, both MUC1/MMTV and MMTV mice in the treatment groups (4 nmol and 8 nmol <sup>t</sup>MUC1 dosage) exhibited strong tumor cell binding for B16MUC1 (MUC1-positive) and minimal binding for B16F10 (MUC1-negative). As expected, the sera from the mice in the control groups displayed significantly lower binding for both B16MUC1 and B16F10 cells when compared to the sera from the mice in the treatment groups (**Fig. 13**). These results reveal that both <sup>t</sup>MUC1 dosages can produce potent anti-<sup>t</sup>MUC1 antibody

response for strong tumor cell binding. From a practical point, we used the lower  $^t$ MUC1 dosage (4 nmol) for further studies and analysis.

a.



b.

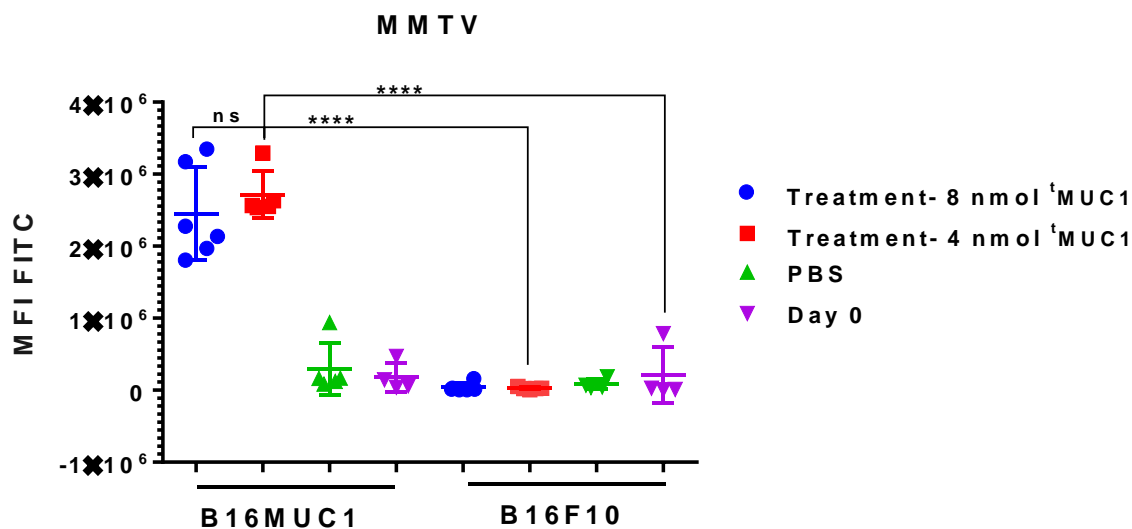
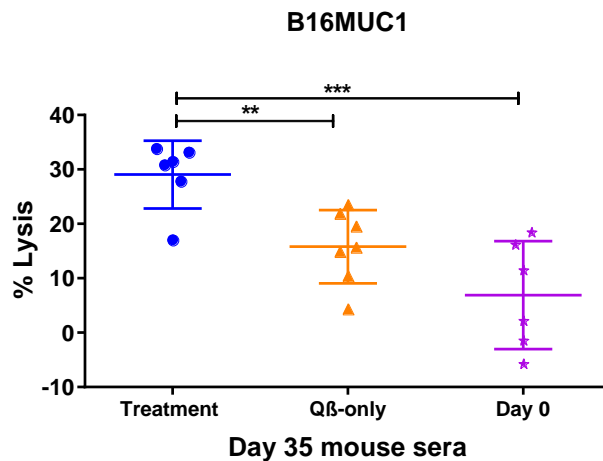


**Figure 13. Mean fluorescence intensities for B16MUC1 and B16F10 cell binding by post-immune sera (day 35).** The treatment group received Q $\beta$ - $^t$ MUC1 with 4 nmol and 8 nmol  $^t$ MUC1 per dose. Mice in the control groups were vaccinated with the protein carrier Q $\beta$ -only or PBS. Mice were immunized when they were 2-month of age. a) MUC1/MMTV mice. b) MMTV mice. Statistical significance was determined by two-tailed unpaired Student's t-test using GraphPad Prism, ns:  $*p > 0.05$ ,  $**p < 0.01$ ,  $***p < 0.001$ ,  $****p < 0.0001$ . Each symbol represents one mouse (n = 4–8 mice for each group).

**2.1.5 Antibodies induced by Q $\beta$ -<sup>125</sup>I-MUC1 vaccine in MUC1/MMTV mice exhibited potent tumoricidal activities *in vitro*, significantly reduced tumor burden and prolonged mouse survival in the spontaneous breast cancer model**

With the strong binding of post-immune sera in mice vaccinated with Q $\beta$ -<sup>125</sup>I-MUC1, the tumoricidal activities of the sera were analysed by the complement dependent cytotoxicity (CDC) assay (Fig. 14).

a.



b.

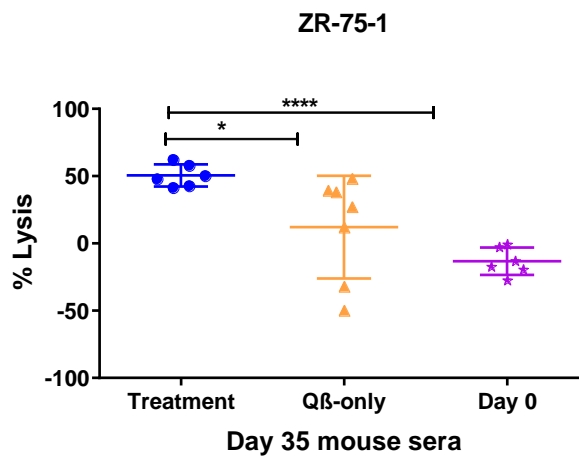
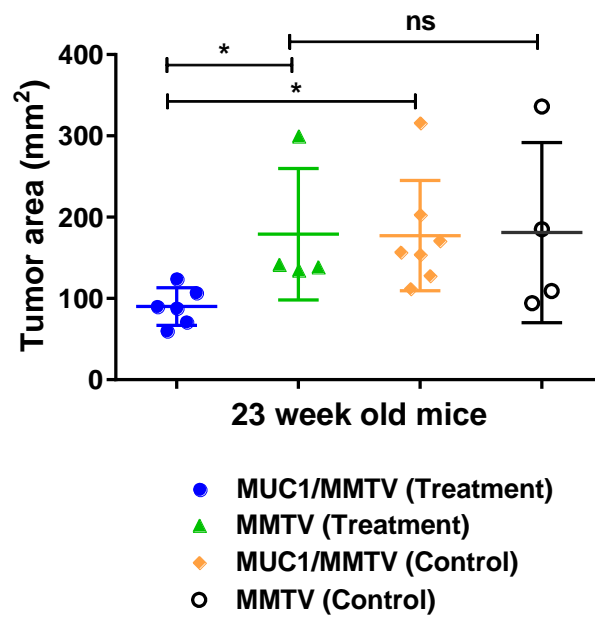


**Figure 14. Percentage lysis of MUC1-positive cancer cells for the post-immune sera (day 35) of MUC1/MMTV mice.** The treatment group received Q $\beta$ -<sup>125</sup>I-MUC1 with 4 nmol <sup>125</sup>I-MUC1 per dose. Mice in the control groups were vaccinated with the protein carrier Q $\beta$ -only or PBS. Mice were immunized when they were 2-month of age. a) Percentage lysis for B16MUC1 cells b) Percentage lysis for ZR-75-1 cells. Statistical significance was determined by two-tailed unpaired Student's t-test using GraphPad Prism, \* $p < 0.05$ , \*\* $p < 0.01$ , \*\*\* $p < 0.001$ , \*\*\*\* $p < 0.0001$ . Each symbol represents one mouse (n = 6–8 mice for each group).

MUC1-positive cultured breast cancer cells (ZR-75-1 and B16MUC1) were incubated with post-immune sera from the treatment group of MUC1/MMTV mice followed by rabbit complement. The results revealed that in comparison to the MUC1/MMTV mice in the control group (Q $\beta$ -only) and pre-immune sera (day 0), a significantly higher percentage of tumor cells was killed by the sera from the treatment group, suggesting the efficacy of the vaccine in tumor protection.

The tumor burdens of immunized mice were analyzed at 23-week of age (**Fig. 15a**). It was observed that the treated MUC1/MMTV mice showed significantly lower tumor burden in comparison to treated MMTV mice or mice in the control group. This result is supported by the *in-vitro* experiment displaying strong tumor binding data observed for MUC1/MMTV mice in the treatment group (**Fig. 10**). Significantly higher percentage of mice in treated MUC1/MMTV (n=6) group survived compared to the MUC1/MMTV receiving the mock control (83% vs 14%) at week 23. For the MMTV mice in the treatment group, no mice survived in MMTV treatment group (**Fig. 15b**) at week 23.

a.



b.

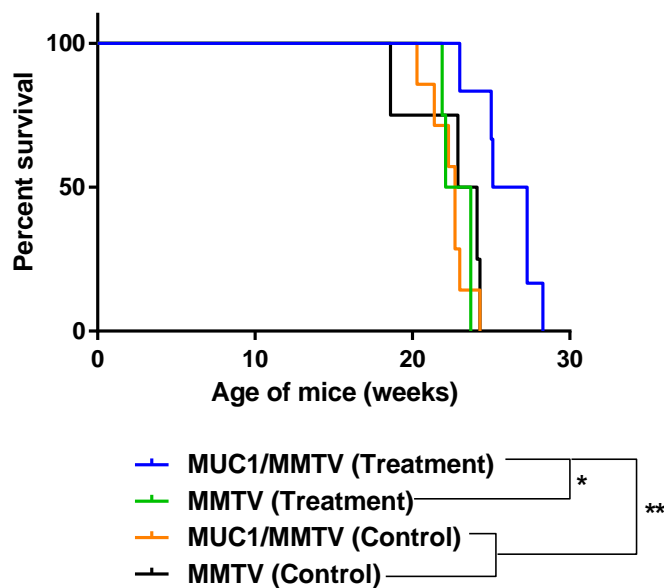


**Figure 15.** a) Tumor burden analysis of MUC1/MMTV and MMTV mice in the treatment group receiving Q $\beta$ -<sup>t</sup>MUC1 at 2-month of age. Mice received 4 nmol of <sup>t</sup>MUC1 per dose. Mice in the control groups were vaccinated with (the protein carrier; Q $\beta$ -only or placebo; PBS). The tumor burden was analyzed twice a week. For each 23-week old mouse, tumor burden was calculated by averaging the area (length x width) of the three biggest tumors and reported in mm<sup>2</sup>. b) The days of survival since birth of MUC1/MMTV and MMTV mice in both treatment and control groups were plotted. Based on the health conditions of the tumor bearing mice observed, mice were euthanized when the biggest tumor area > 200 mm<sup>2</sup> and/or their feeding conditions were affected. Statistical significance was determined by Log-rank Mantel-Cox test using GraphPad Prism, \* $p < 0.05$ . Each symbol represents one mouse (n = 3–8 mice for each group).

While these mice produced high levels of antibodies capable of binding MUC1-expressing tumor cells *in vitro* (Fig. 11), the tumors developed in MMTV mice lack the <sup>h</sup>MUC1 antigen required for binding. Therefore, the treated MMTV mice showed no significant difference in their tumor burden when compared to the mice in the control group, highlighting the importance of <sup>h</sup>MUC1 antigen. Overall, the treated MUC1/MMTV mice lived for more than 4 weeks longer than the treated MMTV mice or control mice. This significant prolongation in the survival of mice with the aggressive tumors resembling the TNBC in the humans, highlights the translational potential of our Q $\beta$ -<sup>h</sup>MUC1 vaccine.

## 2.2 Conclusion

In this study, we evaluated the efficacy of Q $\beta$ -<sup>h</sup>MUC1 vaccine in MUC1/MMTV and MMTV mice. As all these female mice spontaneously develop breast cancer, this model can more closely mimic human conditions as compared to xenograft models of breast cancer. We immunized MUC1/MMTV and MMTV mice at two different timepoints: 1-month of age and 2 months of age. It was discovered that despite a strong antibody response, the treatment group of mice immunized at 1-month did not show any significant differences in tumor burden and their overall survival was also unaffected. Interestingly, immunization of MUC1/MMTV mice at 2 months of age elicited a potent IgG response and strong tumor cell binding to MUC1-expressing cells (B16MUC1, PANC-O2 and ZR-75-1). Post-immune sera from treated MUC1/MMTV mice had significantly higher complement dependent cytotoxicity (CDC) toward MUC1-expressing tumor cells (B16MUC1 and ZR-75-1) cells than control MUC1/MMTV mice. Both dosages of <sup>h</sup>MUC1 (4 nmol and 8 nmol) exhibited similar immune response enabling further studies at lower doses. The treatment group of MUC1/MMTV mice experienced a significantly lower tumor burden compared to MMTV mice in the treatment group. Additionally, 83% of treated MUC1/MMTV mice outlived the treated MMTV. These results emphasize the significance of <sup>h</sup>MUC1 peptide antigen that is lacking in MMTV mice.

This tumor-associated antigen <sup>125</sup>I-MUC1 played a key role in delaying tumor development in the treated MUC1/MMTV mice and ultimately prolonging their overall survival. In conclusion, Q $\beta$ -<sup>125</sup>I-MUC1 vaccine proved to be an effective immunotherapy tool in an aggressive and rapidly growing spontaneous tumor model, laying the groundwork for its clinical translation.

## **2.3 Materials and Methods**

### **2.3.1 Reagents and instruments**

All chemicals were reagent grade and were used as received from the manufacturer, unless otherwise noted. The Q $\beta$ -<sup>125</sup>I-MUC1 was synthesized following a published procedure.<sup>15</sup> Centrifugal filter units of 10,000 and 30,000 molecular weight cut-off (MWCO) were purchased from EMD Millipore. Liquid chromatography-mass spectrometry (LCMS) analysis was performed on Q $\beta$ -<sup>125</sup>I-MUC1 conjugate. The samples for LCMS were prepared with the following procedure: 1:1 v/v of 40  $\mu$ g mL<sup>-1</sup> of Q $\beta$ -<sup>125</sup>I-MUC1 stock solution and 100 mM DTT was mixed and incubated in a water bath at 37 °C for 30 min. One drop of 50% formic acid was added into the mixture. LCMS was performed on Waters Xevo G2-XS quadrupole/time-of-flight UPLC/MS/MS. The liquid chromatography was done on ACQUITY UPLC® Peptide BEH C18 column, 130Å, 1.7  $\mu$ m, 2.1 mm  $\times$  150 mm, using gradient eluent from 95% 0.1% formic acid in water to 95% 0.1% formic acid in CH<sub>3</sub>CN (0.3 mL min<sup>-1</sup> flowrate) at column temperature 40 °C. The multiple charge mass spectra were transformed to single charge by using algorithm MaxEnd148a. The average numbers of MUC1/subunit were analyzed by signal intensity of mass spectrum. Protein concentration was measured using the Coomassie Plus Protein Reagent (Bradford Assay, Pierce) with bovine serum albumin (BSA) as the standard.

### **2.3.2 Cell lines**

All cell lines were purchased from American type culture collection (ATCC) or kindly provided by Profs. O. J. Finn (Univ. of Pittsburgh) and S. J. Gendler (Mayo Clinic). B16-MUC1 melanoma cells were cultured in DMEM supplemented with 10% FBS, 100 U/mL/100  $\mu$ g/mL

Pen/Step, 2 mM L-glutamine, 1 mM sodium pyruvate and 0.3 mg mL<sup>-1</sup> G418. B16F10 cells were cultured in DMEM supplemented with 10% FBS, 100 U/mL/100 µg/mL Pen/Step, 2 mM L-glutamine, 1 mM sodium pyruvate. ZR-75-1 breast cancer cells were cultured in RPMI-1640 supplemented with 10% FBS, 100 U/mL/100 µg/mL Pen/Step, 2 mM L-glutamine, 1 mM sodium pyruvate. PANC-O2 pancreatic cancer cells were cultured in RPMI-1640 supplemented with 10% FBS, 100 U/mL/100 µg/mL Pen/Step, 2 mM L-glutamine, 1 mM sodium pyruvate and 0.3 mg mL<sup>-1</sup> G418. These cell lines were maintained in a humidified incubator at 37°C in a 5% CO<sub>2</sub>, 95% air atmosphere.

### **2.3.3 Mouse immunization and evaluation of tumor burden**

All animal care procedures and experimental protocols were approved by the Michigan State University Institutional Animal Care and Use Committee (IACUC). A spontaneous mouse tumor model was developed by genetically crossing mouse mammary tumor virus (MMTV)-polyoma middle T (PyMT) mice with MUC1.Tg mice. The female offspring of the resulting mice double transgenic in MUC1 and PyMT (referred to as MUC1-MMTV) spontaneously develop palpable breast cancer at 5-7 primary sites resembling human TNBC in 8-10 weeks. Mice were injected subcutaneously at the scruff of the neck with 0.2 mL vaccine construct that included monophosphoryl lipid A (MPLA, 20 µg) as the adjuvant on day 0 plus weekly booster injections given subcutaneously on days 7, 14, 21 and 28. Serum samples were collected weekly on days 0 (before immunization), 6, 20, 27 and 35. For treatment groups, mice received two different Q $\beta$ -<sup>125</sup>I-MUC1 vaccine constructs with 4 nmol and 8 nmol <sup>125</sup>I-MUC1-N antigen dosage per mouse. For the control groups, MUC1/MMTV group of mice received equivalent amount of Q $\beta$  protein carrier and MMTV group of mice received placebo (PBS).

For tumor burden analysis, MUC1/MMTV and MMTV mice in both treatment and control groups were monitored twice a week when they started developing palpable mammary

gland tumors. The tumor burden ( $\text{mm}^2$ ) was calculated by averaging the tumor area (length x width) of three-biggest tumors developed on 23-week old mice. Health conditions of the tumor bearing mice were observed and mice were euthanized when the biggest tumor area  $> 200 \text{ mm}^2$  and/or their body conditions were significantly deteriorated.

#### 2.3.4 Synthesis of $^1\text{MUC1-NPL}$ glycopeptide

The  $^1\text{MUC1}$  glyco-peptide was synthesized using Fmoc based solid phase support peptide synthesis (SPPS) on *p*-nitrophenyl carbonate Wang resin pre-loaded with Fmoc-1,4-diaminobutane 40 using Fmoc chemistry. The *N*-terminal protecting group, Fmoc, was deprotected by 20% piperidine in DMF. The amino acid coupling was carried out with Fmoc amino acids (5 eq.) using (2-(1H-benzotriazol-1-yl)-1,1,3,3-tetramethyluronium hexafluorophosphate (HBTU)/hydroxybenzotriazole (HOBt) (4.9 eq.) and DIPEA (10 eq.). For glyco-peptide synthesis, Fmoc-Tn building block Fmoc-GalNAc-Thr 33 (2 eq.) was used as a building block, which was introduced into the peptide chain mediated by 1-[bis(dimethylamino)methylene]-1H-1,2,3-triazolo[4,5-b]pyridinium3-oxide hexafluorophosphate (HATU)/1-hydroxy-7-azabenzotriazole (HOAt) (1.9 eq.) and DIPEA (4 eq.). After assembly of glyco-peptide, the *N*-terminal Fmoc group was removed and capped with acetic anhydride. The peptide was cleaved from resins by TFA/TIPS/ $\text{H}_2\text{O}$  = 95/2.5/2.5 for 2 h. The excess TFA was evaporated. The glyco-peptide was precipitated by diethyl ether and centrifuged to pellet the solid. To remove the acetyl protecting groups of the Tn, the crude glyco-peptide was treated with 5% (v/v) hydrazine in water for 6 h. The crude reaction was neutralized to pH 7. The deprotected  $^1\text{MUC1-N}$  glyco-peptide was purified on a Shimadzu HPLC (LC-8A Liquid Chromatograph Pump, DGU-14A, Degasser and SPD-10A UV-Vis Detector), using S6 reverse phase column SUPERCOSIL LC18, 25 cm  $\times$  10 mm 5  $\mu\text{m}$  with gradient solvent  $\text{CH}_3\text{CN}$  and  $\text{H}_2\text{O}$  (0.1% TFA) gradient 0–5% in 2 min, 5–40% in 2–40 min. The yield of purified  $^1\text{MUC1}$  glycopeptide was 30-40%. For conjugation of the  $^1\text{MUC1}$  glyco-

peptide onto Q $\beta$ , the purified <sup>125</sup>I-MUC1-N was treated with adipate bis(4-nitrophenyl) ester and then purified by HPLC to obtain <sup>125</sup>I-MUC1-NPL glyco-peptide with 95% yield.

### **2.3.5 Synthesis and characterization of Q $\beta$ -<sup>125</sup>I-MUC1 vaccine**

The amount of antigen added was based on the ratio of antigen per accessible capsid surface amines. The Q $\beta$  (with mutation; A38K/A40C/D102C) is comprised of 180 identical subunits with five accessible surface amines per subunit. As a result, the total number of surface accessible amines available for conjugation is 900. For synthesis of Q $\beta$ -<sup>125</sup>I-MUC1, a solution of Q $\beta$  (6.5 mg, 0.46  $\mu$ mol subunit, 1.84  $\mu$ mol reactive amine) in 0.1 M K-Phos buffer (pH = 7.0, 1.123 mL) was cooled on an ice bath, then added to a frozen solution of <sup>125</sup>I-MUC1-NPL (176  $\mu$ L from a 50 mM stock solution in DMSO, 8.8  $\mu$ mol). The mixture was allowed to warm to rt and gently inverted several times to ensure mixing of the reactants. The reaction was incubated at 37 °C for 16 h. The reaction mixture was purified by Amicon Ultra 30 kDa MW cut-off against 0.1 M K-Phos buffer. The total protein concentration was determined by Bradford assay against BSA standards. Percent protein recovery was found to be approximately 85 %. The extent of particle modification was determined by ESI-TOF LC-MS and by reducing SDS PAGE through Image Lab software by Bio Rad.

### **2.3.6 Synthesis of BSA-<sup>125</sup>I-MUC1 conjugate**

For BSA conjugation, <sup>125</sup>I-MUC1 (2.5 mg) functionalized with adipate bis(4-nitrophenyl) ester was added respectively to a solution of BSA (2 mg) in pH = 7.0, 0.1 M K-Phos buffer (~200  $\mu$ L). The reaction was incubated at 37 °C overnight. The product was purified by an Amicon Ultra 10 kDa MW cut-off against 0.1 M K-Phos (5  $\times$  0.5 mL). Total protein content was quantified by Bradford assay against BSA standards. The extent of modification was determined by MALDI MS.

### **2.3.7 Evaluation of antibody titers by ELISA**

A Nunc MaxiSorp® flat-bottom 96 well plate was coated with a solution of the

corresponding BSA-<sup>t</sup>MUC1 conjugate (10 µg mL<sup>-1</sup>, 100 µL/well) in NaHCO<sub>3</sub>/Na<sub>2</sub>CO<sub>3</sub> buffer (0.05 M, pH 9.6) and incubated at 4 °C overnight. The coated plate was washed with PBS/0.5% Tween-20 (PBST) (4 × 200 µL) and blocked by 1 % BSA/PBS (100 µL/well) at rt for 1 h. The plate was washed again with PBST (4 × 200 µL) and incubated with serial dilutions of mouse sera in 0.1 % BSA/PBS (100 µL/well, 4 wells for each dilution). The plate was incubated for 2 h at 37 °C and then washed with PBST (4 × 200 µL). A 1:2000 dilution of HRP-conjugated goat anti-mouse IgG (Jackson ImmunoResearch Laboratory) in 0.1% BSA/PBS (100 µL) was added to the wells respectively to determine the titers of antibodies generated. The plate was incubated for 1 h at 37 °C. A solution of enzymatic substrate was prepared by dissolving 3,3',5,5'- tetramethylbenzidine (TMB, 5 mg) in a mixture of DMSO (2 mL) and citric acid buffer (18 mL) in a 50 mL centrifuge tube covered with aluminum foil. H<sub>2</sub>O<sub>2</sub> (20 µL) was added and the mixture was homogenized by vortexing. The plate was washed with PBST (4 × 200 µL) and a solution of enzymatic substrate was added (200 µL). Color was allowed to develop for 15 min and 0.5 M H<sub>2</sub>SO<sub>4</sub> (50 µL) was added to quench the reaction. The absorbance was measured at 450 nm using a microplate reader. The titer was determined by regression analysis with log<sub>10</sub> dilution plotted with optical density. The titer was reported as the highest fold of dilution giving the optical absorbance value of 0.1 over those of the pre-immune control sera (OD = 0.2). All samples were tested in triplicates replicates.

### **2.3.8 Detection of cellular binding of anti-<sup>t</sup>MUC1 antibodies to tumor cells by FACS**

B16-MUC1 cells, B16F10 cells, ZR-75-1 cells or PANC-O2 cells were respectively cultured till 80% confluency at 37 °C under 5% CO<sub>2</sub> in cell growth medium. The cells were detached using 0.25% trypsin followed by incubation at 37 °C under 5% CO<sub>2</sub> for 5 min. The cell growth medium was transferred to a conical centrifuge tube, and centrifuged at 1,600 rpm for 5 min at 4 °C. The pellet was re-suspended in growth medium (10 mL). The number of cells was determined using a haemocytometer. The cells were transferred based on requirement of

the experiment (between  $0.35 \times 10^6$  cells -  $0.5 \times 10^6$  cells was recommended). The cells were resuspended in 2 mL of 1X PBS and viability dye (Live/Dead blue) was added at 1/1000 dilution. The cells were incubated on ice in dark for 30 min. The cells were then diluted to 10 mL of FACS buffer (1% FBS, 0.1% NaN<sub>3</sub> in 1X PBS, pH 7.4) and centrifuged at 1,600 rpm for 5 min at 4 °C. The pellet was washed twice with FACS buffer and then resuspended in FACS buffer such that each well in the V-bottom 96 well plate receives the required number of cells in 95 µL of volume. The cells were incubated with 1:20 dilution of mouse sera (5 µL) in FACS buffer for 30 min on ice. The incubated cells were washed twice with FACS buffer, followed by incubation with 1/50 dilution of FITC conjugated goat anti-mouse IgG (minimal x-reactivity) antibody for 30 min. The cells were washed thrice and were fixed with 4% formalin in 1X PBS for 10 min at room temperature. The fixed cells were washed thrice with FACS buffer and then re-suspended in FACS buffer and analyzed by Cytex Aurora. Data was processed by FlowJo software.

### **2.3.9 Complement dependent cytotoxicity**

Complement dependent cytotoxicity of B16-MUC1 or ZR-75-1 cells was determined by MTS assay. B16-MUC1 or ZR-75-1 cells (10,000 cells/well) were cultured for 12–72 h (12 h for B16- MUC1, 72 h for ZR-75-1), and incubated with a 1/20 dilution of mouse sera in 50 µL of culture medium at 37 °C for 30 min from different groups of immunized MUC1/MMTV mice. Rabbit serum complement at 1/15 dilution in 60 µL of culture medium was added and then incubated at 37 °C for 4 h. MTS (CellTiter 96® AQueous One Solution Cell Proliferation Assay; Promega, 20 µL) was added into each well and further incubated at 37 °C for 2 h. The optical absorption of the MTS assay was measured at 490 nm. Cells cultured in MTS were used as a positive control (maximum OD), and the culture medium was used as a negative control (minimum OD). All data were performed in four replicates. Cytotoxicity was calculated as follows: Cytotoxicity (%) = (OD positive control – OD experimental) / (OD positive control –

OD negative control)  $\times 100$ . The lowest cell viability values were used as baseline and all other data points were calibrated accordingly.

## REFERENCES

- (1) Mellman, I.; Coukos, G.; Dranoff, G. Cancer immunotherapy comes of age. *Nature* **2011**, *480* (7378), 480-489. DOI: 10.1038/nature10673.
- (2) Riley, R. S.; June, C. H.; Langer, R.; Mitchell, M. J. Delivery technologies for cancer immunotherapy. *Nat Rev Drug Discov* **2019**, *18* (3), 175-196. DOI: 10.1038/s41573-018-0006-z.
- (3) Zhu, S. Y.; Yu, K. D. Breast Cancer Vaccines: Disappointing or Promising? *Front Immunol* **2022**, *13*, 828386. DOI: 10.3389/fimmu.2022.828386.
- (4) Guo, C.; Manjili, M. H.; Subjeck, J. R.; Sarkar, D.; Fisher, P. B.; Wang, X. Y. Therapeutic cancer vaccines: past, present, and future. *Adv Cancer Res* **2013**, *119*, 421-475. DOI: 10.1016/B978-0-12-407190-2.00007-1.
- (5) Ying, H.; Zeng, G.; Black, K. L. Innovative cancer vaccine strategies based on the identification of tumour-associated antigens. *BioDrugs* **2001**, *15* (12), 819-831. DOI: 10.2165/00063030-200115120-00004.
- (6) Siddiqui, J.; Abe, M.; Hayes, D.; Shani, E.; Yunis, E.; Kufe, D. Isolation and sequencing of a cDNA coding for the human DF3 breast carcinoma-associated antigen. *Proc Natl Acad Sci U S A* **1988**, *85* (7), 2320-2323. DOI: 10.1073/pnas.85.7.2320.
- (7) Gendler, S. J.; Burchell, J. M.; Duhig, T.; Lamport, D.; White, R.; Parker, M.; Taylor-Papadimitriou, J. Cloning of partial cDNA encoding differentiation and tumor-associated mucin glycoproteins expressed by human mammary epithelium. *Proc Natl Acad Sci U S A* **1987**, *84* (17), 6060-6064. DOI: 10.1073/pnas.84.17.6060.
- (8) Xi, X.; Wang, J.; Qin, Y.; Huang, W.; You, Y.; Zhan, J. Glycosylated modification of MUC1 maybe a new target to promote drug sensitivity and efficacy for breast cancer chemotherapy. *Cell Death Dis* **2022**, *13* (8), 708. DOI: 10.1038/s41419-022-05110-2.
- (9) Chen, W.; Zhang, Z.; Zhang, S.; Zhu, P.; Ko, J. K.; Yung, K. K. MUC1: Structure, Function, and Clinic Application in Epithelial Cancers. *Int J Mol Sci* **2021**, *22* (12). DOI: 10.3390/ijms22126567.
- (10) Cheever, M. A.; Allison, J. P.; Ferris, A. S.; Finn, O. J.; Hastings, B. M.; Hecht, T. T.; Mellman, I.; Prindiville, S. A.; Viner, J. L.; Weiner, L. M.; et al. The prioritization of cancer antigens: a national cancer institute pilot project for the acceleration of translational research. *Clin Cancer Res* **2009**, *15* (17), 5323-5337. DOI: 10.1158/1078-0432.CCR-09-0737.
- (11) Brockhausen, I.; Melamed, J. Mucins as anti-cancer targets: perspectives of the glycobiologist. *Glycoconj J* **2021**, *38* (4), 459-474. DOI: 10.1007/s10719-021-09986-8.
- (12) Zhou, R.; Yazdanifar, M.; Roy, L. D.; Whilding, L. M.; Gavrill, A.; Maher, J.; Mukherjee, P. CAR T Cells Targeting the Tumor MUC1 Glycoprotein Reduce Triple-Negative Breast Cancer Growth. *Front Immunol* **2019**, *10*, 1149. DOI: 10.3389/fimmu.2019.01149.

- (13) Kovjazin, R.; Volovitz, I.; Kundel, Y.; Rosenbaum, E.; Medalia, G.; Horn, G.; Smorodinsky, N. I.; Brenner, B.; Carmon, L. ImMucin: a novel therapeutic vaccine with promiscuous MHC binding for the treatment of MUC1-expressing tumors. *Vaccine* **2011**, *29* (29-30), 4676-4686. DOI: 10.1016/j.vaccine.2011.04.103.
- (14) Ibrahim, N. K.; Yariz, K. O.; Bondarenko, I.; Manikhas, A.; Semiglazov, V.; Alyasova, A.; Komisarenko, V.; Shparyk, Y.; Murray, J. L.; Jones, D.; et al. Randomized phase II trial of letrozole plus anti-MUC1 antibody AS1402 in hormone receptor-positive locally advanced or metastatic breast cancer. *Clin Cancer Res* **2011**, *17* (21), 6822-6830. DOI: 10.1158/1078-0432.CCR-11-1151.
- (15) Wu, X.; Yin, Z.; McKay, C.; Pett, C.; Yu, J.; Schorlemer, M.; Gohl, T.; Sungsuwan, S.; Ramadan, S.; Baniel, C.; et al. Protective Epitope Discovery and Design of MUC1-based Vaccine for Effective Tumor Protections in Immunotolerant Mice. *J Am Chem Soc* **2018**, *140* (48), 16596-16609. DOI: 10.1021/jacs.8b08473.
- (16) Becher, O. J.; Holland, E. C. Genetically engineered models have advantages over xenografts for preclinical studies. *Cancer Res* **2006**, *66* (7), 3355-3358, discussion 3358-3359. DOI: 10.1158/0008-5472.CAN-05-3827.
- (17) Maglione, J. E.; Moghanaki, D.; Young, L. J.; Manner, C. K.; Ellies, L. G.; Joseph, S. O.; Nicholson, B.; Cardiff, R. D.; MacLeod, C. L. Transgenic Polyoma middle-T mice model premalignant mammary disease. *Cancer Res* **2001**, *61* (22), 8298-8305.
- (18) Lin, E. Y.; Jones, J. G.; Li, P.; Zhu, L.; Whitney, K. D.; Muller, W. J.; Pollard, J. W. Progression to Malignancy in the Polyoma Middle T Oncoprotein Mouse Breast Cancer Model Provides a Reliable Model for Human Diseases. *Am. J. Pathol.* **2003**, *163*, 2113-2126. DOI: 10.1016/s0002-9440(10)63568-7.
- (19) Weng, D.; Penzner, J. H.; Song, B.; Koido, S.; Calderwood, S. K.; Gong, J. Metastasis is an early event in mouse mammary carcinomas and is associated with cells bearing stem cell markers. *Breast Cancer Res* **2012**, *14* (1), R18. DOI: 10.1186/bcr3102.

## APPENDIX

**Figure 16.** Mass spectrum of functionalized  $^t$ MUC1-NPL.

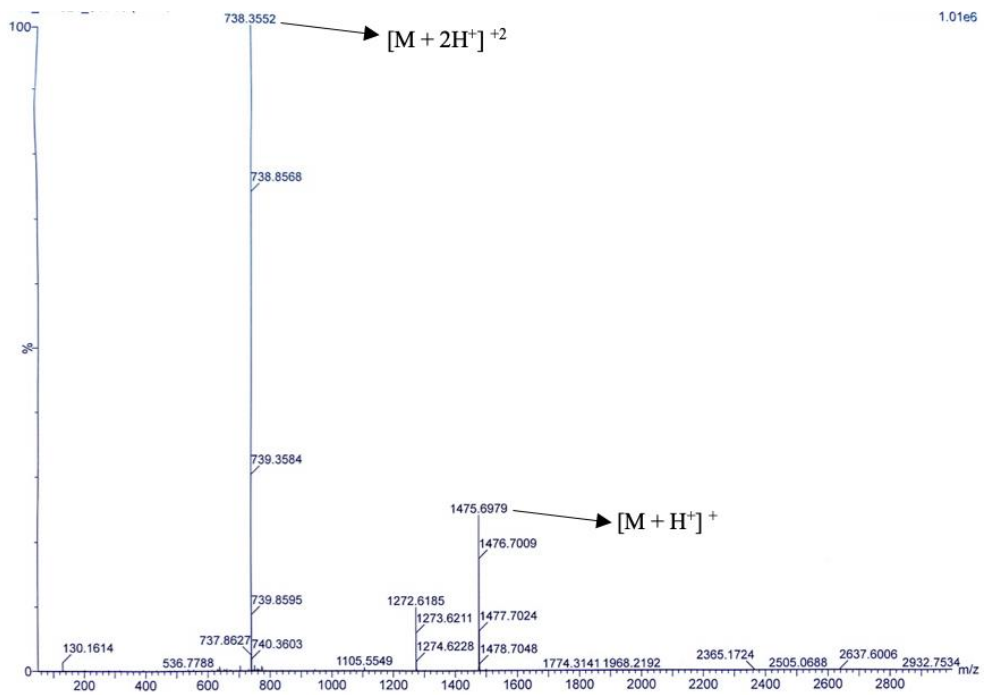
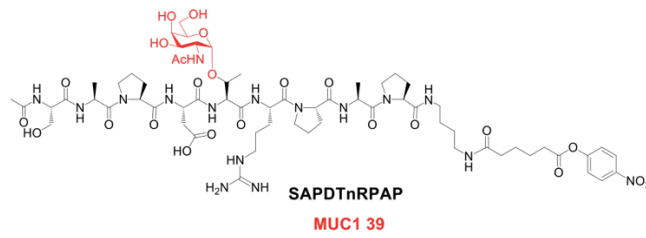


**Figure 17.** Electrophoresis analysis (SDS-PAGE) of Q $\beta$ -<sup>125</sup>I-MUC1 vaccine conjugates showing the number of <sup>125</sup>I-MUC1 copies on each viral capsid subunit is 280 as calculated by Image Lab software.

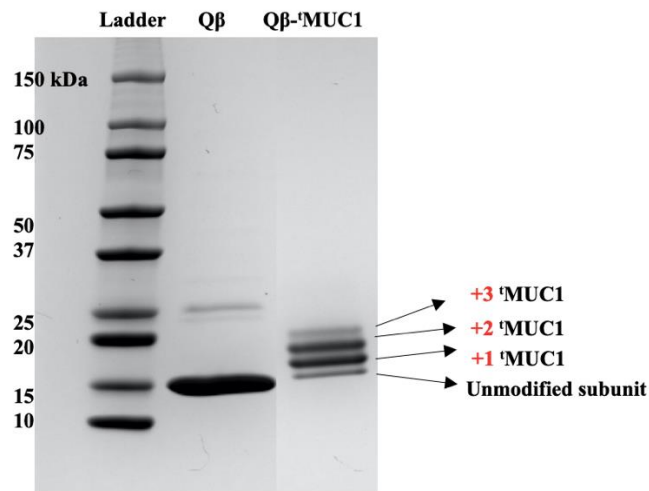
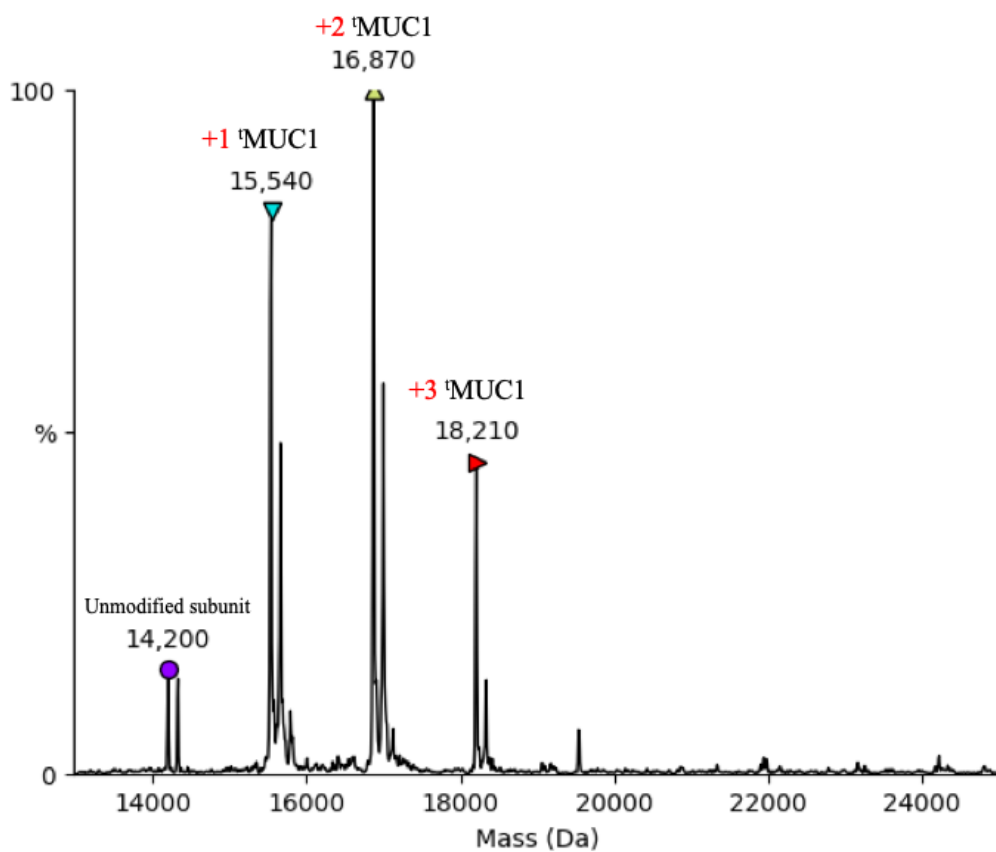


**Figure 18.** ESI-TOF HRMS spectra of Q $\beta$ -<sup>125</sup>I-MUC1 vaccine conjugate showing the number of <sup>125</sup>I-MUC1-NPL copies on each viral capsid is 280 on average.



## **Chapter 3 Investigating Epitopes of MUC1-C Protein as an Antigenic Target for Anti-Cancer Vaccine Development**

### **3.1 Introduction**

Vaccination is a powerful tool that harnesses the immune system of the body to combat diseases, which can potentially provide long term immunity with few side effects. One of the attractive targets for the development of anti-cancer vaccine is human mucin-1 (MUC1) protein. It can be aberrantly overexpressed (>100-fold) on the cell surface of a wide range of human carcinoma including prostate, lung, ovarian pancreatic, colon and more than 90% of breast cancer.<sup>1, 2</sup> MUC1-C protein is cleaved into two subunits MUC1-N (N-terminus) and MUC1-C (C-terminus), which are associated by non-covalently interactions. Many studies have utilized various epitopes of the MUC1-N subunit as antigens for cancer vaccines but have not yet met with clinical successes.<sup>3-11</sup> On the other hand, the transmembrane MUC1-C domain has been shown to have oncogenic potential.<sup>12, 13, 14, 15</sup> MUC1-C is composed of a 58-amino acid extracellular domain (ECD), a 28 amino-acid transmembrane (TM) domain followed by a 72-amino acid cytoplasmic tail (CT). Several studies have investigated the MUC1-C subunit as an alternative antigen for immunotherapy development targeting cancer as discussed in chapter-1.<sup>16-21</sup> However, to date, it has not been reported in a vaccination strategy.

In this study, we report two epitopes of the MUC1-C domain for the development of Q $\beta$ -based vaccine. Bacteriophage Q $\beta$  is a virus like particle (VLP) that displays antigens in a highly organized 3-dimensional orientation. It helps in stimulating the immune system against the antigen to generate high and long-lasting antibody response.<sup>22</sup> The two epitopes span through the MUC1-C domain from N-1098-1155-C (58mer) and N-961-1152-C (192mer). The MUC1-C epitopes (58mer and 192mer) were conjugated to a mutant Q $\beta$  using the maleimide linker chemistry to yield Q $\beta$ -MUC1-C (58mer and 192mer) vaccine constructs. Various aspects of immune response generated by these vaccines were evaluated in this report through ELISA, FACS and cell invasion assay (CIA).

## 3.2 Results and Discussions

### 3.2.1 Expressing and characterizing un-glycosylated-MUC1-C (58mer and 192mer)

Monoclonal antibodies generated against the ECD of MUC1-C 58mer (N-1098-1155-C) had previously displayed potent anti-tumor activities with strong binding to the MUC1-C protein and MUC1-expressing tumor cells through ELISA, FACS and various other immunological assays.<sup>20</sup> In this work we successfully expressed 58 a.a protein from the MUC1-C domain in *E. coli* (pET-28a(+)-TEV vector) with a histidine-tag and a cysteine at the C-terminus. The cysteine moiety was added to enable the covalent conjugation during the vaccine construction and the histidine-tag rendered it convenient for its purification and characterization. The protein was characterized through reducing sodium dodecyl-sulfate polyacrylamide gel electrophoresis (SDS-PAGE) and western blot analysis through an anti-his secondary antibody (**Fig. 19**).

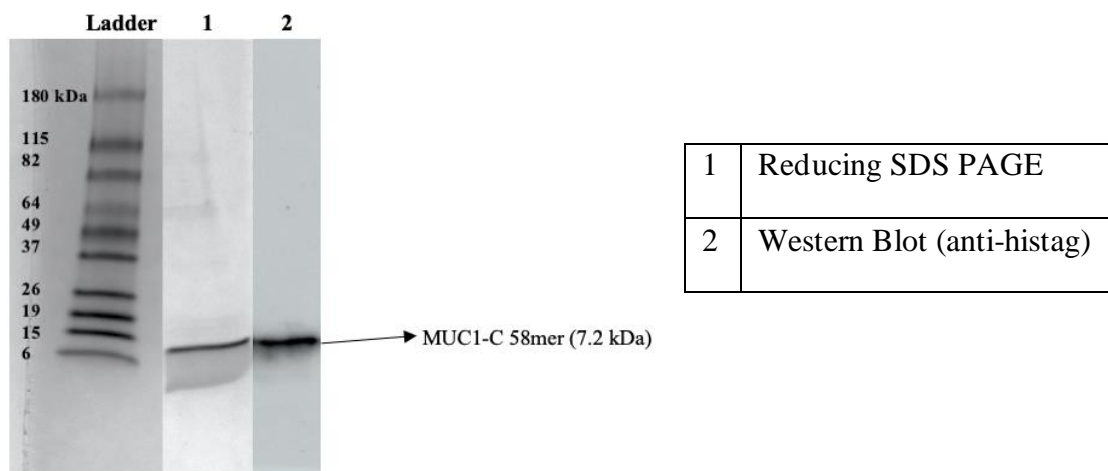


**Figure 19. Characterization of *E. coli* expressed un-glycosylated MUC1-C (58mer) from ECD.** Electrophoresis (SDS-PAGE and Western blot) of MUC1-C (58mer; M.W. 7.2 kDa) displaying ladder and lane 1 (reducing SDS-PAGE, Coomassie blue stain) and lane 2 (anti-histag Western blot).

Another study utilized the 192mer protein sequence (N-961-1152-C) from the MUC1-C ECD to express a monoclonal antibody, which successfully demonstrated specific binding to human MUC1-C in its native form through western blot and immunoprecipitation analysis.<sup>21</sup> This result suggested that the 192 mer may be a suitable antigen. The native MUC1-C 192mer

sequence undergoes auto-proteolysis into two fragments that makes it difficult to target the full-length MUC1-C 192mer as an antigen for vaccine development. A point mutation (S1098A) was introduced into the sequence to prevent the auto-proteolysis leading to the design of the histidine-tagged un-glycosylated MUC1-C 192mer expressed in *E. coli* (N-961-1152-HHHHHH-C; pET30a vector) for our study (**Fig. 20**).

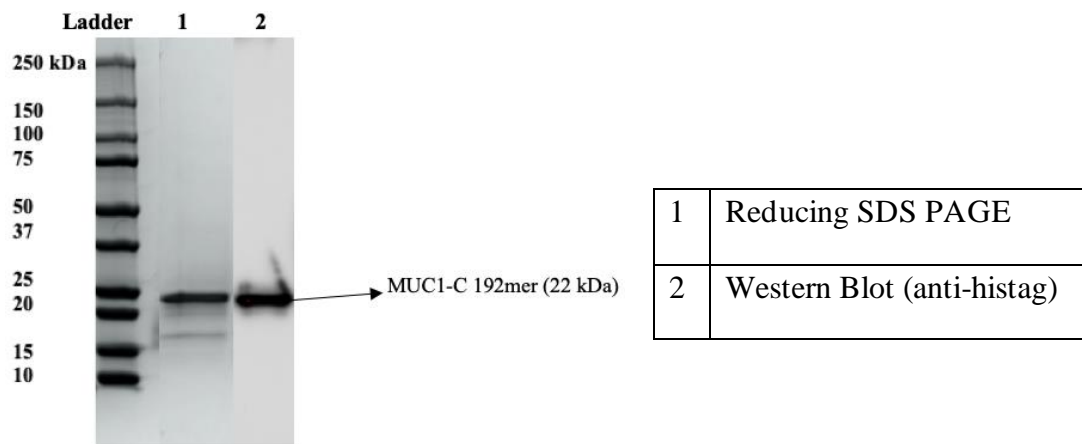
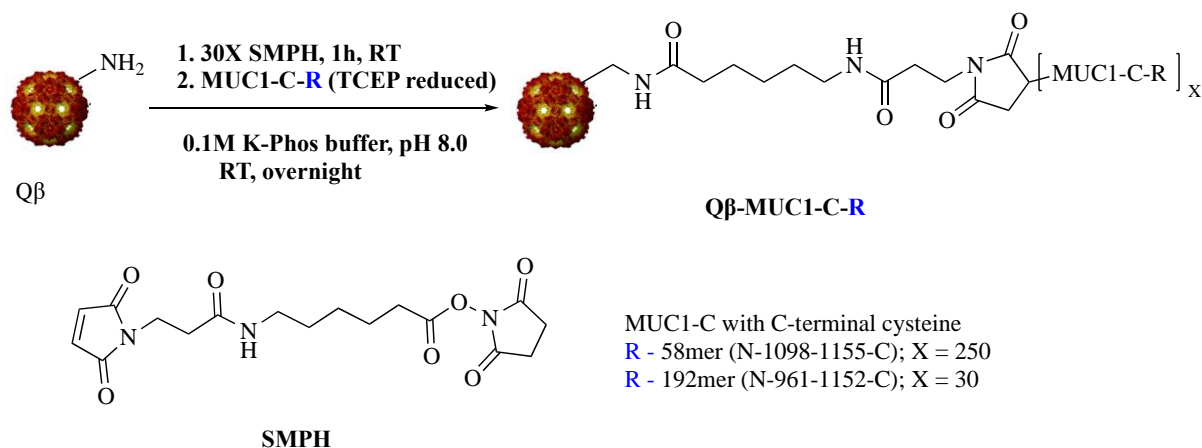


**Figure 20. Characterization of *E. coli* expressed un-glycosylated MUC1-C (192mer) from ECD.** Electrophoresis (SDS-PAGE and Western blot) of MUC1-C (192mer; M.W. 22 kDa) displaying ladder and lane 1 (reducing SDS-PAGE, Coomassie blue stain) and lane 2 (anti-histag Western blot).

### 3.2.2 Bio-conjugation and characterization of MUC1-C (58mer and 192mer) to Q $\beta$ for constructing Q $\beta$ -MUC1-C vaccine

A mutant bacteriophage Q $\beta$  (A38K/A40C/D102CQ $\beta$ ) has been developed in our lab as a potent carrier for conjugate vaccine development.<sup>23</sup> Q $\beta$ -based vaccine constructs have induced robust antibody response against the target antigen with reduced anti-carrier antibodies.<sup>23</sup> For bioconjugation, freshly expressed Q $\beta$  was first oxidized to ensure no free sulfhydryl groups on Q $\beta$  carrier to minimize any interference during lysine-based conjugation with a cysteine reactive bifunctional linker *N*-succinimidyl 6-(3-maleimidopropionamido) hexanoate (SMPH). Oxidized Q $\beta$  was functionalized with the SMPH linker (100 mg/ mL in DMSO; 30X molar ratio) in 0.1M KPB, pH 8 for 1h at room temperature. Excess SMPH was removed by filtration through a membrane filter (30,000 MW cut-off). Simultaneously, purified MUC1-C (58mer and 192mer) was reduced using tris-(2-carboxyethyl)-phosphine (TCEP)

immobilized beads. TCEP-reduced MUC1-C (58mer and 192mer) was then added to Q $\beta$ -SMPH for an overnight incubation at room temperature to construct Q $\beta$ -MUC1-C vaccine (**Scheme 1**).

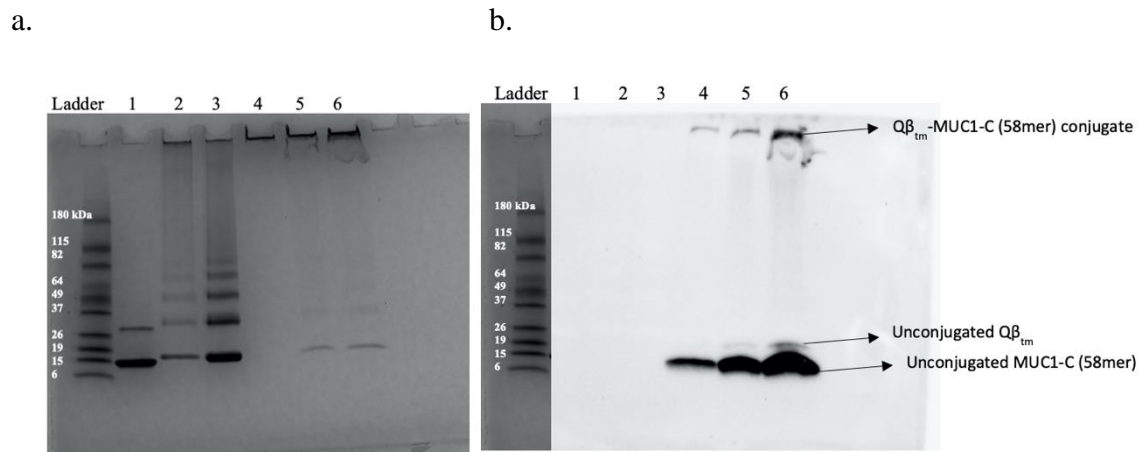


**Scheme 1. Schematic demonstration of Q $\beta$ -MUC1-C (58mer and 192mer) conjugates.** Oxidized Q $\beta$  functionalized with 30X SMPH linker in 0.1M KPB buffer, pH 8 for 1h at room temperature. After removing excess SMPH linker, TCEP reduced MUC1-C (58mer and 192mer) was immediately added to oxidized Q $\beta$  in 1M KPB buffer, pH 8 for overnight incubation at room temperature. The Q $\beta$ -MUC1-58mer vaccine had 250 copies of MUC1-C (58mer) per Q $\beta$  capsid and Q $\beta$ -MUC1-C (192mer) vaccine had 30 copies of MUC1-C (192mer) per Q $\beta$  capsid.

Q $\beta$ -MUC1-C (58mer) conjugate was characterized through qualitative analysis using reducing sodium dodecyl-sulfate polyacrylamide gel electrophoresis (SDS PAGE) and western blot analysis using anti-histag antibody (**Fig. 21a, b**). As demonstrated in lanes 4, 5 and 6 in SDS-PAGE and western blot, the Q $\beta$ -MUC1-C (58mer) conjugate remained stuck in the well in the stacking gel due to the high molecular weight of the conjugate. The unconjugated Q $\beta$  and MUC1-C (58mer) migrated down the resolving gel.

The Q $\beta$ -MUC1-C conjugates were purified with FPLC-SEC (**Fig. 21c**) and the antigen loading levels for MUC1-C (58mer) were quantified by using MUC1-C (58mer) calibration curve obtained by a method adapted from ELISA (**Fig. 21d**). The ELISA plate was coated overnight with 0-50 ng/well of MUC-C 58mer to create a standard curve. A known amount of Q $\beta$ -MUC1-C (58mer) conjugate mixture, which was pre-washed with 0.1 M KPB buffer in

(100,000 MW cut-off) centrifuge filter after the bioconjugation. was also coated in the same ELISA plate. Absorbance was measured at 450 nm and the antigen loading level for MUC1-C (58mer) in the Q $\beta$ -MUC1-C (58mer) conjugate mixture was calculated. On average, 250 copies/Q $\beta$  capsid was obtained.



Row	Sample
1	Q $\beta$ -only
2,3	Q $\beta$ -SMPH
4-6	Q $\beta$ -MUC1-C (58mer) conjugate

c.

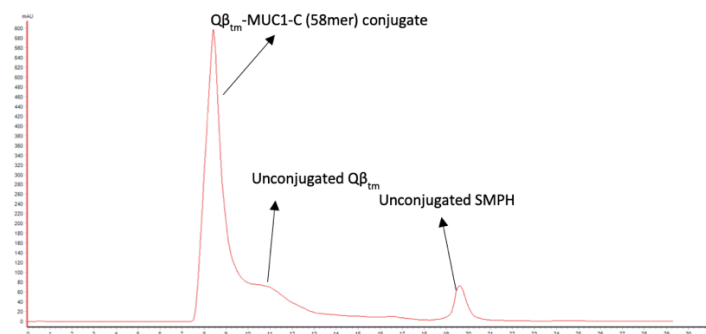
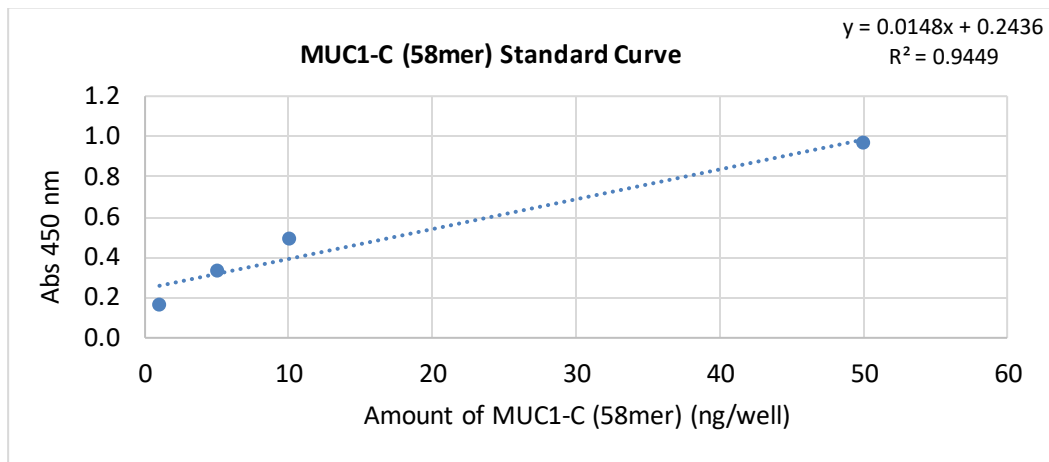


**Figure 21. Characterization of Q $\beta$ -MUC1-C (58mer) vaccine construct.** Analysis of Q $\beta$ -only (lane 1), Q $\beta$ -SMPH (lanes 2, 3) and Q $\beta$ -MUC1-C (58mer) conjugate (lanes 4-6). The pre-washed and Q $\beta$ -MUC1-C (58mer) conjugate mixture consists of unconjugated Q $\beta$  (14 kDa) and unconjugated MUC1-C (58mer) (7.2 kDa) along with the Q $\beta$ -MUC1-C (58mer) conjugate. a) SDS-PAGE with Coomassie blue stain b) Western blot analysis with anti-histag antibody c) FPLC-SEC analysis of Q $\beta$ -MUC1-C (58mer) conjugate mixture. It was performed on a GE ÄKTA Explorer (Amersham Pharmacia) instrument equipped with a Superose-6 column. Microfluidic capillary gel electrophoresis was performed on a Bioanalyzer 2100 Protein 80 microfluidics chip (Agilent Technologies). d) Calibration curve of MUC1-C (58mer) by using Bradford dye and reading absorbance.

**Figure 21 (cont'd)**

d.



The antigen loading levels for MUC1-C (192mer) with 30 copies/Q $\beta$  capsid were calculated by using MUC1-C (192mer) calibration curve obtained by FPLC-SEC (**Fig. 22a**). After the overnight bioconjugation, the Q $\beta$ -MUC1-C (192mer) conjugate mixture was injected in the FPLC-SEC column (**Fig. 22b**) and the amount of unconjugated MUC1-C (192mer) was calculated using the calibration curve. The purified fraction for Q $\beta$ -MUC1-C (192mer) conjugate was then injected in mice for evaluating the immune response.

a.

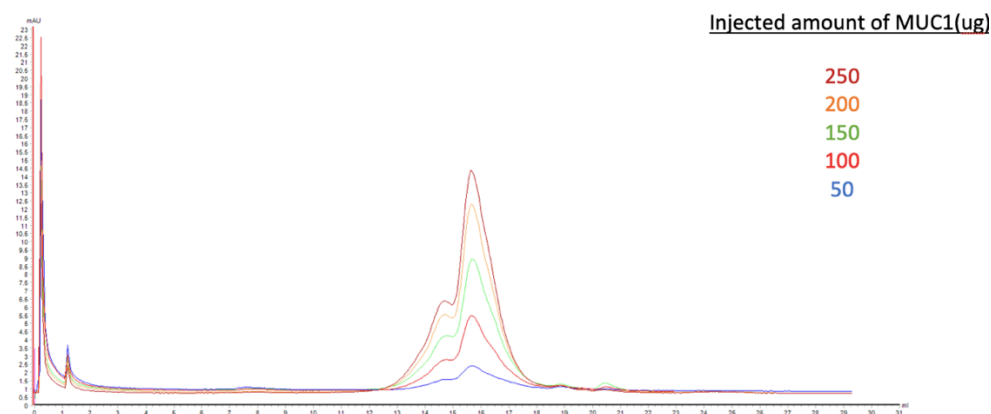
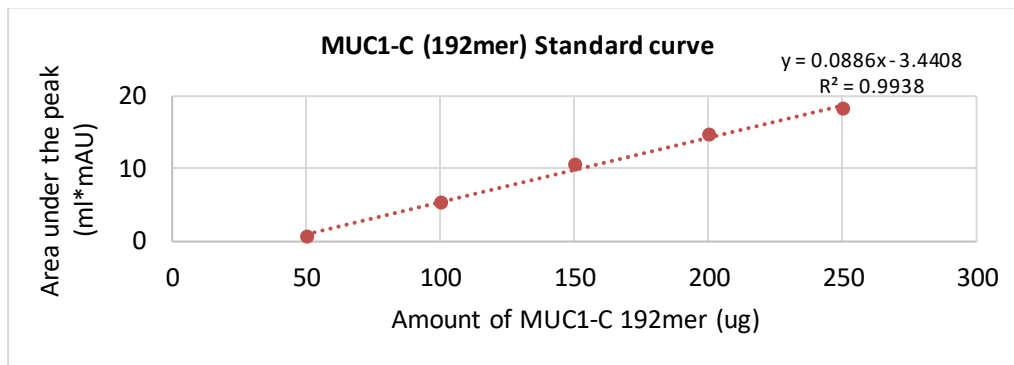


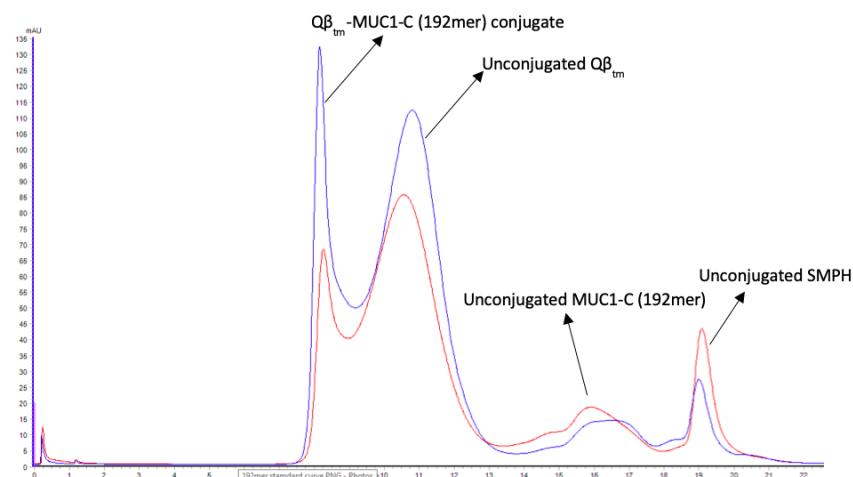
**Figure 22. Characterization of Q $\beta$ -MUC1-C (192mer) vaccine construct.** a) Calibration curve of MUC1-C (192mer) by using FPLC-SEC and calculating area under the peak for each peak corresponding to a known amount of MUC1-C (192mer) injected into the column b) FPLC-SEC analysis of Q $\beta$ -MUC1-C (192mer) conjugate mixture consisting of unconjugated Q $\beta$  (14 kDa), unconjugated MUC1-C 192mer (22 kDa) and unconjugated SMPH linker along with the Q $\beta$ -MUC1-C (192mer) conjugate.

**Figure 22 (cont'd)**

a.



b.



### 3.2.3 Immunization of MUC1.Tg mice with Q $\beta$ -MUC1-C (58mer and 192mer) elicited strong antibody responses

MUC1 transgenic (Tg) mice (n=4-5) were immunized subcutaneously with the Q $\beta$ -MUC1-C (58 mer and 192 mer) using one primer plus 2 booster injections, 2 weeks apart (**Fig. 23a**). Each dose contained 0.83 nmol dosage for the MUC1-C (58mer) and 0.27 nmol dosage for MUC1-C (192mer) with monophosphoryl lipid A (MPLA) as an adjuvant. On day 35 after the initial injection (1 week after the 2<sup>nd</sup> booster), blood was collected from mice to harvest serum followed by ELISA analysis of the IgG antibody titers. The ELISA plates were coated with MUC1-C (58mer) for anti-MUC1-C (58mer) IgG response and MUC1-C (192mer) for anti-MUC1-C (192mer) IgG response.

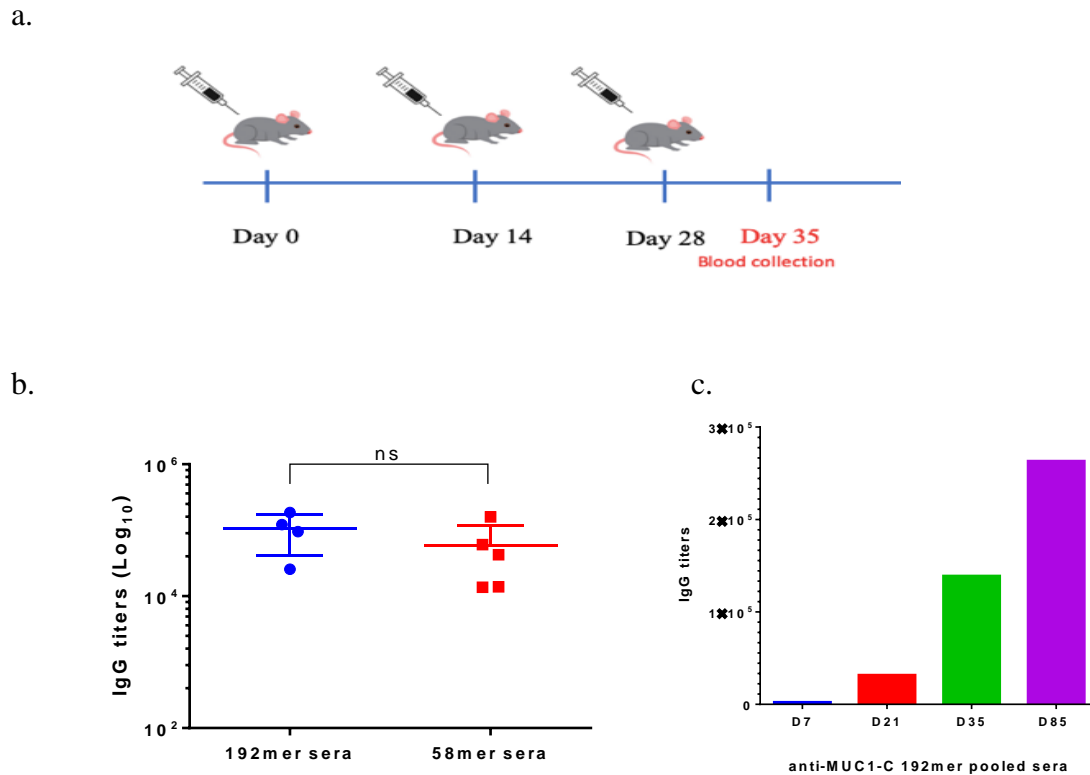


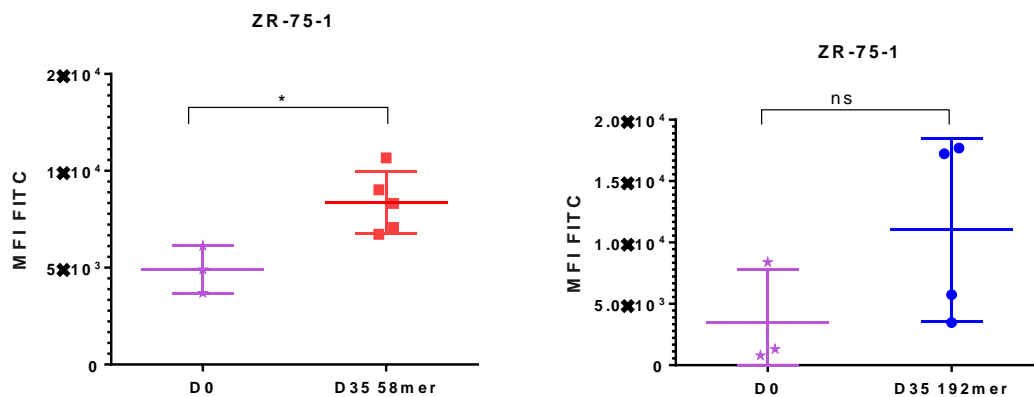
**Figure 23. Immunization protocol and assessment of anti-MUC1-C antibody in mice.** a) Schematic representation of the immunization protocol for C57BL/6 mice (n=4-5) using Q $\beta$ -MUC1-C (58 mer and 192 mer) vaccine constructs. Mice were vaccinated on days 0, 14 and 28 with 0.43 nmol MUC1-C (58 mer and 192 mer) per dose using MPLA adjuvant. Blood was collected on from mice injected with both vaccine constructs on days 0, 7, 21, 35 and on day 85 post-immunization for mice injected with Q $\beta$ -MUC1-C (192 mer) vaccine. b) Anti-MUC1-C (58 mer and 192 mer) IgG titers of different vaccine groups on day 35 post-immunization. c) Persistence of antibody titers for mice injected with Q $\beta$ -MUC1-C (192mer) vaccine.

As shown in **Fig. 23b**, both Q $\beta$ -MUC1-C (192 mer and 58 mer) vaccine constructs elicited robust IgG responses, averaging  $1.4 \times 10^5$  and  $7.5 \times 10^4$  ELISA units, respectively. The persistence of IgG antibody responses elicited by Q $\beta$ -MUC1-C (192 mer) vaccine was monitored over time (**Fig. 23c**). On day 85 post-immunization, the average anti-MUC1-C (192 mer) IgG titer was  $2.6 \times 10^5$  ELISA units (**Fig. 23b**). These results suggested that the MUC1-C vaccines were successfully able to generate long-lasting plasma cells capable of continuous production of anti-MUC1-C antibodies.

### 3.2.4 Antibodies induced by Q $\beta$ -MUC1-C (58 mer and 192 mer) vaccine elicited binding to MUC1-expressing cancer cells

In the next step, the binding ability of the anti-MUC1-C (192 mer and 58 mer) antibodies was tested with MUC1-positive (ZR-75-1) and MUC1-negative (MDA-MB-231) tumor cells through FACS analysis *in vitro* (Fig. 24). For ZR-75-1 cells, anti-MUC1-C (58mer) antibodies bound significantly higher to ZR-75-1 tumor cells than pre-immunized sera (D0) whereas anti-MUC1-C(192mer) antibodies produced non-significant binding to ZR-75-1 cells. As a control, MUC1-negative MDA-MB-231 cells were used and anti-MUC1-C (58 mer and 192 mer) antibodies had minimal binding as compared to pre-immune sera.

a.



b.

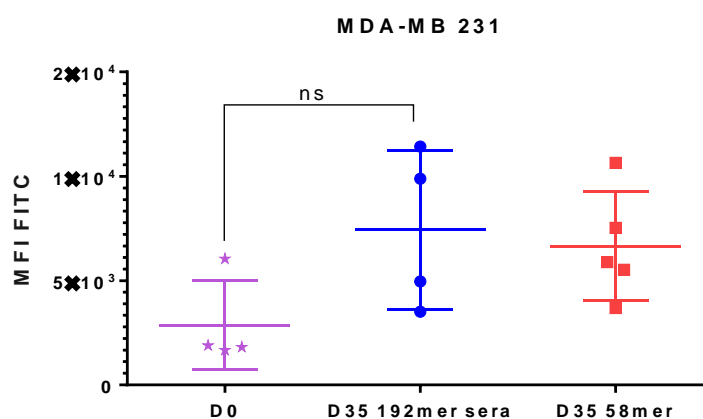


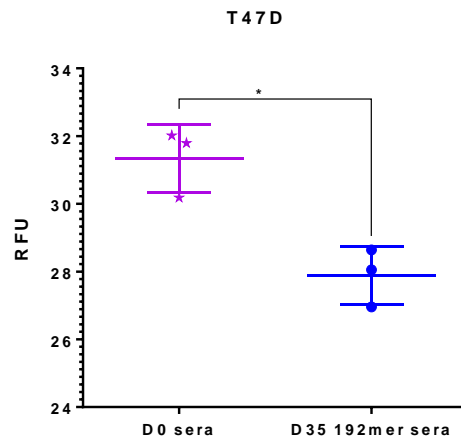
**Figure 24. Results for flow cytometry analysis of cell binding by post-immune sera (day 35) elicited by mice receiving Q $\beta$ -MUC1-C (58mer and 192mer) vaccine constructs.** a) MUC1-positive ZR-75-1 cells. b) MUC1-negative MDA-MB-231 cells. Statistical significance was determined by two-tailed unpaired Student's t-test using GraphPad Prism, ns:  $p > 0.05$ ; \* $p < 0.05$ . Each symbol represents one mouse ( $n = 3-5$  mice for each group).

Even though the post-immune sera (D35) for both MUC1-C vaccines produced similar IgG titers (**Fig. 23b**), the FACS analysis results showed that only anti-MUC1-C (58 mer) antibodies in the post-immune sera (D35) had significantly higher binding to MUC1-positive cells than pre-immune sera (D0). This was due to the dispersion of mean fluorescence intensity (MFI) within the group of mice with anti-MUC1-C (192mer) antibodies. The average MFI for mice immunized with Q $\beta$ -MUC1-C (192mer) was higher than that of Q $\beta$ -MUC1-C (58mer). This demonstrated that both MUC1-C (58 mer and 192 mer) epitopes showed promises in binding to MUC1-expressing cell lines.

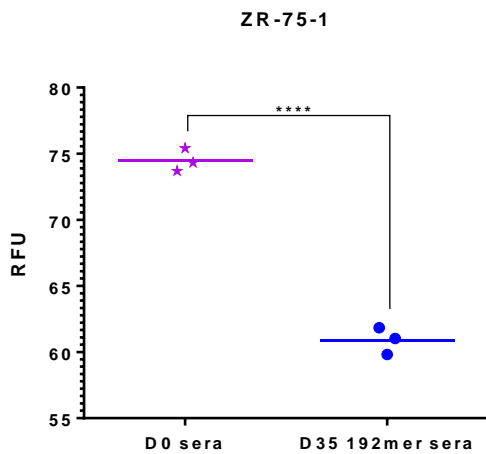
### **3.2.5 Anti-MUC1-C (192 mer and 58 mer) antibodies strongly inhibited invasive activity of MUC1-expressing cancer cells**

MUC1-C domain is known to regulate the metastatic invasion by cancerous cells.<sup>24</sup> MUC1-C (192 mer) epitope was investigated for its role in cancer cell invasion assay by utilizing MUC1-expressing tumor cells in an invasion chamber setting. Antibodies elicited from Q $\beta$ -MUC1-C (192 mer) vaccine (D35 192 mer sera) successfully displayed high levels of migration inhibition for MUC1-positive cells (ZR-75-1 and T47D; **Fig. 25a, b**). In contrast, the antibodies did not exhibit any significant effects on MUC1-negative cells (MDA-MB-231; **Fig. 25c**) when compared with pre-immunized sera (D0 sera) highlighting the important role MUC1 plays in this assay.

a.



b.



c.

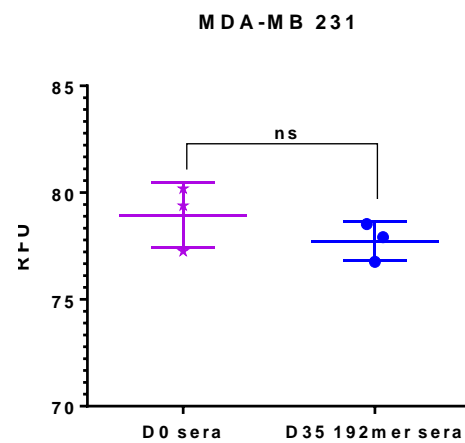


**Figure 25. Evaluation of metastatic activity of anti-MUC1-C (192 mer) antibodies in-vitro Matrigel invasion assay.** A suspension of  $0.3 \times 10^6$  cells/well was incubated with pooled pre-immunized (D0) and post-immunization (D35 sera) for 24-48h at 37 °C in 5% CO<sub>2</sub>. The fluorescence of the cells that migrated to the lower chamber containing CyQuant GR dye was read at 480nm/520nm. a) MUC1-positive T47D cells. b) MUC1-positive ZR-75-1 cells. c) MUC1-negative MDA-MB-231 cells. Statistical significance was determined by two-tailed unpaired Student's t-test using GraphPad Prism, \* $p < 0.05$ , \*\*\*\* $p < 0.0001$ . Each symbol represents one mouse (n = 3 technical replicates).

### 3.3 Conclusion

The Q $\beta$ -MUC1-C (58mer and 192mer) vaccines when administered to MUC1.Tg mice yielded high and robust anti-MUC1-C IgG antibody response as determined through ELISA. The IgG titers of  $2.6 \times 10^5$  ELISA units on day 85 post-immunization depicted the long-lasting antibody response elicited by Q $\beta$ -MUC1-C (192mer) vaccine. Both MUC1-C vaccines elicited similar IgG titers (D35 titers) but the antibodies obtained from Q $\beta$ -MUC1-C (58mer) vaccine

produced a significantly higher cellular binding to MUC1-expressing tumor cells when compared with pre-immunized sera (D0). Even though the cellular binding for anti-MUC1-C (58mer and 192mer) antibodies as evaluated by FACS for ZR-75-1 cells were similar but anti-MUC1-C (192mer) antibodies in 50% of the treated mice did not produce any significant binding compared to D0 sera. Alternatively, the anti-MUC1-C (192mer) displayed successful inhibition of metastatic invasion by MUC1-expressing tumor cells through cell invasion assay (CIA). These results are encouraging and show that these epitopes have the potential to be anti-metastatic therapeutic candidates. However, the results are still preliminary, which will require a broader range of cell lines to be explored for cellular binding experiments. Additionally, the results obtained from un-glycosylated MUC1-C (58mer and 192mer) epitopes provided a strong foundation to explore the glycosylated versions of these MUC1-C proteins.

### **3.4 Materials and Methods**

#### **3.4.1 Reagents and instruments**

All chemicals were reagent grade and used as received from the manufacturer unless otherwise noted. The plasmids for MUC1-C 58mer and MUC1-C 192mer were purchased from GenScript. The cell lysis detergent, DNase I and lysozyme were purchased from Sigma. Protease inhibitor cocktail was purchased from Roche and cobalt his-tagged resin from Takara Bio. Cell invasion assay kit (CBA-111-T) was purchased from Cell Biolabs. Centrifugal filter units of 3,000 10,000 and 100,000 molecular weight cut-off (MWCO) were purchased from EMD Millipore

#### **3.4.2 Cell lines**

All cell lines were purchased from American type culture collection (ATCC). T47D cells were cultured in DMEM supplemented with 10% FBS, 100 U/mL/100 µg/mL Pen/Step, 2 mM L-glutamine, 1 mM sodium pyruvate. ZR-75-1 cells were cultured in RPMI-1640 supplemented with 10% FBS, 100 U/mL/100 µg/mL Pen/Step, 2 mM L-glutamine, 1 mM

sodium pyruvate. These cell lines were maintained in a humidified incubator at 37°C in a 5% CO<sub>2</sub>, 95% air atmosphere. MDA-MB-231 cells were cultured in Leibovitz medium (L15) supplemented with 10% FBS, 100 U/mL/100 µg/mL Pen/Step, 2 mM L-glutamine, 1 mM sodium pyruvate. This cell line was maintained in a humidified incubator at 37°C in a 0% CO<sub>2</sub>.

### **3.4.3 MUC1-C (58mer and 192mer) expression**

For MUC1-C(58mer)-Histag-Cysteine (N-1098-1155-C), DNA encoding residues N-1098-1155-C of human MUC1 (SWISS PROT entry P15941) was inserted into the pET-28a(+)-TEV vector. The plasmid was transformed into BL21 (DE3) competent cells for *E.coli* bacteria over-expression. Multiple colonies of BL21(DE3) *E.coli* cells were grown on LB-agar plates with 20µg/mL kanamycin antibiotic for MUC1-C 58mer. DNA encoding for MUC1-C 192mer (N-961-1152-C) was inserted into pET30a vector that was expressed in BL21 Star™ (DF3) *E.coli* cells. Multiple colonies of bacterial cells were grown with 25µg/mL each of chloramphenicol and ampicillin for MUC1-C 192mer. The expression, lysis and purification protocols were the same for both MUC1-C 192mer and 58mer proteins. A single bacterial colony was selected to inoculate a 25 mL starting culture of Super Optimal Broth (SOB) media containing 20 µg/mL kanamycin. The starter culture was incubated overnight at 37°C, 220 rpm. The following morning, the cloudy starter culture was transferred into 1L SOB culture medium with 20 µg/mL kanamycin and cultured at 37°C, 220 rpm until the OD<sub>600</sub> was between 1.5-1.7. At that point, 1 mL of 1M isopropyl β-D-1-thiogalactopyranoside (IPTG) was added to induce protein expression and cultured overnight at 30°C, 220 rpm. Cells were then pelleted at 12,000 rcf for 30 min, culture media discarded and pelleted cells were re-suspended in 30 mL 50 mM potassium phosphate (KPB) buffer with 0.2 mM NaCl pH 8 and stored at -80°C until lysis.

### **3.4.4 Lysis of cells expressing MUC1-C (192mer and 58mer)**

Cells collected after IPTG induced protein expression were lysed by adding 1X cell lytic buffer. Volume of 1X cell lytic buffer is 1.5X per gram of the pellet. Lysozyme (2 mg/mL final

concentration) and protease inhibitor cocktail (one tablet in water makes 7X concentration; use 0.5X for final concentration) was added. The cell paste was gently mixed with a spatula to avoid any foaming and sonicated with a probe sonicator in a iced water beaker for 20 min with pulsation. After sonication, the cell paste was stirred while adding 100  $\mu$ L Dnase I (5000 U) for 20 min at 4°C. Lysed cells were centrifuged at 20,000 rcf for 30 min using a Fiberlite F21-8x50y at 4°C and the supernatant with the capsid protein was collected into a 50 mL centrifuge tube. The resultant pellet was washed thrice with 20mL of 50 mM KPB with 0.2 M NaCl buffer and all three wash-fractions were pooled together and filtered through 0.45 micron syringe filter. The leftover cell pellet was then digested overnight by using 6M guanidine chloride in 50 mM KPB with 0.2 M NaCl at 4°C. The cell paste was stirred with 500 U of DNase I similar to previous lysis and washed similarly with KPB and the lysates were pooled and then subjected to affinity column purification as described below.

### **3.4.5 MUC1-C (192mer and 58mer) Purification**

The pooled lysates were incubated with 5 mL cobalt his-tagged resin pre-washed with 5 column-volume of 50 mM KPB buffer for 2h at 4°C The mixture was then transferred to a column and the flow through was collected and analyzed for unbound proteins later. The column was washed with 20 column volumes of 50 mM KPB buffer and then subjected to gradient elution (1 mM, 10 mM, 20 mM and 150 mM imidazole in 50 mM KPB with 0.2M NaCl. MUC1-C was eluted at 150 mM imidazole and 1 mL aliquots (25 mL final volume) were collected and concentrated using (3,000 MW cut-off) centrifuge filters. Protease inhibitor was added to the protein to prevent degradation during storage. The eluted fractions and the flow-through was analyzed by SDS-PAGE stained with Coomassie and western blot using anti-his antibody against the histag. For MUC1-C (58mer), the yield was 1 mg/L of broth and the yield for MUC1-C (192mer) was 10 mg/L of the broth.

### 3.4.6 Synthesis of Q $\beta$ -MUC1-C (58mer and 192mer) vaccine

Q $\beta$  (5 mg, 0.5 mL) capsid protein was oxidized using hydrogen peroxide (0.015 mL from 30% stock solution) for 30 min at room temperature and the excess hydrogen peroxide was removed by washing oxidized Q $\beta$  in the 0.1 M KPB, pH 8 buffer. Oxidized Q $\beta$  was functionalized with the SMPH linker (100 mg/ mL in DMSO; 30X molar ratio) in 0.1M KPB, pH 8 for 1h at room temperature. Excess SMPH was removed by a buffer exchange (5 x 0.5 mL) with centrifuge filters (30,000 MW cut-off). Simultaneously, purified MUC1-C (58mer and 192mer) was reduced using TCEP immobilized beads for 1h on a rotator at room temperature. Immediately after the reduction reaction, MUC1-C (58mer and 192mer) was added to Q $\beta$ -SMPH. For Q $\beta$ -MUC1-C (58mer) vaccine, 5 eq. of TCEP-reduced MUC1-C per surface accessible amine was utilized. For Q $\beta$ -MUC1-C (192mer) vaccine, 0.11 eq. of TCEP-reduced MUC1-C per surface accessible amine was utilized.

### 3.4.7 Immunization Studies

All animal care procedures and experimental protocols were approved by the Michigan State University Institutional Animal Care and Use Committee (IACUC). Five MUC1.Tg 7-10-week female mice were used for *in-vivo* studies for each Q $\beta$ -MUC1-C (58mer and 192mer) vaccine. Mice were subcutaneously injected at the scruff with 0.83 nmol dosage of MUC1-C 58mer (0.006 mg, 0.016 mL from 0.92 mg/mL Q $\beta$ -MUC1-C in 0.1 M KPB) and 0.27 nmol dosage of MUC1-C 192mer (0.006 mg, 0.007 mL, 2.2 mg/mL Q $\beta$ -MUC1-C in 0.1 M KPB) per injection. The total volume of each injection was 0.2 mL per construct that included monophosphoryl lipid A (MPLA; 0.02 mg, 0.02 mL from 1 mg/mL MPLA in DMSO) as the adjuvant on day 0 plus booster injections given subcutaneously on days 14 and 28. Serum samples were collected on days 0 (before immunization), 7, 21, and 35. For mice injected with Q $\beta$ -MUC1-C (192mer), additional blood was collected on day 85 to monitor the persistence of antibody response. The IgG antibody titers were evaluated by enzyme-linked immunosorbent

assay (ELISA).

### **3.4.8 Evaluation of antibody titers by ELISA**

A Nunc MaxiSorp® flat-bottom 96-well plate was coated with MUC1-C protein (10 µg/mL, 100 µL/well) in NaHCO<sub>3</sub>/Na<sub>2</sub>CO<sub>3</sub>/NaN<sub>3</sub> coating buffer (0.05 M, pH 9.6) and incubated overnight at 4°C. The coated plate was washed 4 times with PBS/0.5% Tween-20 (PBST), followed by addition of 1% (w/v) BSA in PBS to each well and incubated at room temperature for 1h. The plate was washed again 4 times with PBST (4 x 200 µL). Serial dilutions of mouse sera in 0.1% BSA/PBS (100 µL) were added to each well and incubated for 2 h at 37°C. Wells were then washed with PBST (4 × 200 µL) and a 1:2,000 dilution of HRP-conjugated goat anti-mouse IgG (Jackson ImmunoResearch Laboratory catalog # 115-005-062) in 0.1% BSA/PBS (100 µL) was added to each well and incubated for 1 h at 37°C. Enzymatic substrate was prepared by dissolving 3,3',5,5'-tetramethylbenzidine (TMB, 5 mg) in DMSO (2 mL) and citric acid buffer (18 mL) in a 50 mL centrifuge tube covered with aluminum foil. H<sub>2</sub>O<sub>2</sub> (20 µL) was added and vortexed to homogeneity. The plate was washed with PBST (4 × 200 µL) and enzymatic substrate was added (200 µL). Color was allowed to develop for 15 min, and then 0.5 M H<sub>2</sub>SO<sub>4</sub> (50 µL) was added to quench the reactions. Absorbance was measured at 450 nm using a microplate reader (BioRad). Titers were determined by regression analysis with log<sub>10</sub> dilution plotted against optical density. The titer was reported as the highest fold dilution giving an optical absorbance value of 0.1 over pre-immune control sera (OD = 0.2). Samples were tested in triplicate.

### **3.4.9 Detection of cellular binding of anti-MUC1-C (192mer and 58mer) antibodies to tumor cells by FACS**

ZR-75-1 cells and MDA-MB-231 cells were cultured respectively till 80% confluency at 37 °C under 5% CO<sub>2</sub> in cell growth medium. The mixture of cells was detached using 0.25% trypsin followed by incubation at 37 °C under 5% CO<sub>2</sub> for 5 min. The cell growth medium was

transferred to a conical centrifuge tube, and centrifuged at 1,600 rpm for 5 min at 4 °C. The pellet was re-suspended in growth medium (10 mL). The number of cells was determined using a haemocytometer. The cells were transferred based on requirement of the experiment with the recommended cell number between  $0.35 \times 10^6$  -  $0.5 \times 10^6$  cells. The cells were resuspended in 2 mL of 1X PBS and viability dye (Live/Dead blue) was added at 1/1000 dilution. The cells were incubated on ice in dark for 30 min. The cells were then diluted to 10 mL of FACS buffer (1% FBS, 0.1% NaN<sub>3</sub> in 1X PBS, pH 7.4) and centrifuged at 1,600 rpm for 5 min at 4 °C. The pellet was washed twice with FACS buffer and then resuspended in FACS buffer such that each well in the V-bottom 96 well plate received the required number of cells in 95 µL of volume. The cells were incubated with 1:20 dilution of mouse sera (5 µL) in FACS buffer for 30 min on ice. The incubated cells were washed twice with FACS buffer, followed by incubation with 1/50 dilution of FITC conjugated goat anti-mouse IgG (minimal x-reactivity) antibody for 30 min. The cells were washed thrice and were fixed with 4% formalin in 1X PBS for 10 min at room temperature. The fixed cells were washed thrice with FACS buffer and then re-suspended in FACS buffer and analyzed by Cytex Aurora. Data was processed by FlowJo software.

#### **3.4.10 Migration inhibition of MUC1-expressing cells by anti-MUC1-C (192mer) antibodies in fluorometric cell invasion assay**

The cell invasion assay protocol was adapted from CytoSelect™ 24-well cell invasion assay (basement membrane, fluorometric format; CBA-111-T). The Matrigel basement membrane in the upper compartment was warmed up at room temperature for 10 min before rehydrating it. After rehydrating it for 1h at room temperature with 0.3 mL of serum free media (DMEM containing 0.5% BSA, 2 mM CaCl<sub>2</sub> and 2 mM MgCl<sub>2</sub>)  $3 \times 10^5$  cells (T47D, ZR-75-1 and MDA-MB-231) in 0.3 mL were seeded directly onto the Matrigel-coated inserts. The cells were incubated with sera containing anti-MUC1-C (192mer) antibodies post-immunization (D35) and pre-immunized sera (D0) with 1:20 dilution in the upper compartment. The lower compartment contained medium supplemented with 10% FBS. After 48h incubation, the

invasive cells passed through the Matrigel basement membrane to the lower compartment after being dissociated by the addition of cell detachment buffer. The number of invasive cells passing through the membrane into the lower chamber was quantified using CyQuant® GR Fluorescent Dye. Technical replicates were taken.

## REFERENCES

- (1) Kufe, D.; Inghirami, G.; Abe, M.; Hayes, D.; Justi-Wheeler, H.; Schlom, J. Differential reactivity of a novel monoclonal antibody (DF3) with human malignant versus benign breast tumors. *Hybridoma* **1984**, *3* (3), 223-232. DOI: 10.1089/hyb.1984.3.223.
- (2) Brockhausen, I.; Yang, J. M.; Burchell, J.; Whitehouse, C.; Taylor-Papadimitriou, J. Mechanisms underlying aberrant glycosylation of MUC1 mucin in breast cancer cells. *Eur J Biochem* **1995**, *233* (2), 607-617. DOI: 10.1111/j.1432-1033.1995.607\_2.x.
- (3) Zhang, S.; Graeber, L. A.; Helling, F.; Ragupathi, G.; Adluri, S.; Lloyd, K. O.; Livingston, P. O. Augmenting the immunogenicity of synthetic MUC1 peptide vaccines in mice. *Cancer Res* **1996**, *56* (14), 3315-3319.
- (4) Xing, P.; Michael, M.; Apostolopoulos, V.; Prenzoska, J.; Marshall, C.; Bishop, J.; McKenzie, I. Phase-I study of synthetic muc1 peptides in breast-cancer. *Int J Oncol* **1995**, *6* (6), 1283-1289. DOI: 10.3892/ijo.6.6.1283.
- (5) Schettini, J.; Kidiyoor, A.; Besmer, D. M.; Tinder, T. L.; Roy, L. D.; Lustgarten, J.; Gendler, S. J.; Mukherjee, P. Intratumoral delivery of CpG-conjugated anti-MUC1 antibody enhances NK cell anti-tumor activity. *Cancer Immunol Immunother* **2012**, *61* (11), 2055-2065. DOI: 10.1007/s00262-012-1264-y.
- (6) Oei, A. L.; Moreno, M.; Verheijen, R. H.; Sweep, F. C.; Thomas, C. M.; Massuger, L. F.; von Mensdorff-Pouilly, S. Induction of IgG antibodies to MUC1 and survival in patients with epithelial ovarian cancer. *Int J Cancer* **2008**, *123* (8), 1848-1853. DOI: 10.1002/ijc.23725.
- (7) Apostolopoulos, V.; Pietersz, G. A.; Tsibanis, A.; Tsikkinis, A.; Drakaki, H.; Loveland, B. E.; Piddlesden, S. J.; Plebanski, M.; Pouniotis, D. S.; Alexis, M. N.; et al. Pilot phase III immunotherapy study in early-stage breast cancer patients using oxidized mannan-MUC1 [ISRCTN71711835]. *Breast Cancer Res* **2006**, *8* (3), R27. DOI: 10.1186/bcr1505.
- (8) Wu, X.; Yin, Z.; McKay, C.; Pett, C.; Yu, J.; Schorlemer, M.; Gohl, T.; Sungsuwan, S.; Ramadan, S.; Baniel, C.; et al. Protective Epitope Discovery and Design of MUC1-based Vaccine for Effective Tumor Protections in Immunotolerant Mice. *J Am Chem Soc* **2018**, *140* (48), 16596-16609. DOI: 10.1021/jacs.8b08473.
- (9) de Bono, J. S.; Rha, S. Y.; Stephenson, J.; Schultes, B. C.; Monroe, P.; Eckhardt, G. S.; Hammond, L. A.; Whiteside, T. L.; Nicodemus, C. F.; Cermak, J. M.; et al. Phase I trial of a murine antibody to MUC1 in patients with metastatic cancer: evidence for the activation of humoral and cellular antitumor immunity. *Ann Oncol* **2004**, *15* (12), 1825-1833. DOI: 10.1093/annonc/mdh472.
- (10) Carmon, L.; Avivi, I.; Kovjazin, R.; Zuckerman, T.; Dray, L.; Gatt, M. E.; Or, R.; Shapira, M. Y. Phase I/II study exploring ImMucin, a pan-major histocompatibility complex, anti-MUC1 signal peptide vaccine, in multiple myeloma patients. *Br J Haematol* **2015**, *169* (1), 44-56. DOI: 10.1111/bjh.13245.
- (11) Ibrahim, N. K.; Yariz, K. O.; Bondarenko, I.; Manikhas, A.; Semiglazov, V.; Alyasova, A.; Komisarenko, V.; Shparyk, Y.; Murray, J. L.; Jones, D.; et al. Randomized phase II trial of

letrozole plus anti-MUC1 antibody AS1402 in hormone receptor-positive locally advanced or metastatic breast cancer. *Clin Cancer Res* **2011**, *17* (21), 6822-6830. DOI: 10.1158/1078-0432.CCR-11-1151.

(12) Ramasamy, S.; Duraisamy, S.; Barbashov, S.; Kawano, T.; Kharbanda, S.; Kufe, D. The MUC1 and galectin-3 oncoproteins function in a microRNA-dependent regulatory loop. *Mol Cell* **2007**, *27* (6), 992-1004. DOI: 10.1016/j.molcel.2007.07.031.

(13) Raina, D.; Kosugi, M.; Ahmad, R.; Panchamoorthy, G.; Rajabi, H.; Alam, M.; Shimamura, T.; Shapiro, G. I.; Supko, J.; Kharbanda, S.; et al. Dependence on the MUC1-C oncoprotein in non-small cell lung cancer cells. *Mol Cancer Ther* **2011**, *10* (5), 806-816. DOI: 10.1158/1535-7163.MCT-10-1050.

(14) Ahmad, R.; Raina, D.; Joshi, M. D.; Kawano, T.; Ren, J.; Kharbanda, S.; Kufe, D. MUC1-C oncoprotein functions as a direct activator of the nuclear factor-kappaB p65 transcription factor. *Cancer Res* **2009**, *69* (17), 7013-7021. DOI: 10.1158/0008-5472.CAN-09-0523.

(15) Kufe, D. W. MUC1-C oncoprotein as a target in breast cancer: activation of signaling pathways and therapeutic approaches. *Oncogene* **2013**, *32* (9), 1073-1081. DOI: 10.1038/onc.2012.158.

(16) Jochems, C.; Tucker, J. A.; Vergati, M.; Boyerinas, B.; Gulley, J. L.; Schlom, J.; Tsang, K. Y. Identification and characterization of agonist epitopes of the MUC1-C oncoprotein. *Cancer Immunol Immunother* **2014**, *63* (2), 161-174. DOI: 10.1007/s00262-013-1494-7.

(17) Raina, D.; Ahmad, R.; Joshi, M. D.; Yin, L.; Wu, Z.; Kawano, T.; Vasir, B.; Avigan, D.; Kharbanda, S.; Kufe, D. Direct targeting of the mucin 1 oncoprotein blocks survival and tumorigenicity of human breast carcinoma cells. *Cancer Res* **2009**, *69* (12), 5133-5141. DOI: 10.1158/0008-5472.CAN-09-0854.

(18) Mahanta, S.; Fessler, S. P.; Park, J.; Bamdad, C. A minimal fragment of MUC1 mediates growth of cancer cells. *PLoS One* **2008**, *3* (4), e2054. DOI: 10.1371/journal.pone.0002054.

(19) Panchamoorthy, G.; Jin, C.; Raina, D.; Bharti, A.; Yamamoto, M.; Adeebge, D.; Zhao, Q.; Bronson, R.; Jiang, S.; Li, L.; et al. Targeting the human MUC1-C oncoprotein with an antibody-drug conjugate. *JCI Insight* **2018**, *3* (12). DOI: 10.1172/jci.insight.99880.

(20) Kim, M. J.; Choi, J. R.; Tae, N.; Wi, T. M.; Kim, K. M.; Kim, D. H.; Lee, E. S. Novel Antibodies Targeting MUC1-C Showed Anti-Metastasis and Growth-Inhibitory Effects on Human Breast Cancer Cells. *Int J Mol Sci* **2020**, *21* (9). DOI: 10.3390/ijms21093258.

(21) Wu, G.; Kim, D.; Kim, J. N.; Park, S.; Maharjan, S.; Koh, H.; Moon, K.; Lee, Y.; Kwon, H. J. A Mucin1 C-terminal Subunit-directed Monoclonal Antibody Targets Overexpressed Mucin1 in Breast Cancer. *Theranostics* **2018**, *8* (1), 78-91. DOI: 10.7150/thno.21278.

(22) Chugh, S.; Swenson, C.; Yuzbasiyan-Gurkan, V.; Huang, X. Design and Synthesis of Bovine Leukemia Virus-Associated Peptide-Based Q $\beta$  Conjugate Eliciting Long-Lasting Neutralizing Antibodies in Mice. *ACS Infect Dis* **2022**, *8* (5), 1031-1040. DOI: 10.1021/acsinfecdis.2c00001.

(23) Sungsuwan, S.; Wu, X.; Shaw, V.; Kavunja, H.; McFall-Boegeman, H.; Rashidijahanabad, Z.; Tan, Z.; Lang, S.; Tahmasebi Nick, S.; Lin, P.-h.; et al. Structure Guided Design of Bacteriophage Q $\beta$  Mutants as Next Generation Carriers for Conjugate Vaccines. *ACS Chem. Biol.* **2022**, in press. DOI: 10.1021/acscchembio.1c00906.

(24) Geng, Y.; Yeh, K.; Takatani, T.; King, M. R. Three to Tango: MUC1 as a Ligand for Both E-Selectin and ICAM-1 in the Breast Cancer Metastatic Cascade. *Front Oncol* **2012**, 2, 76. DOI: 10.3389/fonc.2012.00076.

## **Chapter 4 Design and Synthesis of Bovine Leukemia Virus Associated Peptide Based Q $\beta$ Conjugate Eliciting Long-lasting Neutralizing Antibodies in Mice**

Reprinted (adapted) with permission from {Chugh, S.; Swenson, C.; Yuzbasiyan-Gurkan, V.; Huang, X. Design and Synthesis of Bovine Leukemia Virus-Associated Peptide-Based Q $\beta$  Conjugate Eliciting Long-Lasting Neutralizing Antibodies in Mice. *ACS Infect Dis* **2022**, 8 (5), 1031-1040. DOI: 10.1021/acsinfecdis.2c00001}. Copyright {2023} American Chemical Society.

### **4.1 Introduction**

Bovine leukemia virus (BLV), a C-type retrovirus of dairy and beef cattle, is a major worldwide infectious disease that adversely impacts animal health and well-being, resulting in huge financial losses for producers. The National Animal Health Monitoring System (NAHMS) estimated that BLV is present in 89% of US dairy operations.<sup>1</sup> Canada, South America, and China also have reported similar BLV prevalences.<sup>2-4</sup> BLV causes enzootic bovine leukosis including frequent persistent lymphocytosis and less commonly, lymphoma. Transmission is horizontal *via* contaminated equipment or biting insects and cow to calf<sup>5</sup> transfer can occur by introduction of infected blood or milk lymphocytes. The prevalence of BLV infection is exacerbated by poor cattle management practices.<sup>6</sup> Although severe outward symptoms are uncommon, BLV-infected cattle experience increased infections and impaired immunity.<sup>7</sup> The resultant decreased milk production, reduced life-expectancy, and increased risk of carcass condemnation at slaughter due to lymphoma or other co-infections and diseases causes an estimated \$285 million loss to the dairy industry and a \$240 million cost increase for consumers.<sup>8</sup> In addition, BLV DNA was found at higher frequencies in premalignant and cancerous breast samples (38% and 59% respectively) compared to normal breast tissue (29%), suggesting there may be an association between BLV and human breast cancer.<sup>9, 10</sup> These reports raise concerns amongst consumers.

A variety of methods have been used in efforts to reduce the spread of BLV within a herd, which include segregation of infected cattle from non-infected animals, adopting other laborious and time-consuming practices like single use of disposable syringes, needles and

obstetrical sleeves, sterilization following each use of equipment, or increasing fly control measures. In contrast, over 21 nations eradicated BLV decades ago by culling cattle that tested BLV-positive when the prevalence of infection was low. Due to the current escalated prevalence of BLV infection in US cattle, a herd-wide test then cull approach is no longer economically realistic.<sup>11</sup>

Vaccines against BLV have been explored. Compared to other retroviruses like HIV, the BLV genome is highly stable, especially within the envelope protein sequence.<sup>12</sup> Past efforts to develop vaccines<sup>13</sup> utilizing attenuated provirus and recombinant vaccinia virus (RVV) were fraught with limitations including risk of infection or recombination (live attenuated virus) as well as inadequate protection after BLV challenge (RVV-*env*).<sup>14</sup> Viral subunits or synthetic peptide epitopes have been investigated as alternative immunogens to modified virus. Viral peptides have increased safety, without risk of vaccine-induced infection or recombination with endogenous or exogenous viruses. However, to date, peptide-based vaccines have performed poorly due to insufficient<sup>15</sup> or rapidly declining antibody responses.<sup>16,17</sup> Therefore, an innovative and effective vaccine that provides long-term protection without risk of iatrogenic infection is long overdue.

Herein we report a novel synthetic peptide-vaccine candidate against BLV that eliminates previous barriers such as nominal immunogenicity, rapid waning of vaccine-induced immunity, and risk of infection caused by the vaccine. The immunogenicity of the selected antigen was enhanced by engineering a peptide-antigen to conjugate with the mutant bacteriophage Q $\beta$  (mQ $\beta$ ) carrier with a well-organized 3-dimensional structure. The peptide-antigen investigated in this work was derived from the BLV gp51 envelope protein, which is composed of surface glycoprotein subunits anchored to the core via transmembrane subunits.<sup>18</sup> Membrane glycoprotein gp51 is directly implicated in virus infectivity because a portion of the gp51-peptide (amino acid residues 177-192) present in one of the loops located at the top of the

gp51 “head”, is an accessible antigenic target and potential BLV-receptor binding site.<sup>19</sup>

## 4.2 Results and Discussion

### 4.2.1 Evaluating antigenicity of gp51-peptide epitope using BLV-infected cattle sera

Residues 177-192 of the gp51 envelope protein located at the putative receptor binding site (highlighted as the red star in **Fig. 26a**), is a relevant epitope for vaccine design.<sup>19,20</sup> It has been reported that the 177-192 residues stimulate T cell proliferation and antibodies directed against this sequence inhibit syncytium formation, supporting roles for cell-mediated and humoral immunity.<sup>20</sup> For our vaccine study, two modifications to this peptide sequence were incorporated: 1) addition of a glycine residue to the *N*-terminus to facilitate bio-conjugation; and 2) installation of an amide moiety at the C-terminus to eliminate potential interference in antibody response from a free C-terminus.<sup>21</sup> These considerations led to the peptide sequence, GPDCAICWEPSPPWAPE-NH<sub>2</sub> (**1**) for our vaccine study. Antigenicity of peptide **1** was evaluated by enzyme-linked immunosorbent assay (ELISA) using sera harvested from BLV-infected cattle. Significant serum binding to peptide **1** (average anti-gp51-peptide IgG titer =  $1.6 \times 10^5$  ELISA units, **Fig. 26b**) was observed, supporting the suitability of this antigen for vaccine design.

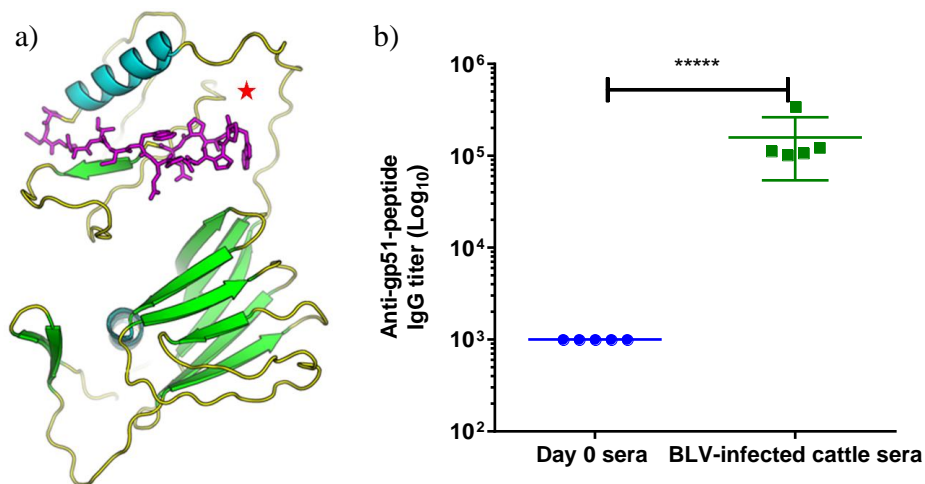
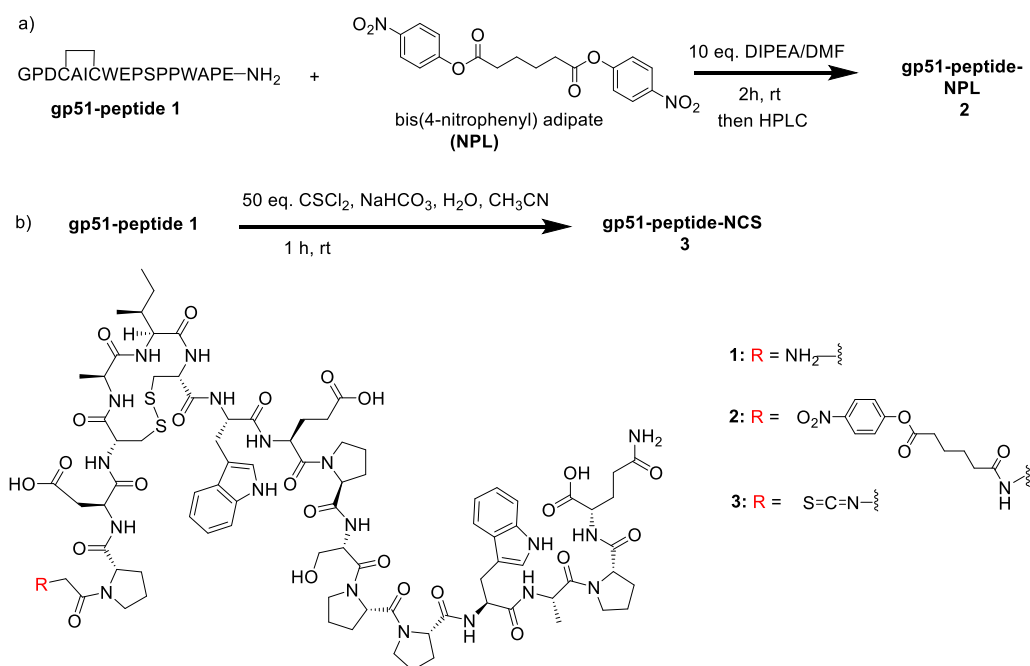


**Figure 26.** a) Structure of BLV gp51 protein by Alphafold structure prediction<sup>22</sup> with amino acid residues 177-192, a putative B-cell epitope on the gp51 envelope protein highlighted in magenta. The red star denotes the potential binding site of gp51 to a receptor on host cells. b) Sera from BLV-infected cattle and pre-immunized mice (day 0) were analyzed by ELISA to demonstrate antigenicity of the peptide epitope. A Nunc MaxiSorp® flat-bottom 96 well plate was coated with BSA-gp51 peptide-1 overnight and sera from both groups were evaluated. Each symbol represents one animal (n=5). Statistical difference was determined through a two-tailed paired Student's t-test of the log(titer). \*\*\*\*\*  $p < 0.00001$ .

#### 4.2.2 Exploring two different linker strategy for functionalizing gp51-peptide epitope

A peptide alone typically has minimal immunogenicity and therefore must be conjugated with a carrier to enhance the immune response. For effective bio-conjugation of gp51-peptide-antigen **1** with a carrier protein, two different linker strategies were explored. In the first approach, the *N*-terminus of the peptide was functionalized with a homo-bifunctional dinitrophenyl adipate linker (NPL) to generate gp51-peptide-NPL **2** (Scheme 2a and Fig. 31).<sup>23</sup> In the second strategy, an isothiocyanate (NCS) group was installed at the *N*-terminus of peptide **1**, producing the gp51-peptide-NCS **3** (Scheme 2b and Fig. 32).<sup>24, 25</sup> The NCS chemistry was more efficient as the isothiocyanate derivatized antigen (gp51-peptide-NCS **3**) could be used directly for bio-conjugation following aqueous workup, whereas the crude gp51-peptides-NPL **2** antigen required an additional HPLC purification step to remove the excess unreacted NPL linker.



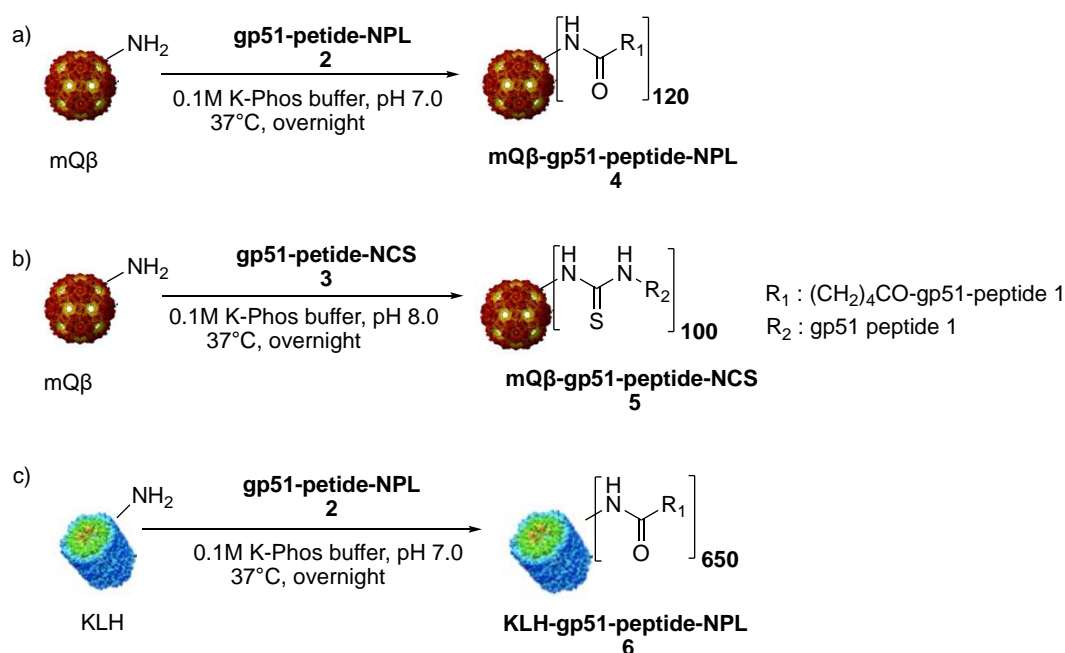
**Scheme 2.** The gp51-peptide antigen **1** was functionalized with two different linker strategies: a) treatment with the homo-bifunctional adipate 4-nitrophenyl diester NPL leading to gp51-peptide NPL **2**; b) conversion of the *N*-terminus of gp51-peptide **1** to an isothiocyanate group producing gp-51-peptide NCS **3**.

#### 4.2.3 Bioconjugation of functionalized gp51-peptide to mQ $\beta$ and control protein carrier Keyhole limpet hemocyanin

Previously, we developed mutant bacteriophage Q $\beta$  (mQ $\beta$ ) as a potent carrier for conjugate vaccine development.<sup>26</sup> The mQ $\beta$ -antigen conjugate can induce a greater antibody response against the target antigen with smaller quantities of non-protective anti-carrier antibodies compared to the corresponding wild type Q $\beta$ .<sup>26</sup> Bioconjugation with mQ $\beta$ (A38K) carrier was achieved by overnight incubation with gp51 peptides **2** and **3** (5 eq. per amine) respectively (**Schemes 3a, b**). The resulting conjugates **4** and **5** were obtained following multiple washes and buffer exchange through membrane filtration (30 kDa MW cutoff) to remove excess reagents. The average numbers of gp51-peptide on the mQ $\beta$  conjugates **4** and **5** were semi-quantified by reducing sodium dodecyl-sulfate polyacrylamide gel electrophoresis (SDS PAGE) using Image Lab software, then further corroborated by LCMS QTOF ESI mass spectrometry (**Figs. 35** and **36**). Loading for both linker-strategies averaged 100-120 copies of

gp51-peptide per mQ $\beta$  capsid. However, besides the aforementioned ease of synthesis, NCS-chemistry permitted recovery of valuable excess peptide as the free gp51-peptide **1** from the flow-through of membrane filtration of the reaction mixture. The recovered free peptide can be re-converted to gp51-peptide **3** enhancing the overall efficiency.

To benchmark the performance of the mQ $\beta$ -gp51-peptide conjugates as potential vaccines, gp51-peptide was conjugated to the gold standard vaccine carrier, keyhole limpet hemocyanin (KLH).<sup>27, 28</sup> Because the alkaline pH (pH 8) required for gp51-NCS **3** coupling is incompatible with KLH protein structure integrity, conjugation of gp51 peptide **1** with KLH was performed using gp51-peptide-NPL **2** (Scheme 3c).<sup>20, 29</sup> The resulting KLH-gp51 construct **6** contained an average of 650 copies of gp51-peptide per KLH.



**Scheme 3.** Schematic demonstration of a) formation of mQ $\beta$ -gp51 conjugate **4** from gp51-peptide-NPL **2**; b) formation of mQ $\beta$ -gp51 conjugate **5** using gp51-peptide-NCS **3**; and c) formation of KLH-gp51 conjugate **6** from gp51-peptide-NPL **2**.

#### 4.2.4 Immunization of WT mice with mQ $\beta$ -gp51 vaccines elicited high antibody titers

C57BL/6 mice (n=5) were immunized subcutaneously with the mQ $\beta$ -gp51 **4**, mQ $\beta$ -gp51 **5**, or KLH-gp51 **6** conjugate constructs using one primer plus 2 booster injections, 2 weeks

apart (**Fig. 27a**). Each dose contained 3  $\mu\text{g}$  of gp51-peptide with monophosphoryl lipid A (MPLA) as an adjuvant. On day 35 after the initial injection (1 week after the 2<sup>nd</sup> booster), blood was collected from mice to harvest serum followed by ELISA analysis of the IgG antibody titers. In order to focus on the anti-gp51 responses and avoid interference by anti-mQ $\beta$  antibodies, BSA-gp51-peptide-NCS conjugate was synthesized as the coating antigen for ELISA analyses. As shown in **Fig. 27b**, mQ $\beta$ -vaccine constructs **4** and **5** elicited robust anti-gp51-peptide IgG responses, averaging  $3.9 \times 10^6$  and  $4.2 \times 10^6$  ELISA units, respectively. These antibody responses were about three orders of magnitude greater than those of pre-immunized mice (day 0) or mice that received only carrier mQ $\beta$  (mQ $\beta$ -only). Mice immunized with KLH-vaccine construct **6** produced an average anti-gp51-peptide IgG titer of  $7 \times 10^5$  ELISA units, or six-fold less than those immunized by the mQ $\beta$ -gp51 constructs, highlighting the advantage of the mQ $\beta$  carrier. The NPL and NCS linker chemistry for mQ $\beta$ -constructs (**4, 5**) did not have a significant impact on the amount of anti-gp51-peptide IgG produced. Analysis of IgG subtypes generated by mQ $\beta$ -constructs (**4, 5**) documented increased quantities of all IgG subtypes, while IgM responses were not significant (**Fig. 27c**). The strong anti-gp51-peptide IgG responses induced by mQ $\beta$ -constructs (**4, 5**) suggest effective activation of helper T cells, facilitating somatic hypermutation and IgG antibody isotype switching.

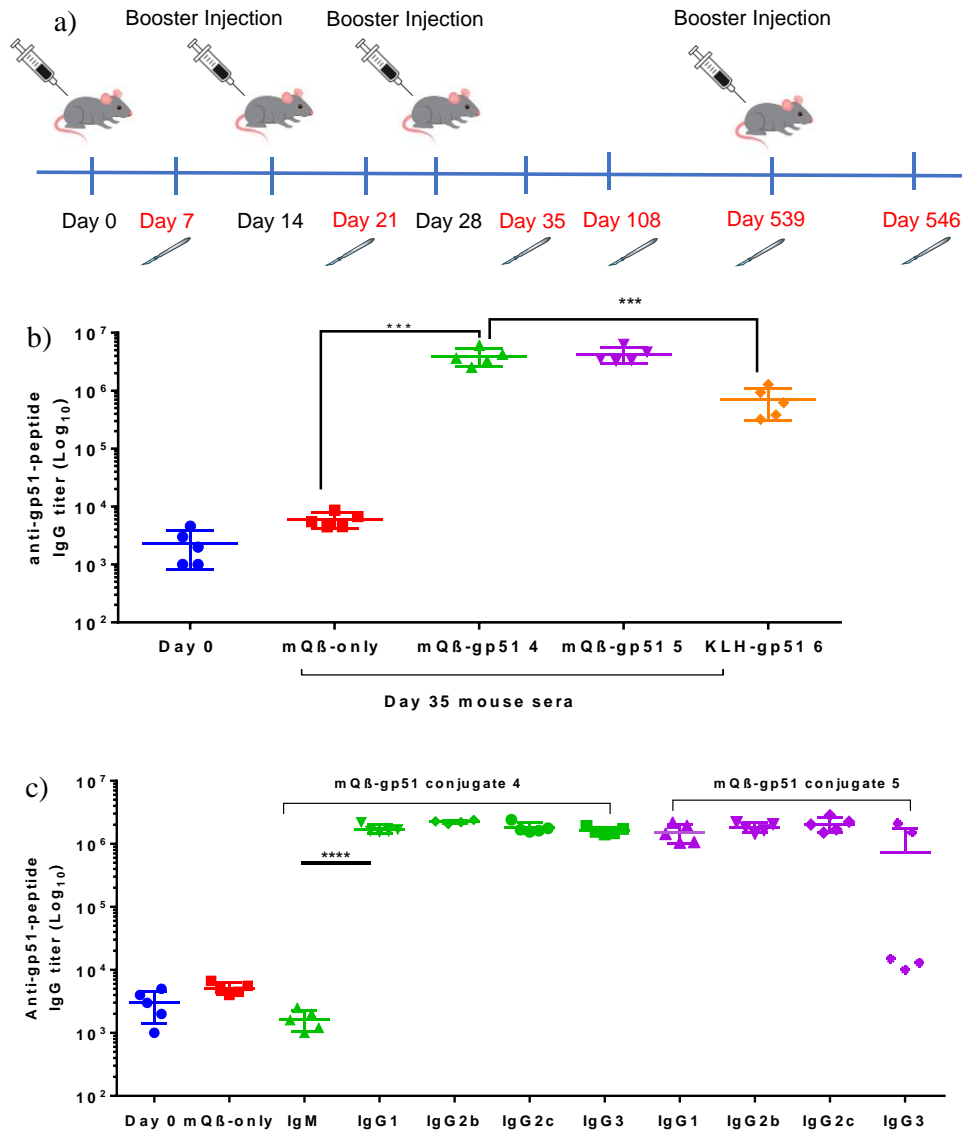


**Figure 27.** Immunization protocol and assessment of anti-gp51 antibody in mice. a) Schematic representation of the immunization protocol for C57BL/6 mice using vaccine constructs (4, 5 and 6). Mice were vaccinated on days 0, 14 and 28 with 3 μg gp51-peptide per dose using MPLA adjuvant. Additional mice were vaccinated with the protein carrier mQβ (mQβ-only) using the same protocol. Mice immunized with mQβ-gp51 and KLH-gp51 were given an additional booster injection on day 539 to test the anamnestic responses. Blood was collected on days 0, 7, 21, 35, 108, 539 and 546 to generate sera for analyses. b) Anti-gp51 IgG titers of different vaccine groups on day 35 post-immunization. Each symbol represents a mouse (n=5 per group). c) Anti-gp51 IgG-subtype antibody titers (4 and 5) and IgM antibody titers. Statistical significance was determined by two-tailed unpaired Student's t-test using GraphPad Prism, \*\*\* $p < 0.001$ , \*\*\*\* $p < 0.0001$ .

#### 4.2.5 mQ $\beta$ -gp51 vaccines induced long-lasting immune response in mice

An important criterion of an efficacious vaccine is the ability to induce long-lasting immunity. The persistence of IgG antibody responses elicited by the mQ $\beta$ -construct **5** was monitored over time (**Fig. 28a**). On day 108 post-immunization, the average anti-gp51-peptide IgG titer for vaccine construct **5** was  $1.1 \times 10^6$  ELISA units. Significant amounts of anti-gp51-peptide IgG antibodies were still present on day 539 post-immunization (average IgG titer was  $2.4 \times 10^5$  and two mice had titer over  $4 \times 10^5$  ELISA units) (**Fig. 28b**), suggesting generation of long-lasting plasma cells capable of continuous production of anti-gp51 antibodies. By comparison, mice immunized with KLH-gp51 **6** had significantly diminished anti-gp51-peptide IgG antibody titers on day 539 compared to mQ $\beta$ -gp51-peptide vaccine immunized mice (**Figs. 28a and 28b**). These results confirm that mQ $\beta$  is a superior carrier compared to KLH.

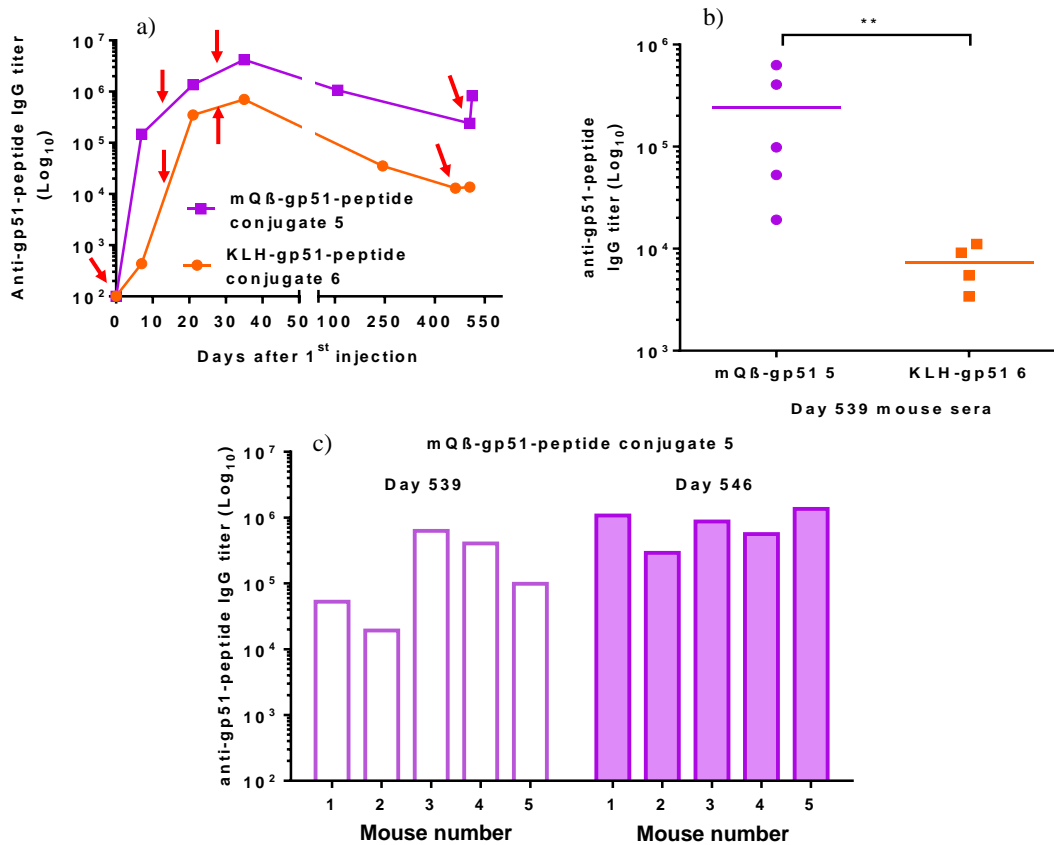


**Figure 28. Anti-gp51 IgG antibody titers monitored over time.** Immunization with mQβ-gp51 induced long-lasting, boostable anti-gp51 IgG antibodies. a) Anti-gp51 IgG antibody titers in mice vaccinated with mQβ-gp51 **5** and KLH-gp51 **6** over time. Immune responses were monitored over 546 days with sera from immunized mice in each group (n=5) pooled and anti-peptide IgG titers reported for days 0, 7, 21, 35, 108, and 539. Circles and squares mark the days of blood collection and arrows represent days of injection with vaccine constructs. b) Individual anti-gp51 peptide IgG antibody titer from mice vaccinated with construct mQβ-gp51 **5** and KLH-gp51 **6** on day 539. Mice that received mQβ-gp51 vaccination had significantly higher levels of anti-gp51 IgG antibodies than those that received KLH-gp51. c) Individual anti-gp51 peptide IgG antibody titer of mice vaccinated with construct **5** on days 539 and 546 post initial injection was analyzed by ELISA to investigate the effect of a booster injection given on day 539; Statistical significance was determined via a two-tailed unpaired Student's t-test using GraphPad Prism. The t-test was performed using log-values for IgG titers for both vaccinated groups. \*\* $p < 0.01$ .

To evaluate whether antibody responses could be boosted, on day 539 after initial immunizations, all five mice in the mQβ-gp51 **5** group received a mQβ-gp51 **5** booster injection, and antibody responses were analyzed by ELISA one week later (day 546). Interestingly, booster injections enhanced anti-gp51-peptide IgG antibody titers 10-fold in mice with anti-gp51 IgG titers less than  $1 \times 10^5$  ELISA units on day 549 (**Fig. 28c**), suggesting that

the initial vaccination series generated memory B cells with resultant boostable IgG antibody production.

#### 4.2.6 Anti-gp51 peptide antibodies effectively recognize and bind to native gp51 epitope and whole BLV particle

In order for anti-peptide antibodies induced by the mQ $\beta$ -peptide conjugate to be effective, they must recognize and bind to the native BLV gp51 epitope. To test this, recombinant gp51 protein was utilized as a coating antigen for measurement of antibodies by ELISA. Sera from negative control groups (day 0 and Q $\beta$ -only) had significantly less anti-gp51 IgG antibody (mean titers =100 and 2,225 ELISA units, respectively) compared to day 35 sera from mice immunized with mQ $\beta$ -gp51-peptide construct **5** (mean titer =  $5.6 \times 10^4$  ELISA units, **Fig. 29**). Similar results were observed for mice immunized with vaccine construct **4** (**Fig. 37**). This data provided evidence that antibodies generated in mice vaccinated with construct **5** recognized both the gp51-peptide **1** as well as the native BLV surface glycoprotein, gp51.

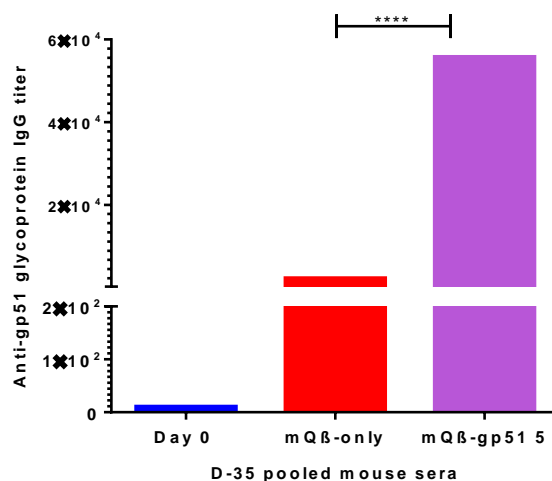


**Figure 29.** IgG antibody titers against native BLV gp51 glycoprotein in sera from pre-immunized mice, mice immunized with mQ $\beta$ -only, or mQ $\beta$ -gp51 **5**, respectively. Mice immunized with mQ $\beta$ -gp51 **5** had significantly increased IgG titers against gp51. Statistical significance was determined through a two-tailed unpaired Student's t-test using GraphPad Prism. \*\*\*\* $p < 0.0001$ .

After the ability of post-immune mQ $\beta$ -gp51 sera to recognize native gp51 was established, we proceeded to assess binding of post-immunized sera to BLV particles. To

accomplish this, we cultured a bovine cell line, BL3.1 (ATCC) that secretes infectious BLV. Cell culture media was harvested, and a double-sucrose gradient protocol was performed to purify BLV particles<sup>30</sup> for examination by transmission electron microscopy (TEM) to confirm the presence and structure of the virus (**Fig. 38a**). Isolated virus particles had typical C-type retrovirus morphology, and their identity was confirmed by western blot analysis using antibodies against BLV viral p24 gag gene and gp51 envelope proteins (**Fig. 38b**). The ability of immunized mouse serum antibodies (mQ $\beta$ -gp51 5) to recognize BLV particles was qualitatively assessed via immunogold labelling, with pooled pre-immunized mouse sera (day 0) serving as a negative control (**Fig. 39**). Gold particles adsorbed with antibodies from mQ $\beta$ -gp51 immunized mouse sera selectively recognized and bound to the surface of isolated BLV particles, while pre-immunized mouse serum antibodies showed minimal non-specific binding to the virus examined by TEM.

#### **4.2.7 Evaluation of neutralizing activities of anti-gp51 antibodies by *in vitro* syncytium inhibition assay**

Finally, the ability of post-immune sera to inhibit virus induced cell-to-cell fusion was investigated using an *in vitro* syncytium inhibition assay (SIA).<sup>31</sup> BLV infects CC81 indicator cells causing syncytium formation, where multiple cells fuse into multinucleated ( $\geq 5$  nuclei) cell mass. The presence of anti-gp51 antibodies decreased CC81 cell fusion and the number of syncytia formed per well presumably through binding to neutralize the virus.

To perform the SIA, BLV particles were pre-incubated with day 0 untreated pre-immunization control pooled sera or day 35 post-vaccination pooled sera before adding the sera/virus mixtures to 96-well plates pre-seeded with CC81 cells. Assays were performed in triplicate. The density of the CC81 cells played an important role for accurate quantification of the number of syncytia formed, with an optimal concentration of  $1 \times 10^4$  cells per well, resulting in a nearly confluent cell monolayer. Monitoring cells incubated with antisera revealed that

after 3 days of incubation (Figs. 40a, b, c), sera from mQ $\beta$ -gp51 peptide immunized mice reduced the number of syncytia formed by ~28% compared to pre-immune sera (Fig. 30), suggesting the potential for mQ $\beta$ -gp51 peptide as a vaccine candidate.

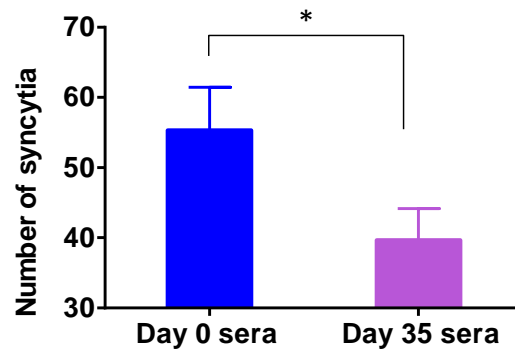


**Figure 30.** Syncytium inhibition assay results. Number of syncytia formed in CC81 cell cultures following challenge with infectious BLV premixed with pooled pre-immune sera (n=5) or pooled mQ $\beta$ -gp51 peptide 5 immunized mouse sera (n= 5). The experiment was performed in triplicate. Statistical significance was determined through a two-tailed unpaired Student's t-test using GraphPad Prism. \* $p < 0.05$ .

#### 4.3 Conclusion

Two vaccine candidates based on mQ $\beta$ -gp51-peptide conjugates 4 and 5 were synthesized using different linkers, NPL and NCS, respectively. Both constructs elicited similarly robust levels of anti-gp51-peptide IgG antibodies following immunization, suggesting comparable effectiveness of these linkers. Due to the relative ease of synthesis and possibility of recycling peptide antigen from the conjugation reaction mixture, the NCS linker was deemed more advantageous. Antibodies induced by mQ $\beta$ -gp51 peptide conjugates exhibited strong binding to both native gp51 envelope protein and infectious BLV particles. In order to benchmark efficacy of our conjugates, induced antibody quantities were compared to the gold standard carrier KLH gp51 peptide conjugate. The mQ $\beta$ -gp51-peptide conjugates generated 6-fold increased IgG antibody titers than the KLH-gp51 conjugate, establishing a clear advantage of the mQ $\beta$  carrier. Importantly, antibodies persisted (IgG titers exceeded  $10^4$  ELISA units on day 539 post-immunization), documenting the first BLV-peptide Q $\beta$  conjugate to induce a

durable antibody response, a characteristic that is crucial for long term protection. Post-immunized sera from mice administered with the mQ $\beta$ -gp51 conjugate also effectively reduced BLV induced cell-to-cell fusion of susceptible target cells. Results of our studies highlight the potential for the mQ $\beta$ -gp51-peptide conjugate to induce long lasting immunity. Compared to more traditional virus-based immunogen designs, peptide conjugates have improved safety profiles. Clinical translational studies are warranted to evaluate the efficacy of this vaccine strategy to prevent BLV infection.

#### **4.4 Materials and Methods**

##### **4.4.1 Reagents and instruments**

All chemicals were reagent grade and used as received from the manufacturer unless otherwise noted. The gp51-peptide **1** was acquired from SynPeptide Co. Ltd. and the recombinant-gp51 was ordered from Bioclone Inc. The cell lysis detergent, DNase I and lysozyme were purchased from Sigma. Centrifugal filter units of 10,000 and 100,000 molecular weight cut-off (MWCO) were purchased from EMD Millipore. Mass spectra were obtained using Waters Xevo G2-XS UPLC/MS/MS.

##### **4.4.2 Cell Lines.**

The feline kidney cell line, CC81 (generously donated by Dr. Luc Willems, University of Liege, Belgium) was maintained in Dulbecco modified Eagle medium supplemented with 10% FBS, 2 mM L-glutamine, and penicillin-streptomycin. The BL3.1 cell line obtained from American Type Culture Collection (ATCC) was cultivated in RPMI-1640 medium supplemented with 10% FBS, 2 mM L-glutamine, and penicillin-streptomycin. These cell lines were maintained in a humidified incubator at 37°C in a 5% CO<sub>2</sub>, 95% air atmosphere.

### **4.4.3 Conjugation of mQ $\beta$ with gp51 peptide 1**

#### **4.4.3.1 Homo-bifunctional nitrophenyl linker (NPL)**

The synthetic procedure was adapted from the literature.<sup>23</sup> Briefly, 5 eq. of adipate bis(4-nitrophenyl)ester (10.5 mg, 27  $\mu$ mol) and 10 eq. of di-isopropyl ethyl amine (DIPEA) (9.6  $\mu$ L, 54  $\mu$ mol) were added to a solution of gp51-peptide **1** (10 mg, 5.4  $\mu$ mol) in dimethylformamide (DMF, 1 mL) and stirred for 2 h at room temperature. Completion of reaction was monitored by LCMS QTOF ESI mass spectrometry. The modified peptide was purified on a Shimadzu HPLC (LC-8A Liquid Chromatograph Pump, DGU-14A, Degasser and SPD-10A UV-Vis Detector), using reverse phase column SUPERCOSIL LC18, 25 cm  $\times$  10 mm 5  $\mu$ m with gradient solvent CH<sub>3</sub>CN and H<sub>2</sub>O (0.1% TFA) gradient 0–5% in 2 min, 5–40% in 2–40 min, with 35% yield of the gp51-peptide-NPL **2**.

#### **4.4.3.2 Isothiocyanate chemistry (NCS)**

The synthetic procedure was adapted from the literature.<sup>24</sup> To a solution of gp51-peptide **1** (5 mg, 0.27  $\mu$ mol) in acetonitrile (70  $\mu$ L), 0.1 M NaHCO<sub>3</sub> was added to adjust pH 8 with a final volume of 1 mL. This solution was layered over chloroform (3.3 mL) containing 50 eq. of thiophosgene (10  $\mu$ L, 13.5  $\mu$ mol). The reaction mixture was then vortexed continuously for 1 h at room temperature. Completion of the reaction was monitored by TLC and LCMS QTOF ESI mass spectrometry. The aqueous layer was extracted four times with chloroform (2 mL) to remove excess thiophosgene. Traces of chloroform were removed by bubbling N<sub>2</sub> gas.

### **4.4.4 mQ $\beta$ (A38K) Expression**

A single colony of BL21(DE3) *E. coli* with the Q $\beta$  mutant-A38K plasmid was selected to inoculate a 25 mL starting culture of Super Optimal Broth (SOB) media containing 20  $\mu$ g/mL kanamycin. The starter culture was incubated overnight at 37°C, 220 rpm. The following morning, the cloudy starter culture was transferred into 1L SOB culture medium with 20  $\mu$ g/mL kanamycin and cultured at 37°C, 220 rpm until the OD<sub>600</sub> was between 0.7-1.0. At that point, 1

mL of 1M isopropyl  $\beta$ -D-1-thiogalactopyranoside (IPTG) was added to induce protein expression and cultured overnight at 30°C, 220 rpm. Cells were then pelleted at 6,000 rpm for 30 min, culture media discarded, and pelleted cells were re-suspended in 30 mL 0.1 M potassium phosphate buffer (KPBS) buffer, pH 7 and stored at -20°C until lysis.

#### **4.4.5 mQ $\beta$ (A38K) Purification**

Cells collected after IPTG induced protein expression were lysed by mixing with 2 mL 1X cell lytic detergent (Sigma) per gram pelleted cells. An equal volume of 0.1 M KPBS buffer plus lysozyme (2 mg/mL final concentration) was added and stirred while adding 100  $\mu$ L Dnase I (5000 U), and stirring was continued for 1h at room temperature. Lysed cells were centrifuged at 14,000 rpm for 30 min using a Fiberlite F21-8x50y and the supernatant with the capsid protein was collected into a 50 mL centrifuge tube containing 5 g of PEG-8000 to a final concentration of 10% (w/v) and placed on a nutating mixer overnight at 4°C to enable complete protein precipitation. The precipitate was pelleted at 14,000 rpm for 30 min, re-suspended in 10 mL 0.1M KPBS, pH 7, added to 10 mL of 1:1 (v/v) chloroform/n-butanol solution and mixed until the solution became colloidal. The colloidal mixture was centrifuged at 7,000 rpm for 20 min in glass centrifuge tubes to separate the layers. The aqueous (top) layer was collected and layered onto freshly prepared linear sucrose gradients (10-40%, w/v), and centrifuged using a swing bucket rotor (SW32) at 28,000 rpm for 4.5 h. The protein band was visualized using LED light directed at the top of the tube and collected in fractions to isolate aggregated protein from pure capsid protein.

#### **4.4.6 mQ $\beta$ (A38K) Characterization**

The fractions were analyzed for purity using Fast protein liquid chromatography (FPLC), performed on a GE ÄKTA Explorer (Amersham Pharmacia) instrument equipped with a Superose-6 column. Fractions showing a single peak at around 10-15 mL elution were determined to be mQ $\beta$  capsid and any aggregated capsid eluted between 8-10 mL. All fractions

containing pure mQ $\beta$ (A38K) were combined and concentrated to ~1mL for quantification by the Bradford assay. After dithiothreitol (DTT) addition, the protein molecular weight was determined by LCMS QTOF ESI mass spectrometry. The multiple charge mass spectrum was transformed to a single charge by Maximum Entropy deconvolution algorithm (Max Ent<sup>TM</sup>).

#### **4.4.7 Synthesis and Characterization of mQ $\beta$ (A38K) Conjugates**

The amount of antigen added was based on the ratio of antigen per accessible mutated capsid surface amines. The mQ $\beta$  (A38K) is comprised of 180 identical subunits with five accessible surface amines per subunit. As a result, the total number of surface accessible amines available for conjugation is 900. To conjugate gp51-peptide **1**, 5 eq. antigen/surface accessible-amine was utilized. The gp51-peptide-NPL **2** (1.85 mg, 0.9 $\mu$ mol) was dissolved in DMSO (25  $\mu$ L), added to a solution containing mQ $\beta$  (A38K) (0.5 mg, 0.2 nmol), suspended in 0.1M KPBS, pH 7 (final protein concentration 2.5 mg/mL), and incubated overnight at 37°C. The conjugate was purified using Amicon ultra (30,000 MW cut-off) centrifugal filtration against 0.1 M KPBS, pH 7 (5  $\times$  0.5 mL).

For conjugation via isothiocyanate derivatization, gp51-peptide-NCS **3** (1.67 mg, 0.9  $\mu$ mol) was solubilized in DMSO (25  $\mu$ L), added to mQ $\beta$  (A38K) (0.5 mg, 0.2 nmol), and suspended in 0.1M KPBS, pH 8 (final protein concentration 5 mg/mL). The reaction mixture was incubated overnight at 37°C, and then purified by Amicon ultra (30,000 MW cut-off) centrifugal filtration against 0.1 M KPBS, pH 8 (5  $\times$  0.5 mL). After achieving an average of 100-120 copies gp51-peptide antigen per capsid, conjugation was repeated at a 1 mg mQ $\beta$  scale for *in-vivo* studies based on 3  $\mu$ g antigen injected per mouse. The antigen loading level was characterized by reducing SDS PAGE through Image Lab software by Bio Rad.

#### **4.4.8 Synthesis and Characterization of KLH-gp51 Peptide 6**

A solution of KLH (1.0 mg, 0.2 nmol) in 0.1 M KPBS (pH = 7.0, 0.2 mL) was cooled using an ice bath and added to gp51-peptide-NPL **2** solution (16  $\mu$ L of 15 mM stock solution

in DMSO, 238  $\mu$ mol). The mixture was gently inverted several times to ensure thorough mixing of the reactants, incubated at 37°C overnight, and purified by Amicon ultra (100,000 MW cut-off) centrifugal filtration against 0.1 M KPBS, pH 7 (5  $\times$  0.5 mL). Total protein concentration was determined via the Bradford assay using bovine serum albumin (BSA) standards. Percent protein recovery was approximately 86%. The number of gp51-peptide-NPL **2** per KLH protein molecule (molecular weight 8,000 KDa) was determined by calculating the amount of unconjugated peptide in the filtrate using the peptide calibration curve generated by HPLC.

#### **4.4.9 Synthesis and Characterization of the BSA-gp51 Peptide Conjugate**

Synthesis of BSA conjugate was similar to that for mQ $\beta$  (A38K) conjugates. The gp51-peptide-NCS **3** (0.5 mg) was added to a solution of BSA (1 mg) in 0.1 M KPBS pH 8, incubated at 37°C overnight followed by buffer exchange to 0.1 M KPBS pH 7 through Amicon Ultra (10 kD MW cut-off) filters. The protein concentration was quantified by the Bradford assay using bovine serum albumin (BSA) standards and the extent conjugation was characterized by MALDI MS.

#### **4.4.10 Immunization Studies**

All animal care procedures and experimental protocols were approved by the Michigan State University Institutional Animal Care and Use Committee (IACUC). Five CB57BL/6 black 7-10-week female mice were used for *in-vivo* studies for each vaccine construct (**4**, **5** and **6**) group. Mice were injected subcutaneously at the scruff of the neck with 0.2 mL vaccine construct that included monophosphoryl lipid A (MPLA, 20  $\mu$ g) as the adjuvant on day 0 plus booster injections given subcutaneously on days 14 and 28. All three vaccine constructs had 3  $\mu$ g of peptide antigen/injection per mouse. Serum samples were collected on days 0 (before immunization), 7, 21, and 35. Mice (n=5) initially immunized with mQ $\beta$ -gp51 **5** were bled additionally on days 109, 539, and 546. These mice received an additional booster injection on day 539 and on day 546 had a final blood collection and were humanely euthanized. The IgG

antibody titers were evaluated by enzyme-linked immunosorbent assay (ELISA).

#### **4.4.11 Antibody Titers (IgG) Measured by ELISA**

A Nunc MaxiSorp® flat-bottom 96-well plate was coated with BSA-gp51-peptide conjugate (10 µg/mL, 100 µL/well) in NaHCO<sub>3</sub>/Na<sub>2</sub>CO<sub>3</sub>/NaN<sub>3</sub> coating buffer (0.05 M, pH 9.6) and incubated overnight at 4°C. The coated plate was washed 4 times with PBS/0.5% Tween-20 (PBST), followed by addition of 1% (w/v) BSA in PBS to each well and incubated at room temperature for 1h. The plate was washed again 4 times with PBST (4 x 200 µL). Serial dilutions of mouse sera in 0.1% BSA/PBS (100 µL) were added to each well and incubated for 2 h at 37°C. Wells were then washed with PBST (4 x 200 µL) and a 1:2,000 dilution of HRP-conjugated goat anti-mouse IgG (Jackson ImmunoResearch Laboratory catalog # 115-005-062) in 0.1% BSA/PBS (100 µL) was added to each well and incubated for 1 h at 37°C. Enzymatic substrate was prepared by dissolving 3,3',5,5'-tetramethylbenzidine (TMB, 5 mg) in DMSO (2 mL) and citric acid buffer (18 mL) in a 50 mL centrifuge tube covered with aluminum foil. H<sub>2</sub>O<sub>2</sub> (20 µL) was added and vortexed to homogeneity. The plate was washed with PBST (4 x 200 µL) and enzymatic substrate was added (200 µL), color was allowed to develop for 15 min, then 0.5 M H<sub>2</sub>SO<sub>4</sub> (50 µL) was added to quench the reactions. Absorbance was measured at 450 nm using a microplate reader (BioRad). Titers were determined by regression analysis with log<sub>10</sub> dilution plotted against optical density. The titer was reported as the highest fold dilution giving an optical absorbance value of 0.1 over pre-immune control sera (OD = 0.2). Samples were tested in triplicate.

#### **4.4.12 Cell-free BLV Preparation, Purification and Characterization**

BLV-producing BL3.1 cells (ATCC) were cultured to obtain cell-free preparations of BLV particles. Briefly, culture media (150 mL) at 72 to 96 h post-sub culturing was centrifuged at low-speed (10,000 x g for 20 min) to harvest cell-free supernatant fluid that was filtered through a 0.45 µm filter, followed by volume reduction by centrifugation through 100kD

membrane filters (Millipore). The final 100-fold BLV concentrate was prepared by pelleting 35mL of cell-free supernatant via ultracentrifugation (110,000 x g for 60 min) and resuspending in 1.5 mL of DMEM.

The concentrated cell-free BLV pellet was purified using a double-sucrose gradient protocol using a procedure adapted from the literature.<sup>30, 31</sup> Four different sucrose solutions were made to create the gradient. The 70% and 20% sucrose solutions were prepared in 0.1 M PBS while the 60% and 30% solutions were prepared in DMEM. The sucrose solutions were added to a 50 mL centrifuge tube in descending gradient concentration order followed by careful addition of the supernatant containing the virus. The gradient tubes were then ultra-centrifuged at 20,000 rpm for 2.5 h at 4°C. The 30-60% fractions were carefully collected into clean tubes, PBS was added to a total volume of 10 mL and the solution was added to another tube containing 2 mL of 20% sucrose, and the tubes were ultra-centrifuged at 20,000 rpm for 2.5 h at 4°C. The supernatant was poured off and all residual liquid was blotted on filter paper by inverting the tubes. The virus-containing pellet was observed at the bottom of the tube. The virus pellet was resuspended in a minimum amount of cold PBS and stored at -80°C. Virus morphology was visualized by transmission electron microscopy (**Fig. 38a**).

To characterize the purified virus concentrate, virus was lysed by adding SDS-PAGE sample loading buffer containing  $\beta$ -mercaptoethanol, boiling for 10 min, loading onto a 4-20% SDS-polyacrylamide gel, and electrophoresing for 1 h at room temperature. The SDS-PAGE bands were transferred onto a nitrocellulose membrane (GE Healthcare) for western blot analysis (**Fig. 38b**). Following blocking with tris-buffered saline (TBS)– 0.1% Tween 20 (TBST) containing 10% of non-fat dry milk, the membrane was incubated overnight at 4°C with primary antibodies using concentrations provided by the manufacturer: anti-gp51 (BLV1; dilution, 1:2,000; VMRD), anti-p24 (kindly provided by Dr. Luc Willems, University of Liege, Belgium, 1:2,000). The nitrocellulose membrane was then washed three times for 5 min with

TBST and incubated for 2 h with a horseradish peroxidase (HRP)-labelled goat anti-mouse IgG secondary antibody (dilution 1:2,000; Santa Cruz Biotechnology). After three TBST washes, bands on the membrane were revealed by chemiluminescence (ECL Plus Western blotting detection kit; GE Healthcare).

#### 4.4.13 Syncytium Inhibition Assay

CC81 cells were cultured at 37°C, 5% CO<sub>2</sub> in cell growth medium. An aliquot of CC81 cells and medium was transferred to a conical centrifuge tube, centrifuged at 1,600 rpm for 5 min at 4°C, supernatant was removed, and the pellet was re-suspended in growth medium (10 mL). The number of cells was determined using a hemocytometer. A suspension of 5x10<sup>3</sup> CC81 cells/well was seeded into a 96-well plate and cultured for 24h at 37°C, 5% CO<sub>2</sub>.

Cell-free BLV concentrate from BL3.1 cells, as described above, was mixed with an equal volume of 1:4 diluted post-vaccination serum and incubated for 30 min at room temperature. Test samples were then added to triplicate CC81 indicator cell wells and incubated for 8h at 37°C, 5% CO<sub>2</sub>, fixed with 10% formalin, and stained (May-Grunwald Giemsa). Each multinucleated fused cell with more than five nuclei visualized using an inverted light microscope was counted as a syncytium and the number of syncytia per well was recorded. Ten randomly selected fields (1 mm<sup>2</sup>) were counted in triplicate wells to reduce counting errors to calculate the total number of syncytia per well. Multinucleated cells were differentiated from clusters of cells via careful visualization at 20× and 40× magnification (**Fig. 40d**). The percentage syncytium inhibition for each virus-serum mixture was calculated as (1- total number of syncytia observed in the presence of post-vaccinated day 35 (D35) pooled serum-inoculated CC81 cells / the number of syncytia observed in pre-vaccinated day 0 (D0) pooled serum-inoculated CC81 cells) x 100 (%). Negative control cells incubated without sera had a total number of 10 syncytia. By comparison, the number of syncytia per well formed in the presence of BLV was significantly higher (> 67).

## REFERENCES

- (1) USDA Bovine Leukosis Virus (BLV) on U.S Dairy Operations. [https://www.aphis.usda.gov/animal\\_health/nahms/dairy/downloads/dairy07/Dairy07\\_is\\_BLV.pdf](https://www.aphis.usda.gov/animal_health/nahms/dairy/downloads/dairy07/Dairy07_is_BLV.pdf). Accessed on March 28<sup>th</sup>, 2022.
- (2) Trono, K. G.; Pérez-Filgueira, D. M.; Duffy, S.; Borca, M. V.; and Carrillo, C. (2001) Seroprevalence of bovine leukemia virus in dairy cattle in Argentina: comparison of sensitivity and specificity of different detection methods. *Vet. Microbiol.* 83, 235-248.
- (3) Nekouei, O.; Stryhn, H.; VanLeeuwen, J.; Kelton, D.; Hanna, P.; and Keefe, G. (2015) Predicting within-herd prevalence of infection with bovine leukemia virus using bulk-tank milk antibody levels. *Prev. Vet. Med.* 122, 53-60.
- (4) Yang, Y.; Fan, W.; Mao, Y.; Yang, Z.; Lu, G.; Zhang, R.; Zhang, H.; Szeto, C.; and Wang, C. (2016) Bovine leukemia virus infection in cattle of China: Association with reduced milk production and increased somatic cell score. *J. Dairy Sci.* 99, 3688-3697.
- (5) Hopkins, S. G.; and DiGiacomo, R. F. (1997) Natural transmission of bovine leukemia virus in dairy and beef cattle. *Vet. Clin. N. Am. Food Anim. Pract.* 13, 107-128.
- (6) Ruiz, V.; Porta, N. G.; Lomonaco, M.; Trono, K.; and Alvarez, I. (2018) Bovine Leukemia Virus Infection in Neonatal Calves. Risk Factors and Control Measures. *Front. Vet. Sci.* 5, 267.
- (7) Erskine, R. J.; Bartlett, P. C.; Sabo, K. M.; and Sordillo, L. M. (2011) Bovine Leukemia Virus Infection in Dairy Cattle: Effect on Serological Response to Immunization against J5 Escherichia coli Bacterin. *Vet. Med. Inter.* 2011, 915747.
- (8) Ott, S. L.; Johnson, R.; and Wells, S. J. (2003) Association between bovine-leukosis virus seroprevalence and herd-level productivity on US dairy farms. *Prev. Vet. Med.* 61, 249-262.
- (9) Gao, A.; Kouznetsova, V. L.; and Tsigelny, I. F. (2020) Bovine leukemia virus relation to human breast cancer: Meta-analysis. *Microb. Pathog.* 149, 104417.
10. Buehring, G. C.; Shen, H. M.; Jensen, H. M.; Jin, D. L.; Hudes, M.; and Block, G. (2015) Exposure to Bovine Leukemia Virus Is Associated with Breast Cancer: A Case-Control Study. *Plos One* 10, e0134304.
- (11) Gutiérrez, G.; Rodríguez, S. M.; de Brogniez, A.; Gillet, N.; Golime, R.; Burny, A.; Jaworski, J. P.; Alvarez, I.; Vagnoni, L.; Trono, K.; and Willems, L. (2014) Vaccination against  $\delta$ -retroviruses: the bovine leukemia virus paradigm. *Viruses* 6, 2416-2427.
- (12) Rola-Łuszczak, M.; Pluta, A.; Olech, M.; Donnik, I.; Petropavlovskiy, M.; Gerilovych, A.; Vinogradova, I.; Choudhury, B.; and Kuźmak, J. (2013) The molecular characterization of bovine leukaemia virus isolates from Eastern Europe and Siberia and its impact on phylogeny. *PLoS One* 8, e58705.

- (13) Abdala, A.; Alvarez, I.; Brossel, H.; Calvinho, L.; Carignano, H.; Franco, L.; Gazon, H.; Gillissen, C.; Hamaidia, M.; Hoyos, C.; Jacques, J.-R.; Joris, T.; Laval, F.; Petersen, M.; Porquet, F.; Porta, N.; Ruiz, V.; Safari, R.; Suárez Archilla, G.; Trono, K.; and Willems, L. (2019) BLV: lessons on vaccine development. *Retrovirology* 16, 26.
- (14) Ohishi, K.; Suzuki, H.; Yamamoto, T.; Maruyama, T.; Miki, K.; Ikawa, Y.; Numakunai, S.; Okada, K.; Ohshima, K.; and Sugimoto, M. (1991) Protective immunity against bovine leukaemia virus (BLV) induced in carrier sheep by inoculation with a vaccinia virus-BLV env recombinant: association with cell-mediated immunity. *J. Gen. Virol.* 72, 1887-1892.
- (15) Kabeya, H.; Ohashi, K.; Ohishi, K.; Sugimoto, C.; Amanuma, H.; and Onuma, M. (1996) An effective peptide vaccine to eliminate bovine leukaemia virus (BLV) infected cells in carrier sheep. *Vaccine* 14, 1118-1122.
- (16) Rodríguez, S. M.; Florins, A.; Gillet, N.; de Brogniez, A.; Sánchez-Alcaraz, M. T.; Boxus, M.; Boulanger, F.; Gutiérrez, G.; Trono, K.; Alvarez, I.; Vagnoni, L.; and Willems, L. (2011) Preventive and therapeutic strategies for bovine leukemia virus: lessons for HTLV. *Viruses* 3, 1210-1248.
- (17) Gatei, M. H.; Naif, H. M.; Kumar, S.; Boyle, D. B.; Daniel, R. C.; Good, M. F.; and Lavin, M. F. (1993) Protection of sheep against bovine leukemia virus (BLV) infection by vaccination with recombinant vaccinia viruses expressing BLV envelope glycoproteins: correlation of protection with CD4 T-cell response to gp51 peptide 51-70. *J. Virol.* 67, 1803-1810.
- (18) Johnston, E. R.; Albritton, L. M.; and Radke, K. (2002) Envelope Proteins Containing Single Amino Acid Substitutions Support a Structural Model of the Receptor-Binding Domain of Bovine Leukemia Virus Surface Protein. *J. Virol.* 76, 10861-10872.
- (19) Callebaut, I.; Portetelle, D.; Burny, A.; and Mornon, J. P. (1994) Identification of functional sites on bovine leukemia virus envelope glycoproteins using structural and immunological data. *Eur. J. Biochem.* 222, 405-414.
- (20) Callebaut, I.; Vonèche, V.; Mager, A.; Fumière, O.; Krchnak, V.; Merza, M.; Zavada, J.; Mammerickx, M.; Burny, A.; and Portetelle, D. (1993) Mapping of B-neutralizing and T-helper cell epitopes on the bovine leukemia virus external glycoprotein gp51. *J. Virol.* 67, 5321-5327.
- (21) Wu, X.; Yin, Z.; McKay, C.; Pett, C.; Yu, J.; Schorlemer, M.; Gohl, T.; Sungsuwan, S.; Ramadan, S.; Baniel, C.; Allmon, A.; Das, R.; Westerlind, U.; Finn, M. G.; and Huang, X. (2018) Protective Epitope Discovery and Design of MUC1-based Vaccine for Effective Tumor Protections in Immunotolerant Mice. *J. Am. Chem Soc.* 140, 16596-16609.
- (22) Jumper, J.; Evans, R.; Pritzel, A.; Green, T.; Figurnov, M.; Ronneberger, O.; Tunyasuvunakool, K.; Bates, R.; Židek, A.; Potapenko, A.; Bridgland, A.; Meyer, C.; Kohl, S. A. A.; Ballard, A. J.; Cowie, A.; Romera-Paredes, B.; Nikolov, S.; Jain, R.; Adler, J.; Back, T.; Petersen, S.; Reiman, D.; Clancy, E.; Zielinski, M.; Steinegger, M.; Pacholska, M.; Berghammer, T.; Bodenstein, S.; Silver, D.; Vinyals, O.; Senior, A. W.;

- Kavukcuoglu, K.; Kohli, P.; and Hassabis, D. (2021) Highly accurate protein structure prediction with AlphaFold. *Nature* 596, 583-589.
- (23) Wu, X.; Ling, C.-C.; and Bundle, D. R. (2004) A New Homobifunctional p-Nitro Phenyl Ester Coupling Reagent for the Preparation of Neoglycoproteins. *Org. Lett.* 6, 4407-4410.
- (24) Smith, D. F.; Zopf, D. A.; and Ginsburg, V. (1978) Carbohydrate antigens: coupling of oligosaccharide phenethylamine-isothiocyanate derivatives to bovine serum albumin. *Meth. Enzymol.* 50, 169-171.
- (25) Wu, X.; Ye, J.; DeLaitsch, A. T.; Rashidijahanabad, Z.; Lang, S.; Kakeshpour, T.; Zhao, Y.; Ramadan, S.; Saavedra, P. V.; Yuzbasiyan-Gurkan, V.; Kavunja, H.; Cao, H.; Gildersleeve, J. C.; and Huang, X. (2021) Chemoenzymatic Synthesis of 9NHAc-GD2 Antigen to Overcome the Hydrolytic Instability of O-Acetylated-GD2 for Anticancer Conjugate Vaccine Development. *Angew. Chem. Int. Ed.* 60, 24179-24188.
- (26) Sungsuwan, S.; Wu, X.; Shaw, V.; Kavunja, H.; McFall-Boegeman, H.; Rashidijahanabad, Z.; Tan, Z.; Lang, S.; Tahmasebi Nick, S.; Lin, P.-h.; Yin, Z.; Ramadan, S.; Jin, X.; and Huang, X. (2022) Structure Guided Design of Bacteriophage Q $\beta$  Mutants as Next Generation Carriers for Conjugate Vaccines. *ACS Chem. Biol.* in press.
- (27) Guo, Z. W.; and Wang, Q. L. (2009) Recent development in carbohydrate-based cancer vaccines. *Curr. Opin. Chem. Biol.* 13, 608-617.
- (28) Harris, J. R.; and Markl, J. (1999) Keyhole limpet hemocyanin (KLH): a biomedical review. *Micron* 30, 597-623.
- (29) Okada, K.; Sonoda, K.; Koyama, M.; Yin, S.; Ikeda, M.; Goryo, M.; Chen, S. L.; Kabeya, H.; Ohishi, K.; and Onuma, M. (2003) Delayed-type hypersensitivity in sheep induced by synthetic peptides of bovine leukemia virus encapsulated in mannan-coated liposome. *J. Vet. Med. Sci.* 65, 515-518.
- (30) Vijayraghavan, S.; and Kantor, B. (2017) A Protocol for the Production of Integrase-deficient Lentiviral Vectors for CRISPR/Cas9-mediated Gene Knockout in Dividing Cells. *J. Vis. Exp.* 56915.
- (31) Graves, D. C.; and Jones, L. V. (1981) Early syncytium formation by bovine leukemia virus. *J. Virol.* 38, 1055-1063.

## PUBLICATION

1. **Chugh, S.**; Swenson, C.; Yuzbasiyan-Gurkan, V.; Huang, X. Design and Synthesis of Bovine Leukemia Virus-Associated Peptide-Based Q $\beta$  Conjugate Eliciting Long-Lasting Neutralizing Antibodies in Mice. *ACS Infect Dis* **2022**, 8 (5), 1031-1040. DOI: 10.1021/acsinfecdis.2c00001

## APPENDIX

**Figure 31.** Mass spectrum of gp51-peptide-NPL 2

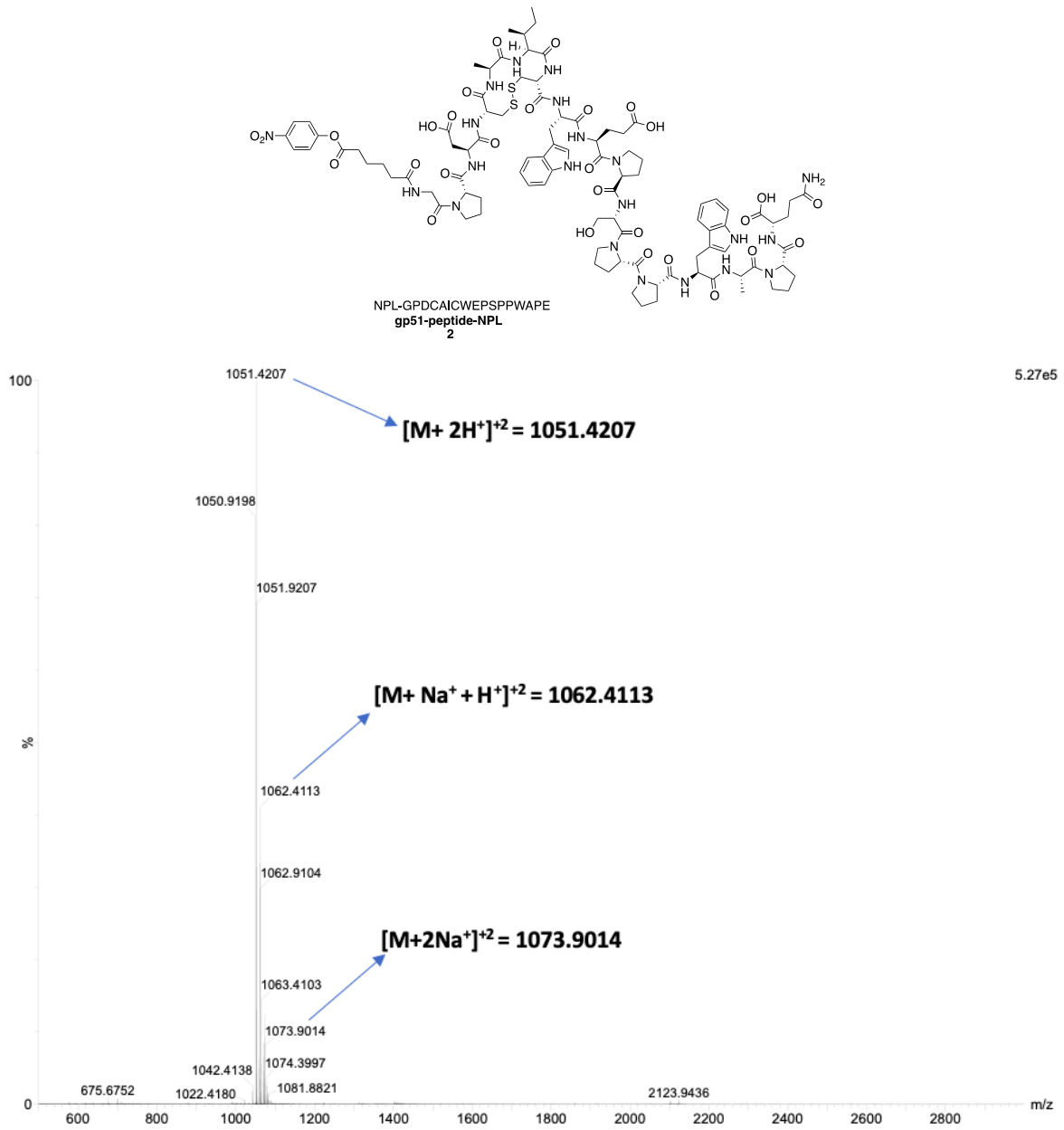


**Figure 32.** Mass spectrum of gp51-peptide-NCS **3**

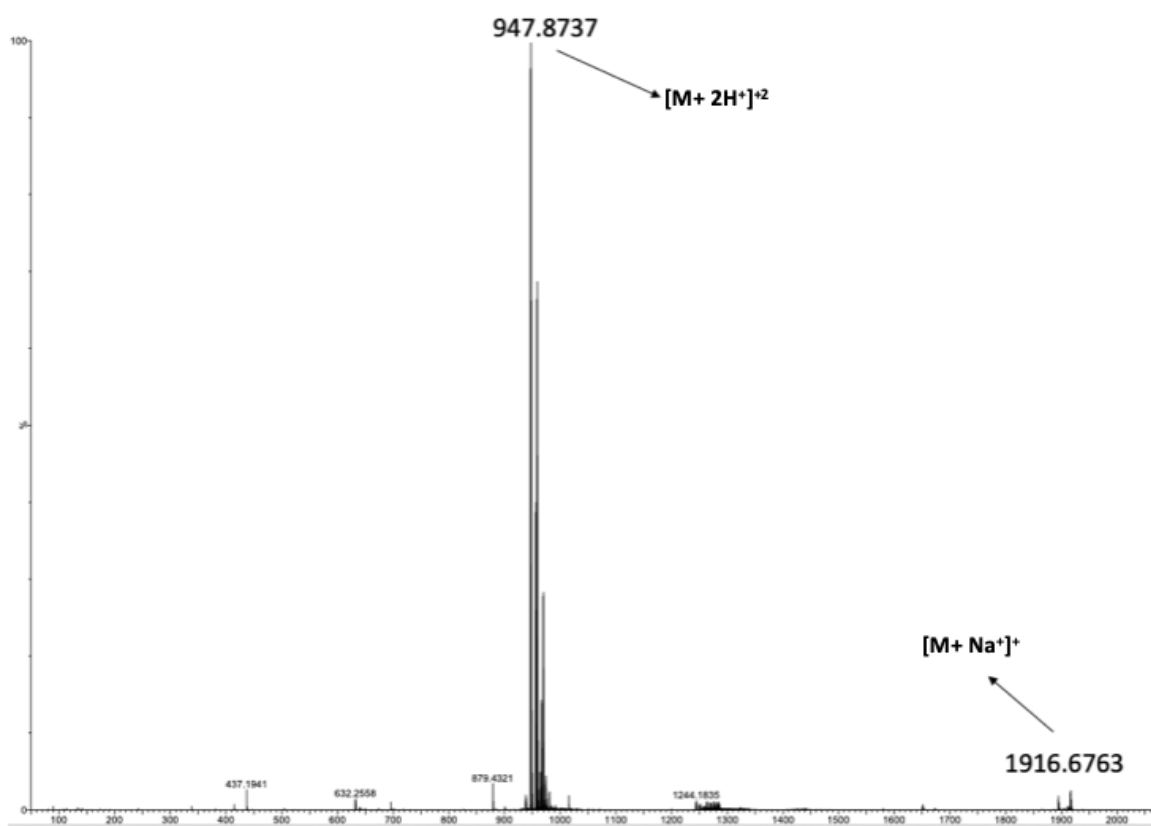
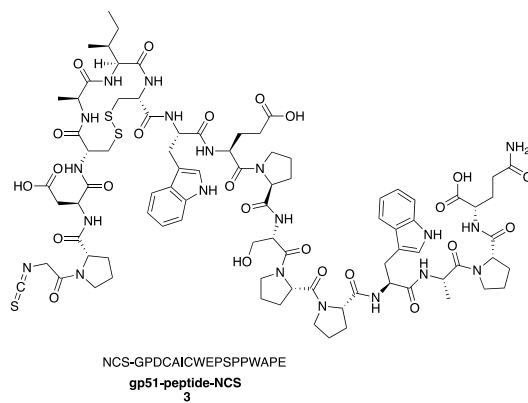


**Figure 33.** ESI-TOF HRMS spectrum of mQ $\beta$ (A38K)

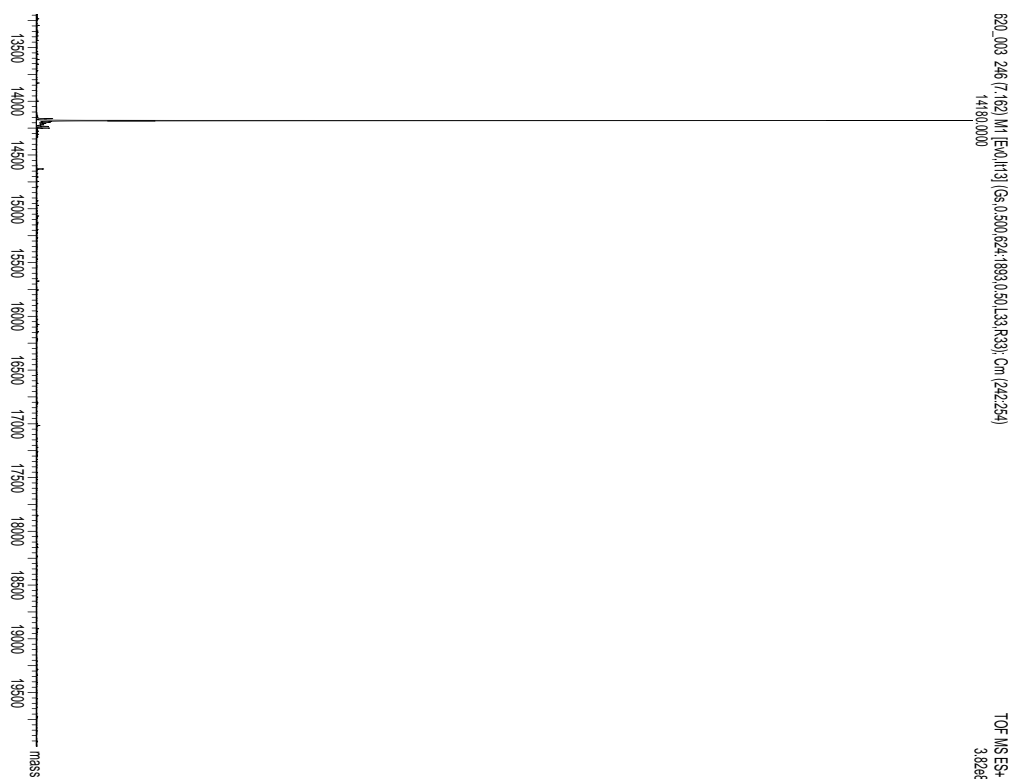


**Figure 34.** (a) Electrophoresis (SDS-PAGE) of mQ $\beta$ (A38K) displaying ladder in lane 1 and mQ $\beta$ (A38K) in lane 2 with two bands for monomer (14kD) and dimer (28kD) and (b) Fast protein liquid chromatography (FPLC) analysis of mQ $\beta$ (A38K). It was performed on a GE ÄKTA Explorer (Amersham Pharmacia) instrument equipped with a Superose-6 column. Microfluidic capillary gel electrophoresis was performed on a Bioanalyzer 2100 Protein 80 microfluidics chip (Agilent Technologies)

a.

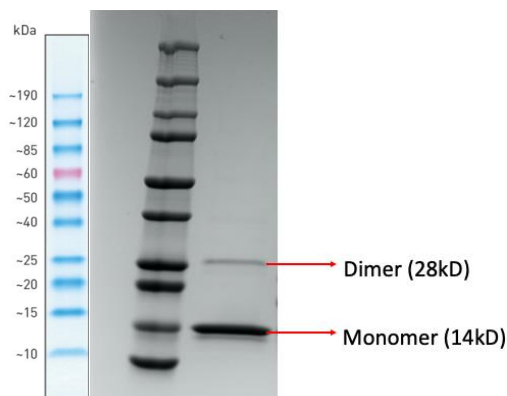


**Figure 34 (cont'd)**

b.

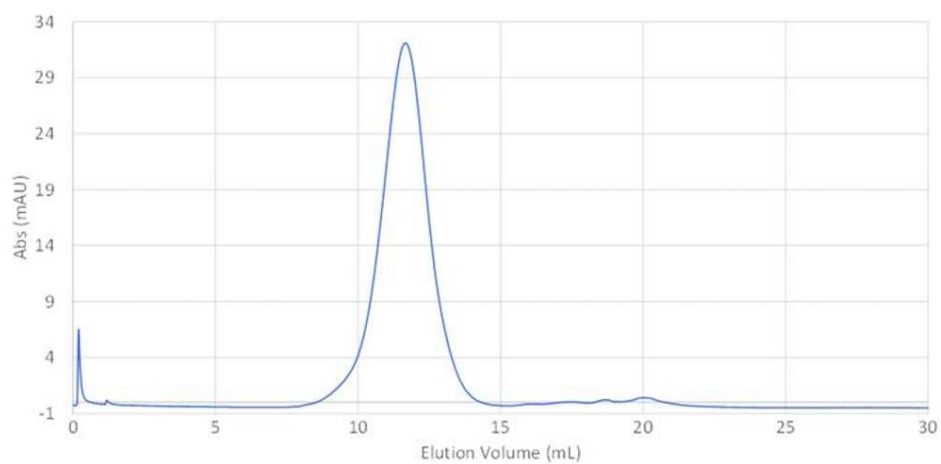


**Figure 35.** ESI-TOF HRMS spectra of mQ $\beta$ -gp51-peptide vaccine conjugate **4** showing the number of gp51-peptide NPL copies on each viral capsid is 120 on average.

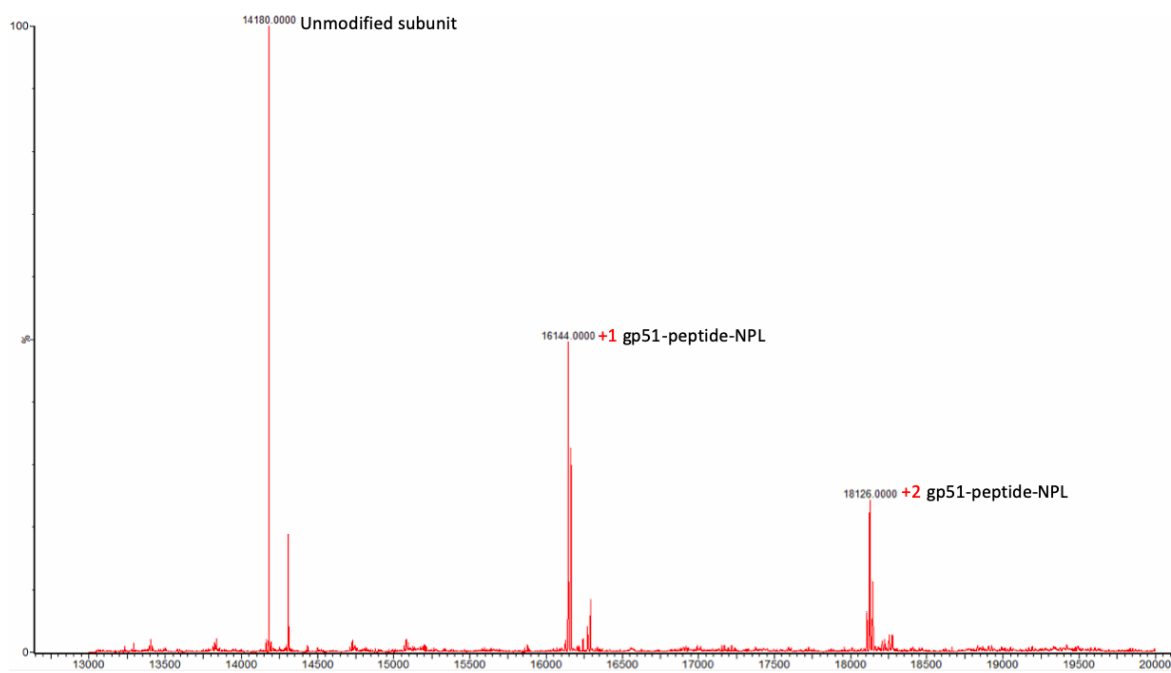


**Figure 36.** Electrophoresis analysis (SDS-PAGE) of mQ $\beta$ -gp51-peptide vaccine conjugates **4** and **5** showing the number of gp51-peptide copies on each viral capsid subunit is 120 and 100 on average respectively as calculated by Image Lab software.

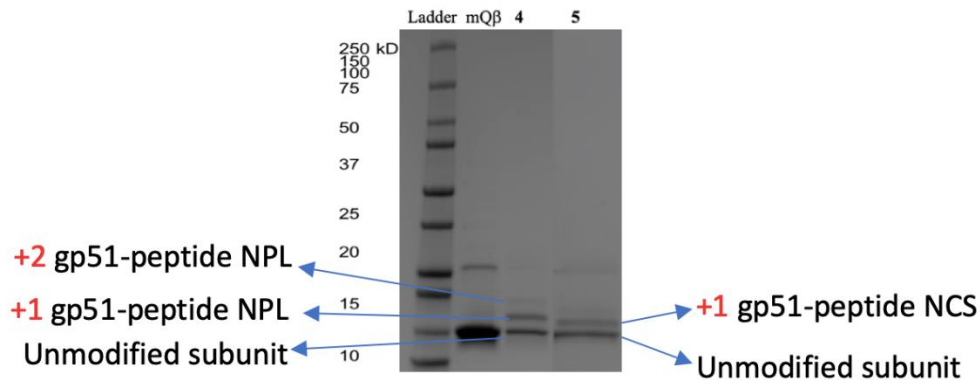


**Figure 37.** Titer of anti-gp51 IgG from mice immunized with mQ $\beta$ -gp51-peptide conjugate **4** or mQ $\beta$ -only.

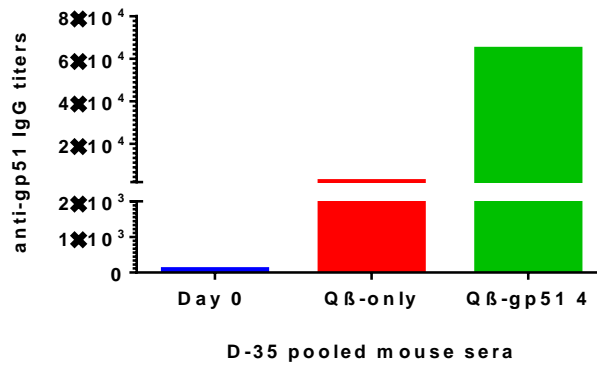


**Figure 38.** a) Double-sucrose gradient protocol for purifying the concentrated cell-free BLV secreted by BL3.1 cells with transmission electron microscopy (TEM) image for BLV particles resembling C-type retrovirus b) Western blot analysis for BLV producing cell line BL3.1 for intracellular gag gene p24 (24kD, Lane 2) protein as an indication of BLV infection, gp51 surface protein (51kD, Lane 3).

a.

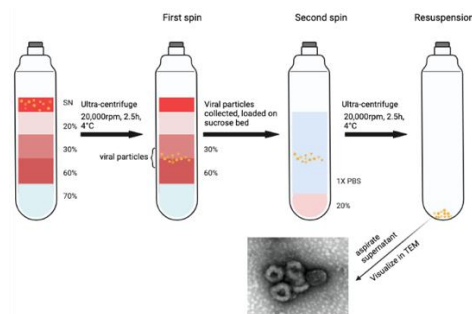


**Figure 38 (cont'd)**

b.

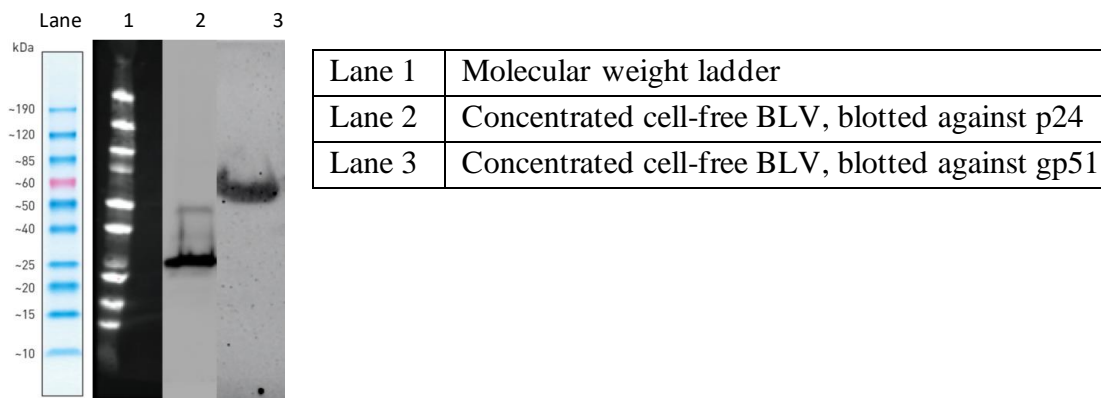
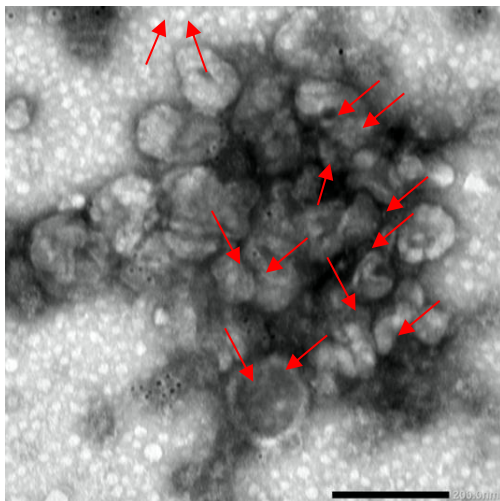


**Figure 39. Immunogold labelling of BLV particles imaged by TEM highlighting (red arrows) the adsorption of gold particles on BLVs incubated with a) pooled sera from mice immunized with mQ $\beta$ -gp51-peptide conjugate **5**; b) pooled sera from pre-immunized mice.** The scale bars for the images are 200 nm. The red arrows indicate the locations of the gold particles on cells. The higher number of red arrows in panel a vs panel b suggests there are more antibodies recognizing the whole BLV particles in sera from mice immunized from mQ $\beta$ -gp51-peptide conjugate **5** than those in sera from pre-immunized mice.

a.



b.

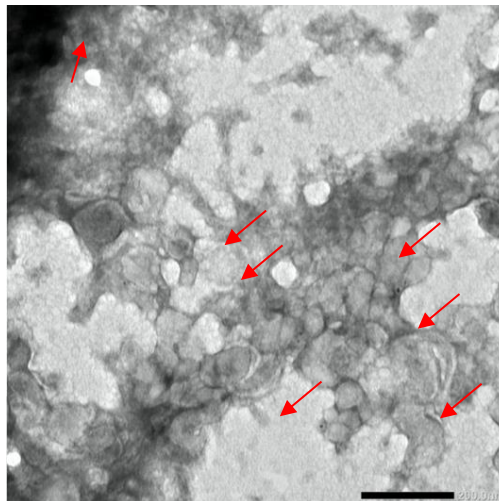
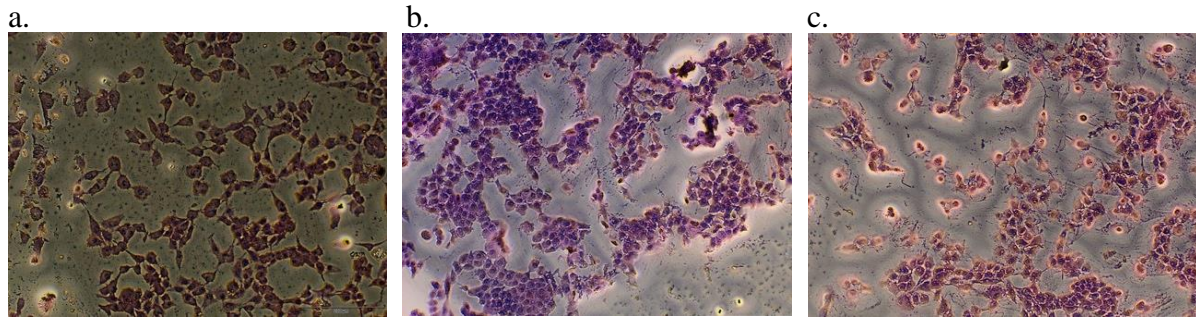


**Figure 40. Light microscope images for syncytium inhibition assay of a) indicator CC81 cells only. b, c) CC81 cells after incubation with BLV mixed with day-35 sera from mice immunized with mQ $\beta$ -gp51-peptide conjugate **5** (panel b) or sera from pre-immunized mice (panel c);** In this assay, multinucleated fused cells with more than five nuclei were counted as syncytia. The number of multinucleate cells (number of nuclei >5) was determined in virus-serum mixtures by visualizing using an inverted light microscope. d) Representative image distinguishing syncytium (circle) vs cell aggregation (rectangle). The cell aggregates have membrane separating the nuclei whereas in syncytium it does not.



d.

